2013

A Microfluidic Platform to Quantify Spatio-Temporal Diffusion of Chemo-Gradients Within 3D Scaffolds: Applications in Axonal Biology

Michael A. Sawonik
Cleveland State University

A MICOFLUIDIC PLATFORM TO QUANTIFY SPATIO-TEMPORAL DIFFUSION OF CHEMO-GRADIENTS WITHIN 3D SCAFFOLDS: APPLICATIONS IN AXONAL BIOLOGY

MICHAEL A. SAWONIK

Bachelor of Science in Industrial Engineering

Cleveland State University

August 2003

Submitted in partial fulfillment of requirement for the degree

Master of Science in Biomedical Engineering

at the

Cleveland State University

May 2013

This thesis has been approved

by the Department of Chemical and Biomedical Engineering

and the College of Graduate Studies by

_____

Thesis Chairperson, Dr. Chandrasekhar Kothapalli

_____

Department & Date

_____

Dr. Joanne M. Belovich

_____

Department & Date

_____

Dr. Parthasarathy Srinivasan

_____

Department & Date

Acknowledgements

First and foremost I would like to thank Dr. Chandrasekhar Kothapalli for being both my advisor and friend throughout my biomedical engineering career at Cleveland State. Over the last two years, I have learned a tremendous amount from Dr. Kothapalli not only from the Biomaterials and Biomechanics courses, but also through daily interaction and discussion of the thesis project.

In addition, I would also like to thank Dr. Joanne Belovich of the Chemical and Biomedical Engineering Department, and Dr. Parthasarathy Srinivasan of the Mathematics Department for their invaluable advice and input on the project and for taking the time to be part of my thesis committee.

Additionally I would like to thank Dr. Peyman Honarmandi from the Mechanical Engineering Department at the City University of New York for his expertise and guidance in COMSOL simulations. Without his assistance with the initial simulation setup, I would have spent many more hours setting up the diffusion experiments and retrieving the data required for the thesis from these simulations. Also, a thank you to Emre Araci, Director of the Microfluidics Foundry at Stanford University for working with me to get all the necessary microfluidic device molds made for use in the fluorescent microscopy experiments. I also would like to acknowledge the support (COMSOL software, licensing, server, etc.) from Dr. Jorge Gatica in our department.

Last but certainly not least, I would like to thank my family (Karen, Ron, Dan, Michele, Marcie, and Larry) and my fiancé, Lexie Shanker, for their continuous support over the past few years and in making sure I stayed on track and never gave up.

A MICROFLUIDIC PLATFORM TO QUANTIFY SPATIO-TEMPORAL DIFFUSION OF CHEMO-GRADIENTS WITHIN 3D SCAFFOLDS: APPLICATIONS IN AXONAL BIOLOGY

MICHAEL A SAWONIK

ABSTRACT

Axonal outgrowth and guidance play an important role in wiring the developing and regenerating nervous system. The critical role of biomolecular gradients in facilitating this axonal sensitivity and directionality along specific trajectories needs to be elucidated for designing effective therapeutic treatments under injury or disease conditions. However, previous *in vitro* approaches based on micropipette assay or gel-turning assay proved to be unsuitable or inefficient for precise generation and quantification of diffusive gradients. In this study, we utilized a microfluidic device to generate and quantify physiologically-relevant biomolecular gradients in a simple and reliable manner. Using a combination of computational and experimental techniques, we designed and developed a microfluidic platform to study the synergistic effects of 3D scaffold concentration (0 - 3 mg/mL), molecular weight of the diffusing molecule (1-1000 kDa) as well as its dosage (0.1-10 µM), on gradient generation and steady-state spatio-temporal evolution. The device was fabricated using standard soft-lithography techniques, and has three separate chambers, flanked by two media channels on the sides. The scaffold (gel) of interest was filled in the left and right chambers (L = 3.6 mm, thickness = 150 µm), and the biomolecule of interest was loaded in the middle

chamber to facilitate diffusion through the gel on both sides. The channels on both sides act as sink for the diffusing biomolecule, creating a gradient across the 3D gel. Two different types of scaffolding materials were used in these studies – collagen-1 or matrigel®. The viscosities of these gels at various concentrations were obtained from commercial vendors, and diffusion coefficients of biomolecules within these gels calculated using the Stokes-Einstein equation. Computational simulations were performed using the finite element methods (COMSOL® Multiphysics), to obtain a gradient profile across the chamber in all three dimensions. The numerical grid for performing the simulations consisted of approximately 250,000 triangular elements for the 2D simulations and tetrahedral elements for the 3D simulations. Primary rat cortical neurons were cultured within 3D 2 mg/mL collagen-1 gel within these devices and exposed to a gradient of 10 μg/mL IGF-1 for 48 h. The neurite outgrowth and turning towards the chemogradient was imaged and quantified, and correlated to the gradient concentrations and steepness at various locations within the device.

Results showed that steady-state diffusion times are strongly dependent on gel concentration and molecular weight of diffusing molecule. For example, while the steady-state condition was reached in 2 h for 1 kDa Dextran diffusing in 1 mg/mL collagen, it took more than 125 h for the 1000 kDa molecule to diffuse in 3 mg/mL collagen. However, the initial concentration of diffusing molecule (0.1-10 μM) appeared to have no significant effect on attainment of steady-state time under these conditions. Molecular diffusion did not exhibit any variation along y and z-axes within the device, and progressed only along x-axis across the

chamber. A generalized equation for the time needed to reach steady-state was proposed, based on scaffold concentration and the molecular weight of the diffusing molecule. The steepness of the gradient at different regions of 3D gel was found to be 1% or less across a 10 µm cross-section, taken at 6 locations across the chamber. Axonal outgrowth and turning was significantly affected by the IGF-I gradient. At the higher IGF-I concentrations in the device, average outgrowth increased to 92 µm compared to only 17 µm in the control samples while the majority of neurites (53%) turned towards the gradient. In conclusion, the device investigated appears to be capable of generating stable chemical gradients across its chambers for the study of axonal regeneration as well as other biological problems where chemogradients play a major role.

TABLE OF CONTENTS

LIST OF TABLES

LIST OF FIGURES

CHAPTER I

INTRODUCTION

1.1 What is bio-microfluidics?

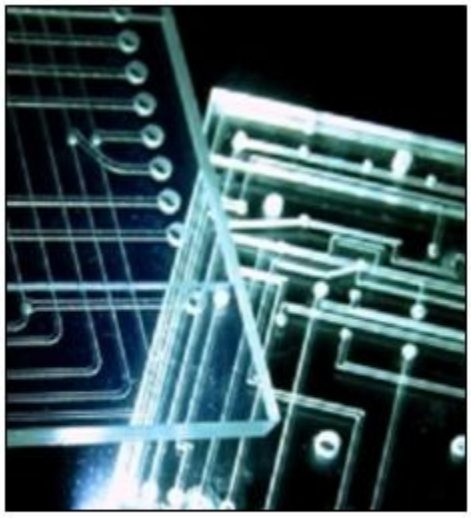

Fig 1: Basic Bio-Microfluidic Device made from PDMS [P1]

Many researchers are unfamiliar with the field of microfluidics or how this field and these devices could potentially benefit their research. Microfluidics is a continuously growing field that deals with manipulating small amounts of fluid through channels with dimensions of tens to a few hundred micrometers [1]. Tabeling defines microfluidics as the study of simple/complex, mono/multiphasic flows that are confined in an artificially created microsystem [2]. Figure 1 depicts a typical microfluidic device created from polydimethylsiloxane (PDMS), a silicon based organic polymer. These devices are similar to integrated circuit boards used in computers, but deal with the flow

of liquids, gels, growth factors, etc. instead of electricity. The origins of this science can be traced back to the mid 1970's when the first miniaturized gas chromatography system was created [2]. After this, the use of microfluidic devices seemed to stall. It wasn't until after 1991 that the true benefit of miniaturization was realized and the field of microfluidics progressed [2]. DNA amplifiers, cytometers, chemical micro-reactors, and even printing heads for ink jet printers began using microfluidic devices.

From these beginnings, microfluidics has found use in many areas of science including both chemical and biological/biomedical engineering. Microfluidics has allowed for the creation of "lab on a chip" devices. These devices can take a small drop of fluid such as blood from a patient, placed into a microfluidic device, and immediately give feedback on contaminants, diseases, etc. found in the blood. For example, Alere Inc. has developed a microfluidic device known as the Alere Triage® Cardiac Panel which can be used to aid the diagnosis of myocardial infarction [3]. This device can take several drops of blood from a patient and draw the sample across a filter by capillary action which separates the blood cells from the plasma. Once filtered, the cells react with fluorescent antibody conjugates as it flows through the device [3]. Once the chip is loaded into the meter, the concentrations of creatine kinase MB (CK-MB), myoglobin, and troponin-I can be determined in as little as 15 minutes compared to several hours by previous pathological screening methods. These three myocardial proteins are produced in abnormal quantities when a patient has

suffered a heart attack [2] and the lab on a chip device gives a quick and easy way to accurately detect them.

Lab on a chip devices are not limited to purely diagnostic applications like the cardiac panel chip described above. Researchers are beginning to use these devices to study a wide variety of biological functions that could not be a precisely controlled as with a conventional cell culture. One area of research currently using these devices is in the study of cancer metastasis. Metastasis has been called one of the most dangerous events in cancer [4], but it is unfortunately poorly understood as to why these cells move or are drawn to certain locations in the body. The hope is that better understanding will lead to better treatment options. The use of microfluidic devices are allowing for studies that look at the external forces, whether they be chemical or mechanical, which cause cell motion. Several research groups have set up both two dimensional and three dimensional devices to generate chemotactic gradients of epidermal growth factor which is thought to be one of the driving factors in breast cancer cell movement [5][6].

The uses of microfluidic devices are finding their way into increasingly higher numbers of studies and applications as time progresses. Depending on the design of the device, gradients of both chemical and mechanical properties can be created across a device allowing researchers to study cell migration, differentiation, neuro-regeneration, among many others biological problems.

1.2 Benefits & limitations of microfluidic devices

The use of microfluidic devices results in many advantages over traditional cell culture and laboratory test techniques. One major advantage over traditional cell cultures is that individual molecule or cell activity can be studied using these devices. In traditional cultures, large quantities of cells are generally isolated and trying to locate and image one particular cell over a long period of time can be difficult to say the least. With the aid of microfluidic devices, a few cells can be loaded and each cell studied and the changes quantified over a longer period of time. This will be discussed in more detail later. Using these devices, gradients of chemical or mechanical properties can be established across the various device chambers to study the effects on cell growth, migration, axonal turning & growth, etc. These devices are generally inexpensive (a couple hundred dollars for a silicon mold) and can be duplicated fairly rapidly [2]. With devices designed in CAD, photolithography methods can be used to quickly build a reusable mold on a silicon wafer [7] and soft-lithography can be used to replica mold the device using a variety of materials such as PDMS.

Other benefits of microfluidic devices include smaller sample volumes and reaction times as well as greater control on experimental parameters. With the various channels and chambers of the devices being on the micron scale, minute amounts of substrate material and reagents are required to successfully setup and run an experiment. If you consider a chamber that is 500 µm X 500 µm X 150 µm, you only need 37.5 *nano liters* of material to fill the chamber. With the

small size and volume of chemicals involved, reaction times are greatly decreased with little waste of expensive reagents.

Microfluidics presents many other important benefits over traditional cell culture techniques. In traditional cultures, the microenvironment around the cell cannot easily be mimicked or controlled. Oxygen content is sometimes unphysiologically high, fluid flow and shear stress seen by the cells is not present, and three dimensional environments cannot be duplicated from one culture to the next [8].

Unfortunately no device is perfect and there are some limitations associated with microfluidic devices. For example, due to the extremely small size of the devices and the chambers and ports used for media, gels, etc. loading of the microfluidic devices can sometimes prove difficult. If you have a steady hand and a keen eye, loading the devices can be fairly straight forward with the use of a micropipette. Otherwise, more sophisticated and more costly devices are needed to accurately fill the chambers and channels with media and gels. While the experiments conducted as part of this thesis deal with static fluid conditions, some devices require specific flow rates through the devices. This requires special plumbing and pump setup to accurately deliver the right amount of flow and media through the channels and chambers without disrupting or damaging (due to shear) the cells or matrices inside the devices. These setups can be relatively simple to extremely complex depending on the study involved as seen in Figures 2 & 3.

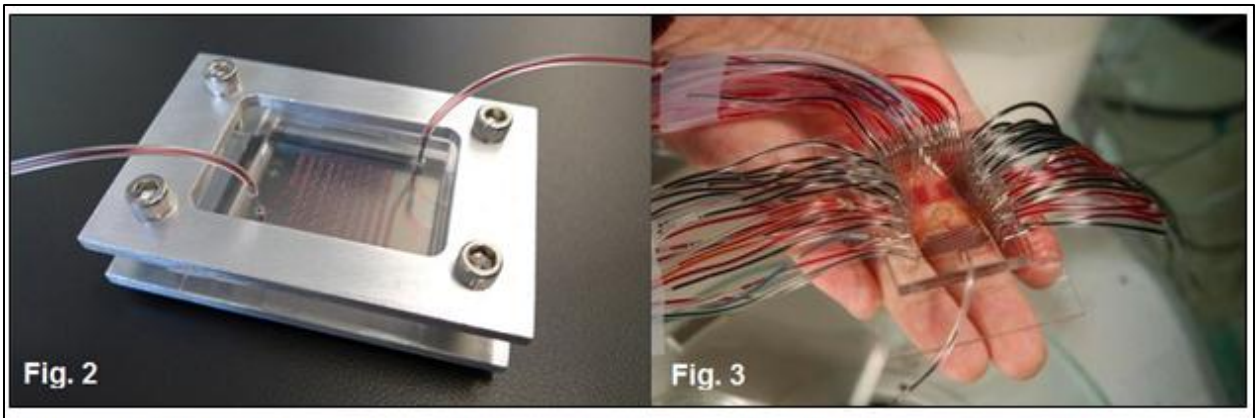

Fig. 2 & Fig. 3: Simple and complex microfluidic pump setups. Simple devices such as those used as mixing devices may only have one pump to flow media through the device. More complex setups, like the one shown in figure 3 can require substantially more pumps and plumbing depending on the reactions being studied. **[P2][P3]**

The completed devices also require a perfect leak proof seal between the PDMS device and the glass cover slip. This relies on air plasma to create an irreversible bond between the two mating surfaces. When done correctly the bond is very strong and will not allow the gel or media to leak. However, if not sealed properly, media and gel will be allowed to leak from one chamber or channel to another and at this point the device cannot be saved and must be discarded and remade. However, the benefits seen from these devices far outweigh the difficulties seen in device fabrication and loading.

1.3 Physiological relevance of gradients

Gradients of chemical, mechanical, and electrochemical properties play a key role in almost every aspect of cell biology. They guide the growth and direction of axons, the differentiation to one cell type or another, the migration of cells through the extracellular matrix and many more. These gradients are responsible for the development of life as we know it today. Since the purpose of

the device was to investigate axonal biology, under healthy and diseased conditions, the importance of gradients to neural cells will be discussed initially, followed by a brief overview of other important gradient functions in the body.

1.3.1 Neuronal development

In nerve cell biology, chemical, mechanical and electrochemical gradients dictate about every function in the cell. During development, growth, and regeneration, axons are guided by specific repulsive and attractive cues in the extracellular environment [9]. During development of the nervous system, the growth cones or the outmost tip of the extending neurites, sense and respond to these chemical cues to reach specific targets in the extracellular environment [10]. It is generally accepted that these extracellular cues help to facilitate the growth cones tunnel through tissue and reach distant targets. Unfortunately, the specific combination of chemical cues and concentrations needed for growth and guidance remains elusive. While valuable information has been discovered from *in vivo* studies on neurite guidance, it is virtually impossible to accurately control all the chemicals involved in the body to be able to conclude the effect of a particular growth factor on the neurite [10]. A multitude of *in vitro* assays have been used to study the effect of particular chemical cues. For instance, in a study conducted by Genc et. al., NT-3 was looked at as a chemoattractive agent for sensory & motor neurons [11]. Mouse dorsal root ganglia (DRG) were dissected and placed on tissue culture inserts. NT-3 and PBS loaded sepharose beads were then inserted into the cultures [11]. Over time, these microbeads released

the guidance cues into the tissue culture where the growth cones could sense and respond to the NT-3. While studies such as these do provide valuable data, they tend to show the overall global response of the culture to the specific chemical cue. Also, due to the overlap of cells, it is difficult to trace individual neurites and their responses over time to particular chemical gradients. Also, it is difficult to quantify the concentration of the gradient seen by the developing neurite.

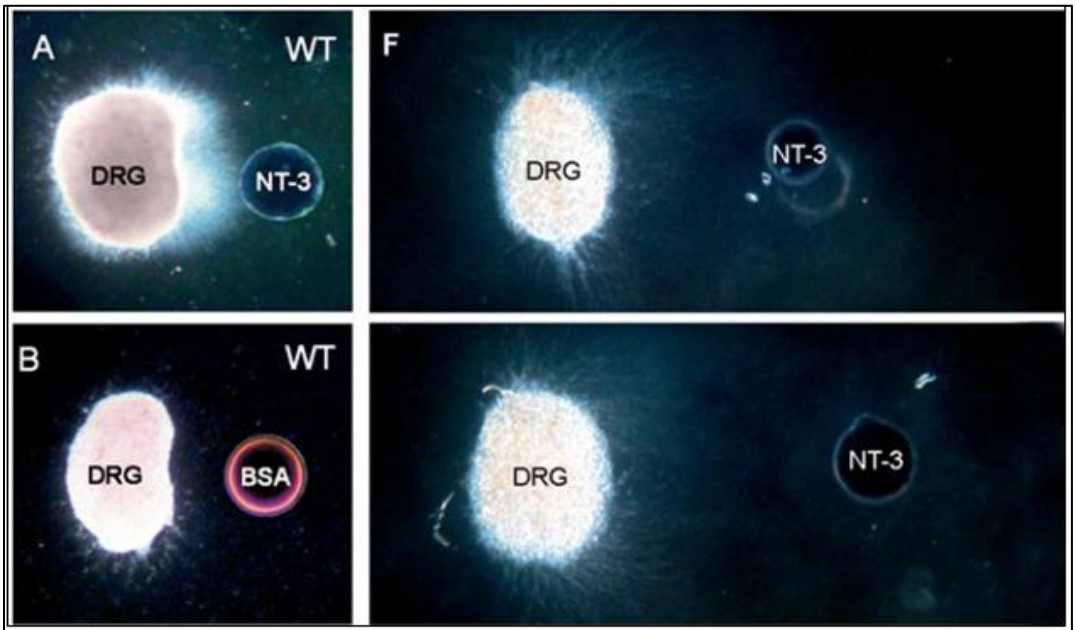

Fig. 4: Chemoattraction of dorsal root ganglia axons to microbeads loaded with Neurotrophin-3 (NT-3) or Bovine Serum Albumin (BSA). While BSA or PBS loaded beads were used as controls, NT-3 was used to show that it acts as a chemoattractant for sensory axons during target direct path finding **[P4]**

1.3.2 Cell migration

Another area of study that is greatly influenced by chemical as well as mechanical gradients is cell movement throughout the extracellular matrix. Of

particular interest in today's world is cancer metastasis. What particular combination of cues causes cancer to migrate and home in a particular area of the body? Since cancer generally spreads via the bloodstream or lymphatic system, what cues causes the cancer to leave the blood and settle in a particular organ? Like neuronal regeneration, it is generally accepted that chemical cues play a role in when and where cancer cells will migrate to and settle. Recent studies have shown that small GTPases, secreted and plasma membrane-tethered proteases, as well as growth-factor signaling, such as that mediated by HGF through the Met receptor, play a role in the chemical guidance of cancer cells [12].

Healthy cells undergo migration through the extracellular matrix (ECM) based on chemical and mechanical cues much like cancer cells. It has been shown in numerous experiments that the growth and movement of cells through the ECM is greatly affected by the matrix stiffness [13][14]. A study by Lo et-al., in 2000 was the first to observe the movement of fibroblast cells with respect to the rigidity of the matrix which they called durotaxis (cell migration guided by gradients in substrate rigidity) [13]. During these experiments, a gradient on the stiffness of the collagen matrix was created and the movement of the cells observed and quantified. This same study also was able to show that the movement of the cell could be guided by creating mechanical strains in the front and rear of the polarized cell. Experiments such as these (examined in detail in Chapter 2) show that not only chemogradients, but also substrate stiffness gradients can affect the direction and mobility of the cell. Since Lo's initial study,

similar phenomena has been observed in other cell types including smooth muscle and epithelial cells as well as neurons.

1.3.3 Immune response

The body's immune response to pathogenic microorganisms that have infected the body depends entirely on the ability of the host immune cells to detect and locate the invading organism [15]. Bacteria and viruses that enter the body are usually first recognized by macrophages, a type of white blood cell that ingests foreign material such as infectious microorganisms. When the macrophages detect and contact the invader, they begin releasing signaling proteins known as cytokines. These cytokines begin to diffuse through the extracellular matrix creating a gradient originating from the site of infection or injury [16]. The cytokines serve multiple purposes in the immune response. First, they stimulate the endothelial cells of nearby vessels to express cell adhesion molecules as well as adhesive proteoglycans [15]. Neutrophils, a second type of white blood cell circulating in the blood stream, are activated by these adhesion molecules and begin to leave the blood stream near the infection site. Once outside the blood stream the neutrophils use the cytokine gradient to migrate towards the site of infection and with the help of the macrophages, phagocytize and destroy the invading organism [15][16]. Without a gradient of protein cytokines, neutrophils would not be able to move out of the blood vessels and migrate toward the source of infection. The biomolecule gradients of the immune

response system play a critical role in eliminating the harmful effects of microorganisms that have infected the body.

Over the past 30 years, methods such as the Transwell assay, Zigmond Chamber, and Micropipette assays have been used to study cellular responses to many molecular signaling cues [6]. While these methods are effective in identifying the global response of cells to delivery of biomolecules, they are not able to generate stable, predictable gradients which is required if reliable accurate correlations between cell movement and chemical cues are to be drawn. The development of microfluidics has helped researchers overcome some of these limitations. Over the past several years, numerous microfluidic assays have been developed to study these chemical gradients in more detail, which will be looked at in Chapter 2.

1.4 Problem statement & thesis objective

Very few studies have been reported on the diffusion of a specific biomolecule within 2D or 3D environments. This is because it is not easy to accurately predict or quantify the biomolecular diffusion using existing *in vitro* or *in vivo* platforms. These prior studies used diffusion coefficients that were referenced from other articles, which could not be verified independently. Thus, till date, a comprehensive understanding of the spatio-temporal evolution of biomolecular diffusion in a physiologically-relevant 3D microenvironment remains elusive. In addition, quantitative analysis of the localized concentrations and steepness of gradients, which could be detected by a single cell (~ 5-10 μm

diameter) or growth cone (< 1 μm diameter) within a 3D microenvironment has not been attempted earlier. Such information is critical to not only understand the role of diffusive gradients on cellular dynamics (chemotaxis, differentiation, migration, turning, etc.) but also elucidate molecular-level signaling pathways (surface receptor activation, integrin binding upregulation, etc.) involved in such processes. Thus, to fill the existing void in literature, the goal of this study is to design, fabricate and implement a microfluidic device which could generate chemo-gradients of physiologically-relevant growth factors. Using this device, we intend to gain a thorough understanding of how biomolecules diffuse through varying gel stiffness, depending on their molecular weights and concentrations. This knowledge would enable us to precisely quantify steady-state times of diffusing molecules (assuming constant source of release), and their gradient and steepness at any location within the 3D device at steady-state. We then applied this knowledge to evaluate the role of diffusing chemogradients on cortical neurite outgrowth and turning within this microfluidic device. Specifically, these outcomes were correlated to the concentration gradients and steepness within the device at specific locations. This device could also be used to study axonal regeneration after injury, which we intend to follow up in the next batch of experiments.

1.5 Organization of the thesis

Chapter 2 provides an in-depth analysis of the past and current methods of mechanical and chemical gradient studies as well as how gradients are

created and verified using microfluidic devices. Although the purpose of this device was originally to study axonal growth and regeneration in healthy and damaged nerve cells, we will also look at how microfluidic devices are being used to study other biological problems such as cell movement, cancer metastasis, as well as how researchers are using these devices to study and quantify these gradients.

Chapter 3 will provide in detail the rationale behind the device design as well as how the devices were fabricated. From here, we discuss in detail how the COMSOL simulations were set up as well as the reasoning behind running both 2 dimensional as well as 3 dimensional simulations. We then detail the procedure for running the fluorescent microscopy studies using the actual microfluidic devices to verify the data obtained from the simulations. The chapter concludes with a description of the in vitro cortical neuron culture within 3D collagen-1 gel within the device, and exposure to 1 μM IGF-1. In Chapter 4, we begin by discussing the calculations and results needed for the initial setup of the COMSOL models and then discuss the results of the simulations and fluorescent imaging experiments. We then quantify and correlate the neurite outgrowth and turning in response to the gradients within this device. The final chapter discusses the conclusions and limitations of this work, and provides direction for future work and experiments that can be built from our findings.

CHAPTER II

LITERATURE REVIEW

A wide range of biological phenomena are influenced by various chemical species diffusing throughout the ECM. Axonal guidance, cell migration & cancer metastasis, cell differentiation, survival, or death, all rely on chemical cues in the body. Unfortunately, the effect of specific cues and combinations of cues which modulate these biological phenomena are yet to be determined. Every cell in an organism is continuously exposed to chemical signals released by other cells. Why cells respond to some cues and ignore others, move toward areas of higher or lower ECM stiffness is at the center of much of the current research. We first begin by looking at various methods of generating gradients, both traditional and using microfluidic devices. Then we focus on examining some of the current research centered on chemical and mechanical gradients. Since the device presented in this work was specifically designed for studying axonal outgrowth and turning, we conclude the chapter with a look at the traditional vs. microfluidic assays used to study axonal biology.

2.1 Quantification & verification of gradients in vitro using traditional methods & microfluidic devices

Prior to the development of microfluidic devices, generating and maintaining stable spatial and temporal gradients was problematic. In the past, generation of chemical gradients *in vitro* relied on methods such as Transwell assay / Boyden chamber, Zigmond and Dunn chambers, micropipette generated gradients, and even biological hydrogels. Over the years, these methods have proved invaluable in identifying molecules that elicit gradient-dependent cell responses. Although invaluable, these methods left a number of questions unanswered, due to their inability in producing sustainable, reproducible, and easily quantifiable molecular gradients. Recent developments in microfluidics have resulted in many innovative approaches to help overcome these difficulties. Two general methods of gradient generation have been described: (a) free diffusion of a molecule across a matrix between a source and sink, and (b) gradient generation perpendicular to continuous streams of varying concentrations [17]. Due to the nature of the goal of this research, the focus here will be on quantifying gradients created between a source and a sink, and so we will look at several different methods previously and currently used to generate and quantify these gradients.

2.1.1 Simple diffusion

The source-sink method of gradient generation relies exclusively on simple diffusion of the molecule through the matrix. Simple diffusion is a means of passive transport whereby net movement of a particular molecule is seen from

an area of higher concentration to one of lower concentration until equilibrium is reached. In simple diffusion, there are six main factors that affect the diffusion rate [18]:

1. concentration gradient
2. molecular weight of the diffusing molecule
3. distance the molecule has to travel
4. temperature
5. solubility of the diffusing molecule and,
6. surface area over which the molecule can work

Unlike other types of transport in the body such as facilitated or active transport, simple diffusion such as the source-sink setup does not involve a protein. Since no proteins or energy is involved, the molecule can only flow down the concentration gradient via an exergonic process, in which the free energy at the final state is less than the free energy at the initial state.

2.1.2 Transwell assay / Boyden chamber

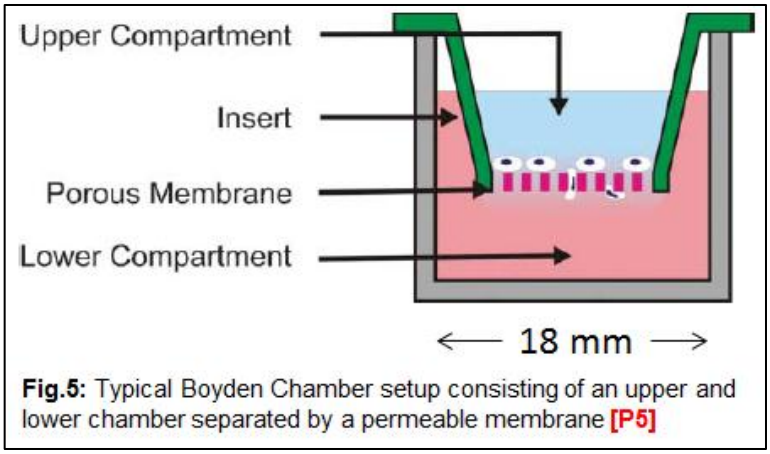

Fig.5: Typical Boyden Chamber setup consisting of an upper and lower chamber separated by a permeable membrane **[P5]**

Transwell assays, also known as Boyden chambers, were developed by Stephen Boyden in the early 1960's to study leukocyte chemotaxis [15][19] and

its use has greatly expanded our understanding of chemotaxis in the body. This assay is relatively straightforward and simple to use making it a popular method for chemotaxis studies. In short, the upper compartment of the chamber contains the seeded cells and has a porous membrane that the cells can migrate through. The lower chamber contains the chemoattractant solution [15]. The chamber setup allows chemoattractant from the lower compartment to diffuse across the porous membrane and through the seeded matrix of the upper compartment thereby setting up a chemical gradient with higher concentration at the bottom and lower concentration at the top (Figure 5). This chemical gradient can induce the cells seeded in the top compartment to migrate though the porous membrane and into the lower compartment. Once in the lower compartment, the cells that have migrated can be fixed, stained, and then counted to quantify the degree of chemotaxis seen.

This method of chemotaxis studies has many benefits. First, cell motility studies can be conducted quickly without having to consider the effects of cell proliferation [19]. Typically, the cells can migrate through the porous membrane of the chamber in as little as a few hours which is considerably shorter than the time needed for the complete cell cycle. Second, this method readily produces a chemotactic response from the seeded cells and provides a simple way to quantify the level of migration due to chemotaxis [15]. Also, the Transwell assay is relatively sensitive to low levels of chemotactic factors and has fairly good reproducibility compared to other cell migration assays [20]. Finally, this assay allows researchers to study migration of cells transfected with a particular gene

of interest. By marking the cells of interest with a particular chemical marker such as β-galactosidase which can be visualized by X-gal staining, migration of cells with particular genes subjected to a particular chemical gradient can be quantified [19].

Compared with more current techniques like microfluidic devices, the Boyden Chambers do have some limitations. While it is simple to generate a chemical gradient across the chamber membrane, this gradient varies over space and time and cannot be readily controlled and an imbalance of fluid between the upper and lower chambers can cause flows through the porous membrane that can distort the chemical gradient [15]. Also, gradients using multiple chemoattractants cannot be created. Lastly, the cost of the porous membranes used in the chamber is relatively high and due primarily to the size of the chamber, the quantification of cell migration is usually only determined for a small portion of the membrane surface [20].

2.1.3 Zigmond chamber

Created in the late 1970's, the Zigmond chamber was conceived to study the rapid migration of polymorphonuclear (PMN) leukocytes [21]. The overall setup and function of the Zigmond Chamber is similar to that of the Boyden (Figure 6) wherein the Zigmond chamber uses a simple source/sink setup, but rather than the two chambers being separated by a porous membrane, they are separated by only a narrow gap [22]. A typical Zigmond chamber setup holds approximately 100 µL in each of the two chambers and is separated by a gap

that ranges from 3 - 10 µm tall and 1 mm in width [15][22]. As the chemoattractant begins to diffuse from the source side of the chamber to the sink, a chemical gradient is established, that like other assays can induce the cells to move from one chamber to the next, either up or down the chemical gradient. What was groundbreaking about this device is that it was the first time that cell behavior could be directly visualized in the presence of a chemical gradient. Until these chambers were introduced, cells needed to be fixed and removed from the devices to be visualized [15]. The thin region between the glass ridge and cover slip allows for simple visualization under the microscope of cell growth, migration, and even cell differentiation. With the tighter dimension of the Zigmond chamber, gradients that are more reproducible and mathematically predictable can be created. Also, unlike the Boyden chamber, since direct visualization is possible, fluorescent dyes can be used to help visualize and quantify the chemical gradient.

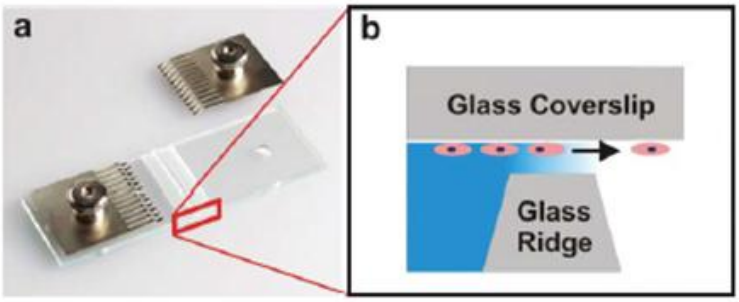

Fig.6: a. Commercially available Zigmond Chamber. b. Narrow gap between the source and sink side of the Zigmond Chamber where chemoattractant cues and cells migrate through **[P6]**

While the Zigmond chamber has many advantages over the Boyden's, it does have one major limitation. While it is simple to create a chemical gradient across the narrow channel, the gradient created only has a lifespan of approximately 1 h before reaching a near steady-state condition [15][22]. This is

due to the physical dimensions of the device itself, specifically the dimensions of the gap compared to the source and sink chambers. Since the gap between the chambers is so small and the volume of fluid contained in the chambers is so large by comparison, an infinite source-infinite sink system is created causing steady state of the gradient to be achieved quickly [23]. Due to this limitation, only cells that respond quickly to chemical cues such as neutrophils or polymorphonuclear (PMN) leukocytes can easily be studied using this method. In addition, similar to a Boyden chamber, the Zigmond chamber cannot create multi-factor chemical gradients. It is only capable of creating two factor gradients along a single line. Lastly, the design of chambers and channels makes the gradient highly susceptible to evaporation [15]. As evaporation occurs, dissolved chemical species in each chamber become more and more concentrated, inducing fluid flow from one chamber to the next, which can disrupt the established gradient.

The Zigmond Chamber has many advantages over previous assays. The fact that cells could be directly imaged was a big step in understanding how cells respond, move, and proliferate in the presence of various cues. However, the short length of stable gradient time, the evaporative effects on fluid flow between chambers, and the fact that multi-factor gradients cannot be created limits the use of the Zigmond chamber.

2.1.4 Biological hydrogels

Biological hydrogels are water-swollen, cross-linked polymeric structures that have received significant attention in recent years due to their exceptional promise for use in biomedical applications. These materials are highly biocompatible and with their hydrophilic characteristics can cause controlled and sustained release of substances trapped within the hydrogel material [16]. This makes them highly desirable especially in pharmaceutical applications. Aside from these applications, hydrogels made from collagen, fibrin, or agarose have been used to create chemical gradients around cells *in vitro* [11].

Recently, these hydrogel gradients have been created in several ways. The most common procedure currently used is to directly deposit an array of droplets or lines of the particular chemical cue onto the surface of the seeded hydrogel, and then allow the chemical cue to diffuse into the hydrogel [24]. These droplets can be easily controlled and dispensed through the use of computer-controlled pumps [24] or ink-jet printing setups [25]. As the droplets diffuse away, they create a chemical gradient diffusing out in all directions from the application site that evolves over space and time. This method of gradient generation has several unique features that have made it a commonly used way of exposing cells to chemotactic gradients. First, the hydrogels are simple to make and they provide the cultured cells with an environment that is more similar to that found in vivo when compared to other two dimensional cell culture substrates [15]. Secondly, due to the high density of the gels, effects from the flow of fluids is greatly reduced. The molecules moving through the gel are only

able to do so by simple diffusion. And unlike other assays, the use of hydrogels offers more control over the gradient than was capable in the Boyden or Zigmond chambers. This control comes from the spatial relation of the chemoattractant to the cells being studied and since multiple types of chemical cues can be injected or printed on the gels, this method is capable of inducing gradients with multiple factors involved.

This method of gradient generation is not reproducible and imaging of the cells in question can be difficult. Imaging of individual cells is made difficult by the 3 dimensional structures of the gel as well as the fact that some gels used for such experiments are not optically clear [15]. With 2D cultures, cells can be tracked and imaged with just a light microscope. Gel cultures require images to be taken at different levels since the cells under study have the capability of moving in all three dimensions requiring the use of 3D tracking algorithms. Lack of gradient control is another disadvantage of this type of gradient generation. The diffusion of the chemical species depends highly on the polymeric chain structure and the porosity of the gel, neither of which can be easily controlled to obtain reproducible results from one experiment to the next. Besides, once the gradient is established, it is difficult to maintain the gradient for long periods of time.

2.1.5 Benefits of microfluidic methods over traditional gradient generation methods

With so many different assays available, what can microfluidic devices offer that cannot be accomplished by one or a combination of other devices?

Advances in micro fabrication techniques over the past 30 years has enabled devices to be designed and built at relatively low cost. In recent years, microfluidics researchers have focused on a need for better gradient generation methods to study cell – chemoattractant interaction. Microfluidic cell culture environments are well suited for achieving the precise gradient control needed to accurately quantify the response of cells to one or multiple chemical gradients. The precise dimensions of these devices coupled with our understanding of fluid behavior at the micrometer scale gives microfluidic devices unique advantages over the traditional gradient generating methods described above [2]. In chapter 1, we looked at the benefits of microfluidic devices in terms of cost, ease of use and fabrication etc. This section will focus more specifically on how microfluidics can solve some of the gradient generation problems seen in traditional assays.

Fluids flowing in the micro channels of a device are dominated by the viscous properties of the fluid and not by the inertial forces generated by that fluid [2][15]. This particular type of flow, known as laminar flow, is very well understood and indicates that the flow of fluids within a microfluidic device can be calculated mathematically with a high degree of accuracy. The equations used to define laminar flow can be used to construct new cell environments with specific control over chemical movement and gradient generation. This technology allows researchers to create gradient generators using multiple chemical species and to have precise control over the spatiotemporal distribution of each chemical under study. This is by far the biggest advantage of microfluidic devices when

compared to traditional methods such as the Transwell Assay or Zigmond Chambers.

During embryological development, the ECM is a highly dynamic environment where cells are constantly secreting signaling molecules. These molecules diffuse through the extracellular matrix causing multiple overlapping chemical gradients inducing nearby cells to migrate, differentiate, or proliferate [26]. The gradients of signaling molecules released by the developing cells rarely ever act independently [27][28][29]. Thus the specific migration or differentiation of a cell is not directed by a single chemical gradient, but by a set of gradients with unique concentrations and spatiotemporal characteristics [15]. But what combination and concentration of these signaling molecules cause the cells to respond one way or another? What combination will cause a nerve cell body to send an axon out in a particular direction and grow and connect to a target organ or muscle potentially on the other side of the body? These are the questions researchers are hoping to answer in treatments for such injuries as nerve or spinal cord damage is to become treatable.

2.2 Chemical gradient studies using microfluidics

Currently, there is a lot of interest in the research community concerning the regeneration of CNS axons and the relationship with growth cones. Normal sensation, motor control and behavior depend on the appropriate wiring of neuronal circuits during fetal development. The neuronal axons are the longest components of these circuits, and come from immature neurons and elongate

precisely through diverse tissues to reach synaptic targets located throughout the body. This embryonic navigation is accomplished by the growth cone, a motile structure at the distal tip of an elongating neuronal axon. The growth cone seeks out molecular “signposts” that are evident throughout developing tissues, by advancing, pausing and turning until it reaches the appropriate target during both embryonic development and regeneration. There are two common forms of guidance cues, diffusible factors secreted by the cells and surface-bounded guidance cues, which are processed by the navigating cones. Scientists have tried to replicate this phenomenon in vitro by periodically injecting chemical solutions in fixed amounts via a micropipette tip near a growth cone to produce approximate, exponentially shaped gradients [15]. Unfortunately, details on how this regulation works is still somewhat of a mystery, partly due to limitations with current experimental techniques. Although studies involving induced flow in microfluidic devices have been successful in generating complex, stable and controlled chemical gradients, use of such devices is limited due to the effects of shear stress, among other factors [15].

Wang et. al. developed a microfluidics-based turning-assay chip designed to overcome the issue of shear stress (Fig. 7). In addition to generating precise gradients of soluble guidance cues, the chip is also capable of fabricating complex composite gradients of diffusible and surface-bound guidance cues that can mimic the conditions of growth cones encounter in vivo [30]. By applying this assay to Xenopus embryonic spinal neurons, it was found that the presence of a surface-bound laminin gradient can finely tune the polarity of growth cone

responses, either repulsion or attraction, to gradients of brain-derived neurotrophic factor (BDNF), with the guidance outcome dependent on the mean BDNF concentration.

In order for Wang to successfully study the guidance response of a growth cone, several design elements needed to be taken into consideration for the device including: (a) the device needed to be compatible with culture conditions for neurite growth, (b) It needed to be capable of creating a stable gradient of diffusible and matrix bound chemical cues, (c) The device must allow for fluorescent imaging of the cells to view and quantify results [30].

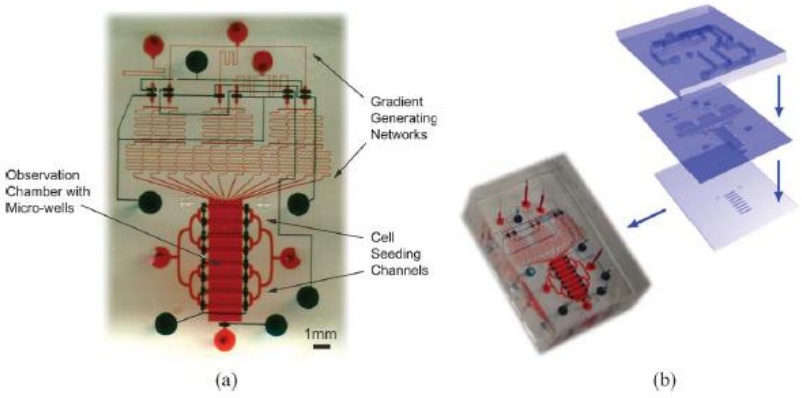

Fig 7: a. Microfluidic composite gradient generator composed of a microfabricated PDMS chip and glass coverslip b. 3D relationship of the multiple layers of the microfluidic device **[P7]**

Using this device, they observed that a gradient of BDNF produced a repulsive turning response in a growth cone on a surface with uniform laminin coating [30]. Time lapse imaging showed that the neurite began to respond to this gradient with repulsive turning in as little as 10 minutes. In this experiment, the average turning angle for the neurites exposed to the gradient was significantly different than that in the control (-12.3˚ +/- 3.3˚ compared to 1.1˚ +/- 2.9˚ in the control, p=0.003) [30]. In addition, this device was able to show that the polarity of the growth cone is regulated by the composite BDNF/laminin

gradient. Results showed that 61.5% of axons extended towards areas of higher laminin concentrations when exposed to a laminin gradient while the growth direction was about 50-50 on a uniformly coated laminin surface [30]. This data suggests that spinal neurons are attracted to higher levels of laminin which is consistent with other previous studies. However, implementation of such a device is very challenging, as multiple Teflon tubes connect the ports within the device to external computer-controlled fluid-flow devices (not seen in Fig. 7).

2.3 Mechanical property gradient studies using microfluidics

One major advantage microfluidic devices have over traditional cell cultures is they allow for the formation of gradients of both mechanical properties as well as chemicals such as growth factors or inhibitory molecules. The flexibility of the microfluidic devices allows researchers to study these gradients in the same device saving both the cost and the time in designing multiple devices for their studies. It has been shown in numerous experiments that the growth and movement of cells through the extracellular matrix is greatly affected by the matrix stiffness [31][32]. A study by Lo et. al. in 2000 was the first to observe the movement of fibroblast cells with respect to the rigidity of the matrix which they called durotaxis (cell migration guided by gradients in substrate rigidity) [33]. Since Lo's initial study, this same phenomenon has been observed in other cell types including smooth muscle and epithelial cells as well as neurons. This is of particular interest for researches working to guide the growth of neurites in hope to be able to repair damage to the peripheral or central nervous system tissues.

During development, the growth of neurites are guided by a multiple cues which can include chemical, adhesion based haptotactic, aligned ECM proteins, other axons and many more [31]. These are all present in the 3D environment during development and the trick is to be able to simulate all these cues in vitro. Microfluidics allows researchers to more accurately replicate these conditions in their experiments.

Surprisingly, few systems have been developed to orient and potentially enhance neurite growth via durotaxis. A study conducted by Sundararaghavan et. al. attempted to accomplish this. Here, a simple H-shaped device was created to induce a gradient across the center channel. This allowed for the introduction of collagen gel into the cross channel that the neurons would be growing through. To establish the stiffness gradient, genipin was introduced to allow for crosslinking of the collagen.

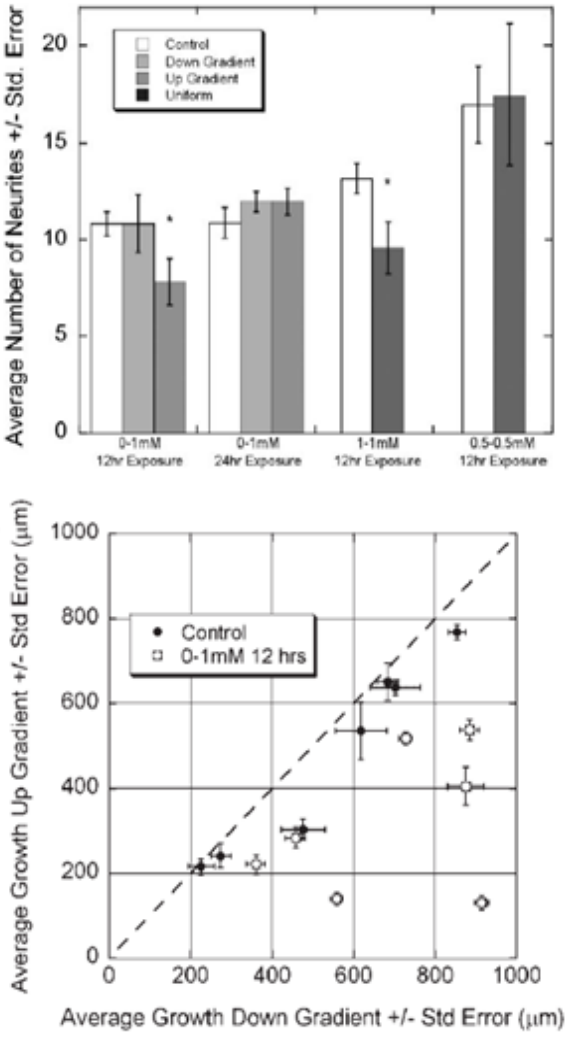

Fig. 8: Top – Number of neurons that turned down versus up the stiffness gradient. Bottom – Average neurite growth seen up and down the stiffness gradient. **[P8]**

These gradients were verified by evaluating the fluorescence intensity emitted by the cross linked collagen. This intensity was shown in a previous study by the same group to strongly correlate with the storage modulus measured in shear of the cross linked collagen gel. This modulus allowed for the calculation/determination of the matrix stiffness across the length of the device channel.

To quantify the results of this experiment, the average length of the axons that grew into the cross channel was measured both in the direction of increasing stiffness and decreasing stiffness. The results of the 1 mM genipin experiments are shown in figure 8. The bottom graph shows that the longer average neurite lengths (greater amount of growth) always occurred in the direction down the gradient (lower stiffness). The top graph depicts the number of neurons that turned away from the gradient compared to towards was significantly higher in both the 0.5 mM and 1 mM genipin concentration experiments ($p = 0.01$) [31]. In contrast, the control setup which had no genipin crosslinking gradient displayed no significant difference in the direction of axon growth or in the length of axon growth after both the 12 h and 24 h time periods.

2.4 Assays to study neurite outgrowth and guidance under healthy and inflammatory conditions

Microfluidics is a multidisciplinary field of study, which can be used in engineering, physics, chemistry, microtechnology and biotechnology. It is becoming an increasingly useful tool for cell biologists due to the ability to precisely control, monitor and manipulate cellular microenvironments. It is

possible to use this technique to isolate and direct growth of central nervous system (CNS) axons without the use of neurotrophins (exogenous factors that signal cells to grow survive or differentiate). This provides a very adaptable system to examine many aspects of CNS development, degeneration and injury, to study their ability or inability to regenerate after injury.

Traumatic spinal cord injury, or SCI, is an important contributing factor to morbidity and mortality in the United States with an incidence rate of 15 - 40 new cases per one million people each year [34]. These injuries can be caused by falls, motor vehicle accidents, violence, sports, etc. and can cost the patient between $500 K and $3 million in medical expenses over their lifetime [34]. The majority of these patients are left paralyzed with no restorative treatment available as of yet. Continued research in this field has led to the identification of growth inhibitory components in the damaged spinal cord that, if properly modulated, could lead to enhanced regenerative capacity and regrowth [35]. Surprisingly, few microfluidic studies have been done to study nerve lesions and how the cells respond and regenerate after. Most studies, as seen in the sections above, focus more on how healthy nerve cells respond to mechanical or chemical gradients. If treatments are going to be produced to help patients who have suffered nerve damage from disease, trauma, etc. it is important to conduct experiments that can mimic the trauma or disease and then see how nerve cells respond to the various gradients. To accomplish this, various in vitro assays have been developed using brain or spinal cord neuronal cells to study axonal growth in an environment that mimics post injury conditions.

Traditional in vitro assays used to study neuronal injury have provided valuable results. For instance, neurite outgrowth and growth cone collapse assays have identified three major inhibitory proteins that suppress axon outgrowth [36]. Neurite outgrowth assays provide a simple means to determine what compounds influence neurite formation and repulsion. Growth cone collapse assays have been successfully used to identify and purify molecules that are repulsive to growth cones or inhibit axonal outgrowth. While these assays have proved useful, they have some major limitations. First, they do not provide a way to probe the axons independently from the cell bodies and second there is no way to induce axonal injury [36]. Traditional methods of inducing injury to axons have included electrically driven shafts (Fig. 9) [37], sharp knives [36], and even glass electrodes [38]. While these methods accurately mimic a crushing injury to the spinal cord, they are only capable of severing a few axons at a time, and they require the use of expensive manipulators, and lack the high degree of control and reproducibility seen in more current methods. In some cases, such as with the glass electrodes or pipettes damaged the surrounding cell matrix to the point

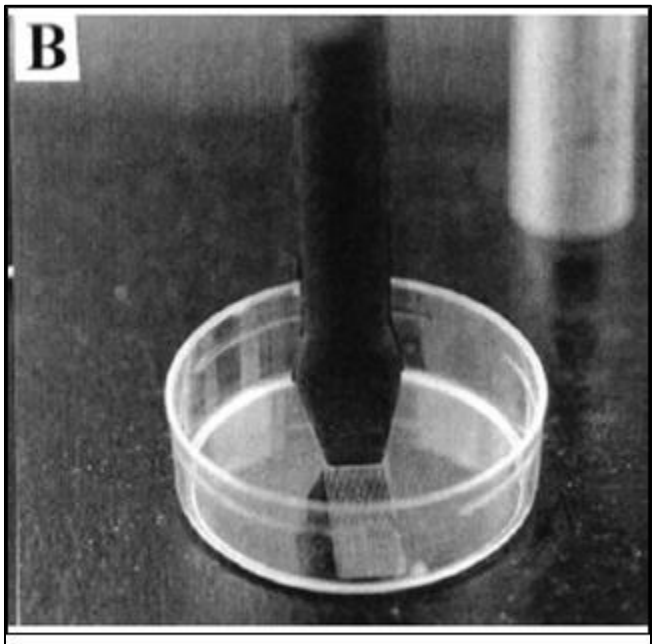

Fig. 9: Rubber Impactor Device Used to Model Neuritic Trauma in vitro **[P9]**

where regrowth of the nerve axons could not be achieved [37]. There are other disadvantages to this sort of approach as well. First, tissue cultures in petri dishes lack the inflammatory response and blood flow changes typically seen around an injury site in vivo. The use of a microfluidics platform and micro fluid pumps allow for this aspect to be studied as well. Second, there is no glial scar formation to impede the regeneration of the neurites or axons. In the environment around the glial scar, regeneration and remyelination typically fails. The damage that occurs to the system causes recruitment of microglia, oligodendrocyte precursors, meningeal cells, astrocytes and stem cells [39]. Various experiments have shown that these cell types release molecules such as NI250, myelin-associated glycoprotein (MAG), and NG2, which can cause inhibited growth and/or collapsing growth cones [40].

Newer methods of studying axonal injury are employing the use of PDMS based microfluidic devices and lasers to more accurately control nerve damage in the lab. In a study conducted by Kim et. al., laser microbeams were used to induce axonal damage to cells cultured in microfluidic devices. Their goal was to study the dynamics of neuronal damage and regeneration in vitro. The general setup for this experiment can be seen in Fig. 10. The nerve cells were cultured in a microfluidic device with alternating surface patters of PLL and aggrecan which helped to control the outgrowth towards specific regions [36]. This helped to force the axons to grow down the channels in the microfluidic device. Once established, a laser microbeam could be used to induce damage to the axons. By varying the intensity of this beam, the researchers could cause partial or

complete transections of the axons. This method produces numerous advantages, but some disadvantages as well. The use of the microfluidic device allows for the manipulations of the spatial organization of the neurons and the microbeams from the laser allow for the accuracy and reproducibility in the experiment. This allowed the researchers to determine important characteristic of nerve damage such as dieback of the proximal segment of the neuron as well as the degeneration of the distal segment [36]. One major disadvantage is that the resulting injury to the axon is not really physiologically relevant. When an injury occurs such as from a car accident or sports injury, etc. more damage would be done to the nerve and surrounding tissue. The laser produces a very fine, clean cut across the neuron which is not typically what would be seen in a normal injury.

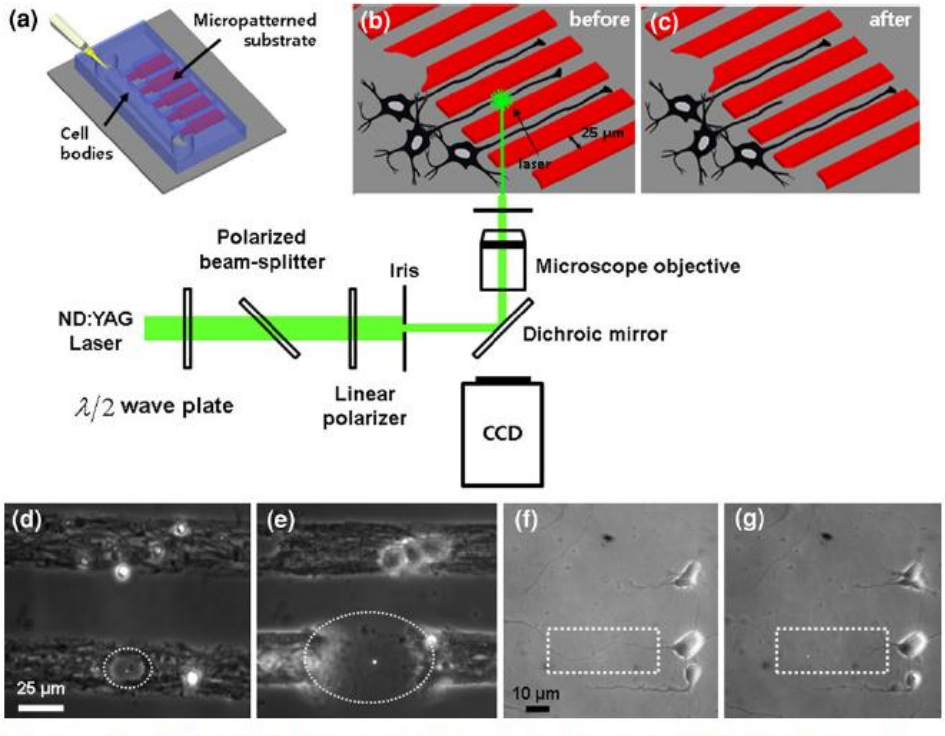

Fig. 10: a. Microfluidic Culture Platform, b & c. Laser Induced Axotomy, d thru e. Micrographs of Laser Induced Axotomy **[P10]**

2.5 Current & future treatment of neuronal injury

Nerve injuries can be the result of a number of different actions, such as the following [41]:

1. Mechanical trauma

2. Crush injury, such as fractures, hematomas, compartment syndrome

3. Penetrating traumas, i.e. stab wounds, surgical incisions where the peripheral nerves are partially or completely severed in an irregular manner

4. Stretch injury from nerves being stretched 10% - 20% before structural damage.

Such injuries are classified based on the nerve components affected, loss of functionality, and the ability to recover spontaneously. There are two systems currently used that stage the extent of nerve injury: Seddon's system and Sunderland's system [41][42].

Peripheral nerve injuries occur more frequently than those involving the central nervous system. The neuron doesn't proliferate through mitosis as do other somatic cell types in various tissues. When its axon is cut from the cell, it's swallowed by macrophages [43]. The remaining axon segment that's connected to the cell starts to grow and interacts with the proliferating Schwann cells present in the nervous fiber membrane, thus forming a new axonal tube. The Schwann cells provide layers of covering myelin that are necessary for synaptic transmission and nervous reflex [43]. As a result, peripheral nerves can have a spontaneous recovery in the 65 - 85% range [43]. However, more severely damaged nerves will need other types of intervention.

The goal of any type of treatment is to return function to the damaged nerve, and at a minimum, improve the individual's quality of life and finally reducing neuropathic pain. The initial course of action is through pharmacologic therapy. Nerve pain is a combination of somatosensory, cognitive and emotional alterations and is characterized by a burning sensation and dysesthesias, or an abnormal sensation produced by normal stimuli [41]. Despite the number of options for reducing pain that are available, only about 70% are adequately managed with drug therapy [41]. This therapy begins with the use of analgesics including non-steroidal anti-inflammatory drugs and opioids. However, these are dose dependent and are limited by side effects. In addtion, antidepressants and anesthetics are also used, as well as antiepileptics [41].

Other approaches include transcutaneous electrical nerve stimulation, antivirals and steroids [41]. Surgical treatment is also an option [44]. The aim of surgery is to repair the damaged nerve, maximize the number of axons that regenerate through the site of the injury, and increase the proportion of axons that grow back to appropriate targets [44]. The most appropriate surgical technique depends on the extent of the nerve damage, the nerve's viability and location, patient's age and medical conditions, whether functional ability can be restored to some certain level, and whether benefits outweigh risks, costs and loss of productivity [44]. Surgical techniques include nerve repair, nerve graft and nerve transfer.

All of the above approaches to repairing peripheral nerve damage have limits and do not guarantee success. Over the past decade, there have been a

variety of ongoing studies, investigating new avenues to treat nerve damage. The following is a discussion of several of these approaches.

Scientists at the University of Utah have identified a worm gene that is essential for regeneration of damaged nerve cells [45]. They have been able to speed regeneration by over-activating the gene. The study used nematode worms since they have the same molecules performing similar functions as in humans. A pathway was found that regenerated nerves in the worm; this pathway also exists in humans [45]. It is hoped that a drug will be developed that could activate the gene, thus stimulating regeneration of diseased and injured nerve cells.

Researchers at Queen Mary, University of London, proposed a theory that suggests that omega-3 fatty acids, found in fish oil, may have the potential to protect nerves from injury and help them regenerate [46]. The study focused on peripheral nerves. In experiments using isolated mouse nerve cells that were damaged, they found that enrichment with omega-3 fatty acids in cells produced significant protection and decreased cell death [46].

A study of the role of folate in regeneration of afferent spinal neurons after injury, showed that axonal regeneration relies upon the integrity of DNA methylation pathways [47]. This study provided insight into an epigenetic mechanism that contributes to neurorepair and suggests that manipulation of the methylation milieu offers promising therapeutic avenues to promote regeneration.

Current research is looking at the use of umbilical cord blood stem cells as a potential therapeutic tool for neural injuries. Recent studies have shown that

human umbilical cord blood stem cells have the potential to generate cells with neuronal characteristics and for neural differentiation [48]. Scientists were able to produce functional neural cells from these stem cells. Recently, scientists have been able to use olfactory ensheathing cells (OEC) to act as a bridge linking damaged and undamaged tissues in the spinal cord [49]. Early experiments performed on dogs with damaged spines have shown that OECs can be helpful in regeneration of the parts of nerve cells that pass on signals, i.e. axons.

CHAPTER III

MATERIALS & METHODS

3.1 Microfluidic device design

The microfluidic device used in the following experiments was created using photolithography and soft lithography / replication molding using polydimethylsiloxane or PDMS. The 3D models of the devices were constructed using the Solid Works® 2011 CAD package (DSS Solidworks Corp).

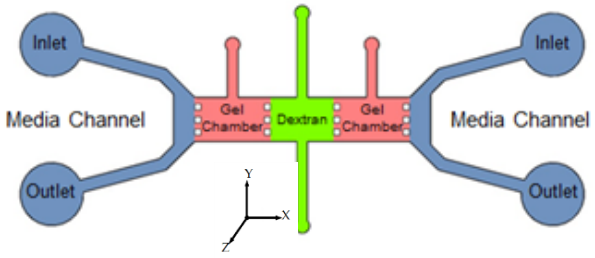

Fig. 11: Design of the microfluidic device used to study gradients across various collagen gel and matrigel concentrations. After replica molding with polydimethylsiloxane, or PDMS, either Type I Rat Tail Collagen or Matrigel (BD Biosciences) was loaded into the gel chambers and allowed to polymerize. Varying molecular weights of FITC-dextran was loaded in the center chamber and allowed to diffuse through the gels.

Figure 11 shows the design and dimensions for the gradient generating microfluidic device which was created using the Solidworks® software package and a dimensioned drawing of the device is shown in Appendix A for reference.

The thickness of all chambers, wells, and channels are 150 µm. The posts between the gel chambers and channels (300 µm sq. posts, 300 µm spacing) are designed to hold the gel within the chamber it was loaded in while still allowing chemicals to diffuse. Capillary force between the posts keeps the gel from flowing out of the chamber when being loaded.

The device was designed with multiple potential applications in mind, the main purpose being to study axonal outgrowth and guidance under healthy and injured conditions *in vitro*. In one application, healthy neuronal cells would be seeded in the left most gel chamber and their axons allowed to grow across the center chamber and into the right. With healthy axons spanning the central chamber a chemical treatment would be introduced to this central chamber which would sever the axons. After injury, removal of the chemical and reestablishment of the various growth factor gradients across the central chamber would allow for the study of how injured axons respond to various chemicals and chemical concentrations. Unfortunately, as mentioned earlier, little information exists on the diffusion of certain chemicals and molecular weights through various matrices. Due to this lack of information, we initially investigated the biomolecular diffusion across the device chambers.

For these experiments, the manner in which the gel and the diffusing molecules were loaded was slightly different. In these experiments, the diffusing molecule (in our case FITC-Dextran) could be loaded into the left and the right media channels and the center chamber could act as the sink. Similarly, the dextran could be loaded into the center chamber and allowed to diffuse out

toward the media channels. From this, fluorescent images could be taken at different time points and the images analyzed in Matlab to generate a gradient profile across the chamber over a period of time. This data will prove vital when biological experiments are conducted in the device. While the cells and axons would be stained with a fluorescent marker, it would be impossible to know from the images what concentration of a particular growth factor the growth cone at the tip of the axons would be experiencing at the time the image was taken. For this reason, this device and thesis has focused on understanding and quantifying these gradients for various molecular weights, matrices, and diffusing molecule concentrations.

The design of this device also makes it suitable for studying other biological problems as well. For example, cell movement through an extracellular matrix with a chemical or even mechanical property gradient across the chambers could be established. Mechanical properties such as matrix stiffness can be setup as a gradient across the chamber and cell movement studies could be conducted to see how the cells respond to varying matrix stiffness.

3.2 Microfluidic device fabrication

These devices were created using a combination of photolithography and soft lithography techniques. Creation of these silicon chips was done at the Microfluidics Foundry at Stanford University and involves the use of photolithography to transfer the design created in CAD to the surface of a silicon wafer [50]. This process involves first printing the Solidworks design onto a

transparency film using a high resolution printer [7]. A photosensitive polymer was then spin coated onto the surface of the silicon chip, the transparency film placed over the photoresist and the entire chip exposed to ultraviolet light [7]. Once developed, the transferred microfluidic design is revealed on the silicon surface. The result of this process is a silicon wafer with the positive relief of the microfluidic device that can be used to replica mold the device as needed [10]. This was shipped to our lab at this stage, which we used to fabricate PDMS devices as described below.

With the silicon molds in hand, the process of replica molding the polydimethylsiloxane, or PDMS, devices via soft lithography could begin. To ease the separation of the PDMS from the silicon wafer, the wafer first underwent a silanization process. This involved the use of tridecafluoro-1,1,2,2-tetrahydrooctly-1-trichlorosilane, also known as silane (United Chemical Technologies Inc. Part # T2492). Due to the hazardous nature of this substance, this portion of the molding process was conducted in a fume hood. To begin, 25 µL of silane was added to a small petri dish using a pipette and placed inside a vacuum desiccator next to the silicon chip. Using a vacuum hose, air inside the desiccator was removed and the silane and silicon wafer was left under vacuum for a minimum of 1 h. Under vacuum, the silane undergoes a phase change from liquid to vapor and, when settles, coats the silicon wafer [51]. Once coated with silane, PDMS could be mixed and applied to the silicon mold.

The individual microfluidic devices used were created from the silicon molds using soft lithography techniques. The PDMS used in these experiments is

a two part mixture: the PDMS polymer and a curing agent and is purchased as a kit (Sylgard® 184 Silicone Elastomer Kit, Dow Corning, USA). The polymer and curing agent were weighed and thoroughly mixed at a 10:1 ratio by weight (polymer : curing agent). The resulting PDMS mixture was placed back into the desiccator to remove the air bubbles introduced from mixing (usually around 30 min). The mixture was then carefully poured over the silicon mold, to minimize additional air bubbles. If bubbles were introduced, the mold was placed back into the desiccator under vacuum to remove the trapped air. To cure, the PDMS was placed into an oven at 70˚C for 24 h. Once the PDMS polymer had cured, the mold was cut to a size to allow for sealing to a glass cover slip and removed from the silicon mold. The next step involved the use of a 4.0 mm and 1.0 mm biopsy punch to punch the various inlet and outlet wells in the device. For these experiments, the 4.0 mm punch was used at both ends of each of the media channels while the 1.0 mm punch was used for the inlet wells for the three gel chambers. Once punched, the PDMS chips were air dusted with compressed air to remove any dust or debris on the device and then placed in boiling DI water to remove any polymer or catalyst that had not been polymerized, as well as to remove any other contaminants that might be on the surface. The glass coverslips that were to be used for sealing the devices were thoroughly cleaned with alcohol and both the PDMS devices and coverslips were placed into the oven to dry for 15 min.

The final step was to close the device with a glass cover slip. To accomplish this, the surface of both the PDMS and the glass cover slip were

oxidized by air plasma which helped to ensure an irreversible bond between the PDMS and cover slip to prevent any leaks of either the gels or growth factors introduced [10]. This process introduces polar functional groups to the surface of the PDMS and glass cover slips to allow for irreversible bonding between the two materials as well as changing the surface characteristics of the PDMS from hydrophobic to hydrophilic [10]. Figure 12 shows a completed microfluidic device ready for gradient studies. The sealing process is one of the most crucial steps of the fabrication process. If an inadequate seal between PDMS and cover slip was created, either the diffusing molecule or collagen gel would be free to flow from one chamber to the next or out from under the device altogether. If this happened, the device would need to be discarded and replaced.

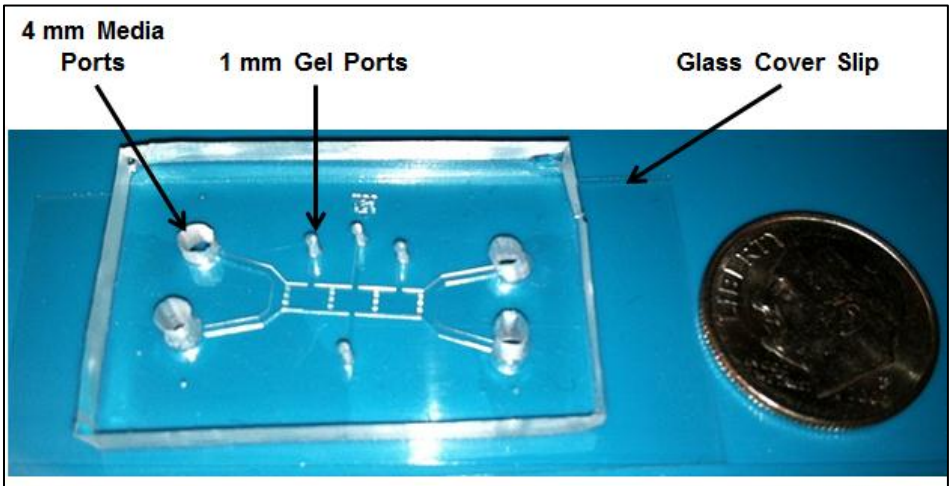

Fig. 12: Completed PDMS Microfluidic Device and its size compared to a dime. At this point, various gels and diffusing molecules can be added to the channels and chambers and the resulting gradient generation imaged using fluorescent microscopy.

3.3 Gradient simulations in COMSOL

Review of the current literature has revealed a surprising lack of information regarding diffusion coefficients. Many studies report specific diffusion

coefficients, but little or no verification had been done to confirm whether these diffusion coefficients were accurate for the particular gel matrix being used. As a starting point for the simulations, diffusion coefficients were calculated using the Stokes-Einstein Equation where k is Boltzmann's Constant, T is absolute temperature (since these experiments were conducted at room temperature, T = 23 ˚C or 293 K), η is the viscosity of the matrix (collagen or matrigel in our case), and R is the Stoke's radius of the molecule diffusing through the gel.

Equation 1: $$D = \frac{kT}{6\pi\eta R}$$

Collagen gel viscosities were provided by Advanced Biomatrix Inc. (San Diego, CA) while the Stokes radii were provided by Pharmacosmos of Holbaek, Denmark (Table II). To get an accurate picture of the diffusion profiles, collagen concentrations of 1.0, 2.0, and 3.0 mg/mL were used with diffusing molecules of 1 kDa, 10 kDa, 100 kDa, and 1,000 kDa. As a reference point, the diffusion of these molecules through water was also calculated and simulated. To see if concentration affects the diffusion rate and time needed to reach steady state, initial concentration values of 0.1, 1.0, and 10.0 µM were used. The rationale behind the choice of these numbers was to ensure their physiological significance and relevance, and to be able to place our findings in the context of the body of literature in this area.

Before the COMSOL models could be created, certain assumptions about the device were needed:

1. The diffusion coefficient, D, remains constant throughout the chamber

2. There are no pressure gradients or fluid flows in the device; all transport occurs by diffusion.

3. Transport is one-dimensional in each region

4. Concentration in the chemoattractant channel remains constant at C_O over the course of the experiment.

5. Concentration in the sink channel remains at zero. The channel volume is much larger than the cell culture chamber volume and it is connected to the large, open media reservoir at two ports, so any chemoattractant build-up in the sink channel will be extremely dilute.

6. The steady state solution to the one dimensional diffusion equation in a single channel with fixed concentrations at both ends is a homogenous linear profile.

To completely study the diffusion across the device, both 2D and 3D simulations were performed. The 2D simulations were run on every combination of molecular weight, collagen gel concentration and diffusing molecule concentration (48 simulations in total). For comparison purposes, matrigel was also simulated using all four molecular weights at a 10 µM concentration. Viscosity data for matrigel was provided by BD Biosciences (San Jose, CA). Diffusion profiles in 3D were run for selected cases using 10 kDa FITC-Dextran in 1.0 and 2.0 mg/mL collagen with a concentration of 1 and 10 µM. These 3D studies were run to help insure that the diffusion of the molecule progressed across the device in a straight line, edge to edge, in the chamber and did not

vary by height across the gel chamber i.e. progress across the chamber is along the x-axis only.

We defined D as the diffusion coefficient of the FITC-dextran in the particular collagen gel according to the Einstein-Stokes Equation, and C_o as the initial concentration of FITC-dextran. Insulating or "no flux" boundaries were defined at the 300 µm posts separating the chambers as well as the outer perimeter of the device. These are boundaries where the diffusing molecule is not permitted to cross or diffuse through. Flux boundaries were defined between the center and left & right chambers long the posts as well as between the gel chambers and media channels. Appendix B depicts the boundary locations as well as boundary conditions and equations used in the COMSOL program. The numerical grid for performing the simulations consisted of approximately 250,000 triangular elements for the 2D simulations and tetrahedral elements for the 3D simulations. Figure 13 shows a snapshot of the COSMOL model broken up into the triangular and tetrahedral elements for the 2D and 3D simulations. With the

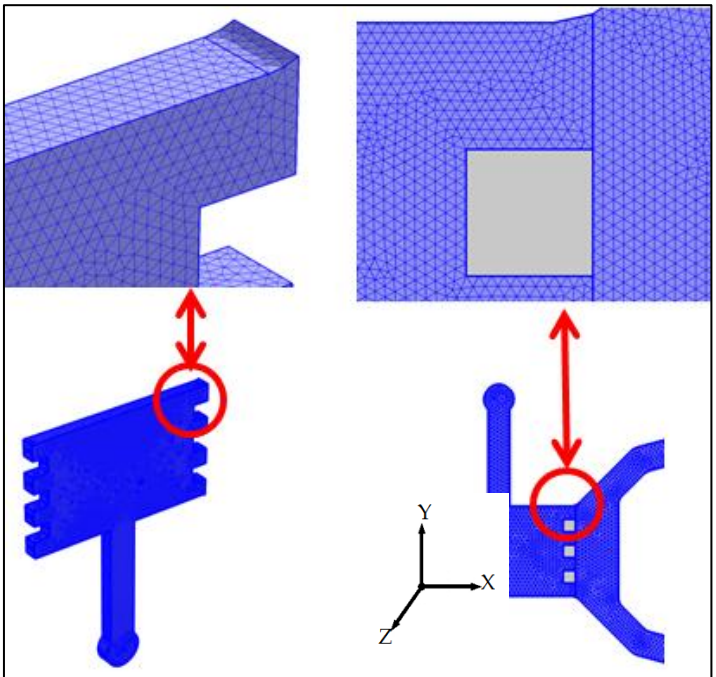

Fig. 13: Tetrahedral (left) and Triangular (right) mesh grid setup used for performing COMSOL simulations. Each mesh used in the simulations contained approximately 250,000 elements.

model setup, simulations over any time range could be conducted. COMSOL uses Fick's Law to determine the concentration gradient over time i.e. $t_{initial}$ to t_{max}. For these simulations, step size for t was set to 60 sec. T_{max} varied from one simulation to the next, since some conditions reached steady state in just a couple hours where some took a couple days or longer to reach steady state conditions. The partial differential equations used for determining the gradient concentrations are:

Equation 2: $$\frac{\partial \phi}{\partial t} = \nabla \cdot (-D \nabla \phi)$$

Φ = concentration in mol/m^3
D = diffusion coefficient in m^2/sec

The initial concentration in the center chamber was defined as $C=C_o$ for time 0 to ∞. Flux boundaries were defined by COMSOL as:

Equation 3: $$(-D \nabla \phi) \cdot \hat{n} = k (c - c_1)$$

K = mass transfer coefficient in m/sec
$(c-c_1)$ = concentration in bulk solution outside

Insulating / No Flux Boundaries:

Equation 4: $$(-D \nabla \phi) \cdot \hat{n} = 0$$

When plotting the 2D gradient profile curves, four curves were initially generated, corresponding to lines AB, CD, EF, & GH as shown in Fig. 14. The four points across the chamber were first examined to ensure that the diffusion of the molecule across the chamber did not exhibit any variation along the y-axis, and that the leading edge of the diffusing molecule moved across the chamber only along the x-axis. Multiple simulations showed insignificant differences between the gradient profiles at the four locations across the chamber, and so for the remaining simulations, profiles at line segment CD were created and analyzed. Similarly, a 3D profile gradient graph was built using the parametric extrusion data set in COMSOL and shows the concentration vs. chamber location vs. chamber depth of the diffusing molecule. As before, these simulations across the depth of the chamber were looked at for multiple gel / molecular weight combinations to show that flow patterns along the y- and z-axes did not exist i.e. flow was one dimensional across the x direction only. For each condition simulated, gradient profile graphs were created at multiple time points

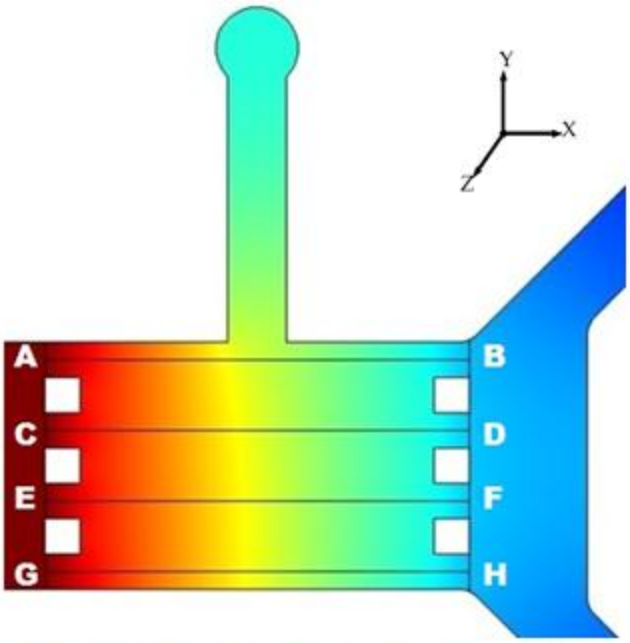

Fig. 14: Gradient profile locations across the gel chamber. Multiple locations were first looked at to ensure that the molecules were diffusing across the chamber in a straight line and did not exhibit random flow patterns (flow was one dimensional across x axis only)

during the simulations. From these graphs, steady state conditions could be determined for each combination of gel concentration / molecular weight / concentration simulated. Figure 15 shows the typical graph obtained from the simulations. In the case of these graphs, COMSOL inputs concentration values in terms of mol/m^3 where 0.001 mol/ m^3 is equal to 1 µM. Data gathered and analyzed from these graphs will be discussed in detail later.

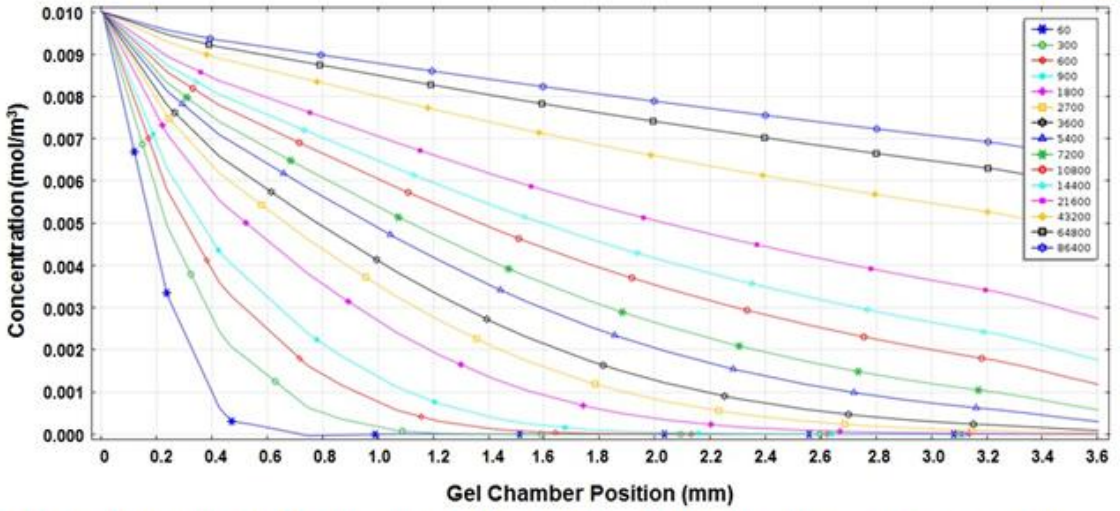

Fig 15: Typical gradient profile graph obtained from COMSOL simulations. The x axis shows the relative position across the gel chamber while the y axis is the concentration of the diffusing molecule. Time points depicted by the legend are in seconds.

3.4 Cortical neuron culture within devices

Primary rat cortical neurons (E-18) cultured in these devices were obtained from Neuromics Inc (Minneapolis, MN). The tissue section provided was digested in a solution of papain and enzymatic solution, as per protocols provided by the company. Once the cells were dissociated from the ECM, the digestate was filtered and cell population purified at a final concentration of 100,000 cells/mL. The neurons were mixed in 2 mg/ml collagen gel at a ratio of

1:10 (cell : gel) by volume, and seeded into the devices (n = 3 devices/ test condition) immediately after dissociation and cultured for 2 day in a humidified incubator at 5% CO_2 and 37 °C. The cell mixture was added in the left and right chambers of the device, and neurobasal medium containing B27 was added to the left and right media channels. For the experimental condition, commercially-obtained IGF-1 (Peprotech Inc.) was added at a concentration of 10 μg/mL concentration in the middle chamber. In this fashion, a gradient of growth factor was generated across both the left and right chambers. The medium was changed at regular intervals to maintain chemogradient at all times. The control devices which received no IGF-1 were cultured in the same procedure as with test cases.

3.5 Characterization of neurite outgrowth and turning

Phase-contrast and fluorescence microscopy were used to characterize neurite distribution and quantify neurite turning in 3D collagen gels within the devices. Images were acquired with a Zeiss Axiovert A1 florescence microscope equipped with a Hamamatsu camera and image acquisition software. Neurite staining was performed after fixation with 2% PFA (30 min). The fixed samples were rinsed thrice with 1X phosphate buffered saline (PBS), treated with 0.1 % Triton-X (5 min), rinsed with 1X PBS twice followed by the infusion of Alexa Fluor 488® phalloidin (Life Technologies) for F-actin (30 min) and a final wash step with 1X PBS. The phalloidin stains both axons and dendrites within the 3D scaffold. The last 100 μm segment along the length of each neurite leading to the

growth cone was traced with NeuronJ, a plugin for the ImageJ program that allows the user to trace and quantify lengths and angles of elongated image structures, and the angle this segment makes with the horizontal line (0°) was measured. For example, for the cells seeded in right chamber of the device, among the four quadrants, values in Q1 (135° to 225°) reflect growth towards guidance cue and in Q3 (45° to 315°) reflect turning away from the guidance cue. The number of neurites in quadrants 1 and 3 were counted for devices cultured under similar conditions, and the statistical significance values between test cases and control cultures (with no guidance cues) were computed using Mann-Whitney test by averaging the data from all the devices under each experimental condition. The neurite outgrowth and turning data obtained at a specific location within the device was correlated to the concentration and steepness of gradient cue at that location. It is important to note that while the neurites were able to grow in all three dimensions, imaging was only possible looking from the top down (one plane of view across the x and y axis only). Due to this, neurite outgrowth could potentially be longer than the NeuronJ software calculates since the z component of the total length is not accounted for.

CHAPTER IV

RESULTS & DISCUSSION

In this chapter we looked at the calculations for the diffusion coefficients of various molecular weight molecules in collagen and matrigel at various concentrations using the Stokes-Einstein equation and compare the results to known experimental data. The bulk of the chapter looks at the results of the COMSOL simulations conducted for both type-I collagen gel and matrigel. Initially, flow patterns were simulated across the chamber both in x-axis (lengthwise) and across the depth of the chamber (z-axis). Next, the effects of varying the concentration of the diffusing molecule were analyzed on the formation of the gradient and the steady-state conditions. We continue by examining the theoretical diffusion times for each case, the steady-state conditions and times for each molecular weight / gel combination, and the average concentration & steepness in various sections across the gel chamber at steady-state. We conclude by correlating our findings with cortical neuron culture experiments, to visualize and quantify the effects of gradient on neurite outgrowth and turning.

4.1 Diffusion coefficients in collagen & matrigel

The diffusion coefficient, D, indicates the mobility of a substance that moves from one area to another due to a concentration difference between the two areas. This diffusion coefficient is unique to a given diffusing molecule and medium (matrix or gel) in which it is diffusing [53]. Thus, values of D will be relatively large when the chemical species is diffusing through a gas, and will get smaller as the density of the matrix increases. To begin, we calculated diffusion coefficients to feed into the COMSOL simulations using the Stokes-Einstein equation:

$$D = \frac{kT}{6\pi\eta R}$$

Where k is Boltzmann's Constant (1.38065×10^{-23} J/K), T is the absolute temperature at which the molecule is in diffusion (in the case of these experiments room temperature), η is the viscosity of the gel that the molecule is diffusing through, and R is the Stokes radius of the diffusing molecule. This equation gives a starting point to feed into the models. Obviously, changes in the viscosity of the gel or temperature differences can greatly affect these coefficients. The calculations for each case and the resulting diffusion coefficients are shown in Table 2.

When compared to diffusion coefficients obtained by experimentation from published literature, we find broad agreement in these results to that calculated from the Stokes-Einstein equation. It is important to remember that changes in

viscosity and temperature can affect the value obtained for the diffusion coefficient, so the values obtained from simulations versus actual

Diffusion Coefficient Calculations - Stokes Einstein Equation

Assume Room Temperature of 23°C = 296.15 K

	Dextran MW (kDa)	Dextran Stokes Radius, R (m)	Matrix Viscosity, η ($kg\ m^{-1}\ s^{-1}$)	Boltzmann Constant, k ($J\ K^{-1}$)	Absolute Temp, T (K)	Stokes - Einstein Equation	Diffusion Coefficient, D ($m^2\ s^{-1}$)
0 mg/mL Collagen (Water)	1	7.50×10^{-10}	0.001	1.38065×10^{-23}	298.15	$D = \frac{kT}{6\pi\eta R}$	2.91×10^{-10}
	10	2.36×10^{-9}					9.25×10^{-11}
	100	6.90×10^{-9}					3.16×10^{-11}
	1,000	1.99×10^{-8}					1.10×10^{-11}
1 mg/mL Collagen	1	7.5×10^{-10}	0.0037	1.38065×10^{-23}	298.15	$D = \frac{kT}{6\pi\eta R}$	7.87×10^{-11}
	10	2.36×10^{-9}					2.50×10^{-11}
	100	6.90×10^{-9}					8.55×10^{-12}
	1,000	1.99×10^{-8}					2.97×10^{-12}
2 mg/mL Collagen	1	7.5×10^{-10}	0.0104	1.38065×10^{-23}	298.15	$D = \frac{kT}{6\pi\eta R}$	2.80×10^{-11}
	10	2.36×10^{-9}					8.90×10^{-12}
	100	6.90×10^{-9}					3.04×10^{-12}
	1,000	1.99×10^{-8}					1.06×10^{-12}
3 mg/mL Collagen	1	7.5×10^{-10}	0.02592	1.38065×10^{-23}	298.15	$D = \frac{kT}{6\pi\eta R}$	1.12×10^{-11}
	10	2.36×10^{-9}					3.57×10^{-12}
	100	6.90×10^{-9}					1.22×10^{-12}
	1,000	1.99×10^{-8}					4.23×10^{-13}
Matrigel (As Received)	1	7.5×10^{-10}	0.0150	1.38065×10^{-23}	298.15	$D = \frac{kT}{6\pi\eta R}$	1.94×10^{-11}
	10	2.36×10^{-9}					6.17×10^{-12}
	100	6.90×10^{-9}					2.11×10^{-12}
	1,000	1.99×10^{-8}					7.32×10^{-13}

Table I: Calculation of diffusion coefficients for 1, 10, 100, and 1000 kDa molecules in various concentrations of Matrigel and Collagen gel. The Stokes-Einstein equation used for the calculations (shown in the table) takes into account the viscosity of the gel and the size of the diffusing molecule which primarily determines how fast or slow a molecule will diffuse through the matrix.

experimentation may slightly differ. For example, in a second study conducted by Guarnieri et. al., 50 kDa dextran was allowed to diffuse through 1.2 mg/mL collagen gel. Calculation of the diffusion coefficient of the dextran was determined by FRAP technique (Fluorescence Recovery after Photobleaching) with the resulting images analyzed in Matlab [55]. This experiment gave a diffusion coefficient of 9.65×10^{-7} cm^2/sec (9.65×10^{-11} m^2/sec). Again plugging the necessary values into the Stokes-Einstein Equations gives a similar result of

8.21×10^{-7} cm^2/sec. Thus it can be seen that the Stokes-Einstein equation gives a good approximation for the diffusion coefficient for various molecules and substrates when the radius of the diffusing molecule and viscosity of the matrix is known. Due to the accuracy of the equation compared to experimental results, the diffusion coefficients determined from the Stokes-Einstein equation were used for each of the simulations conducted.

4.2 COMSOL simulations & steady state conditions

The COMSOL Multiphysics software is a finite element analysis, solver, and simulation package designed to analyze various physics and engineering applications such as diffusion, heat transfer, fatigue, corrosion, etc. This package allows us to input the Solidworks design of the microfluidic device and run diffusion simulations when conditions such as flux and no flux boundaries, diffusion coefficients, and concentration are known. This software allowed for the simulation of all 20 gel / molecular weight combinations and initial diffusing molecule concentrations of 0.1, 1.0, and 10.0 µM. Using this, steady state conditions, average concentrations at various locations across the chamber, and steepness could be determined. Simulations in x and y planes (2D) were run for all conditions, while simulations in all 3 axes (3D) were run on select conditions to analyze the gradient generation along z-axis in the gel chambers.

4.2.1 Random vs. straight line gradient progression

The first sets of simulations were run to determine the shape of the chemical gradient. This was examined using both 2D simulations across the 3.6

mm length of the gel chambers, as well as 3D simulations that looked at diffusion across the 150 µm height of the chamber.

The 2D simulations examined the gradient profiles at four locations across the gel chamber (refer to figure 14). Analysis of the graphs and data obtained from the simulations showed no significant difference in the gradient profiles between any of the four simulated locations. Average steady-state concentration taken at all four locations showed less than a 1% difference. This shows that the resulting gradient profile does not vary across the y direction. For consistency, the remaining simulations were run and gradient profiles generated using a slice corresponding to line CD in Figure 14 (Materials & Methods chapter). Appendix C shows the gradient profile graphs from each of the four segments across the gel chamber.

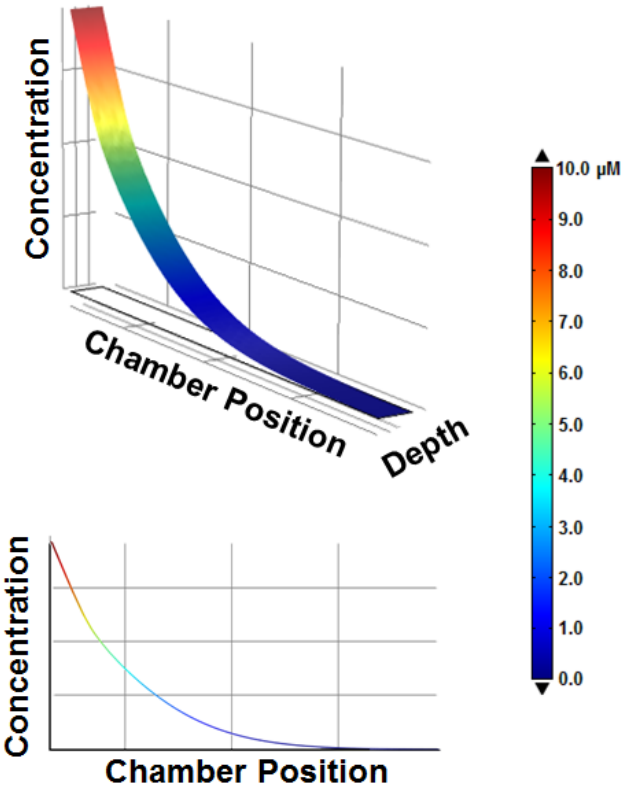

Fig. 16: Top: The three dimensional gradient profile across the 150 µM chamber depth for the case of 10 µM, 10 kDa, 1 mg/mL Collagen shown at the steady state time of 6 hours. If the diffusion across the depth of the chamber were exhibiting any laminar flow patterns, a curve with a more rounded center section would be seen and not a straight line graph as shown in the x-y view in the bottom figure. This held true for all 3D simulations conducted across the gel chamber depth.

Three dimensional simulations were also run to look at the progression of the gradient across the height (z-axis) of the chamber. Results similar to that

observed in the 2D simulations were seen across the 150 µm depth of the gel chambers. The gradient appeared to progress across the gel chamber only in the x direction and did not vary over the z axis or depth of the chamber. Figure 16 shows the 3D gradient profile across the 150 µm height of the gel chamber for the case of a 10 kDa molecule in 1 mg/mL collagen gel. If random flow of the diffusing molecule was seen, a more three dimensional curve would be seen and not the diffusion profile as seen in the bottom image of figure 16. Similar simulations conducted for a 10 kDa molecule in 2 mg/mL and 3 mg/mL collagen showed that the gel concentration had no effect on the diffusion patterns across the z-axis of the chambers. Gradient profiles were generated at two locations across the height of the gel chamber and showed less than a 0.01 µM difference in steady-state concentration in the case of the 10 kDa, 2 mg/mL collagen. Similar results were seen in the 1 mg/mL and 3 mg/mL collagen simulations.

4.2.2 Effect of varying the diffusing molecule concentration

To fully understand the diffusion across a range of conditions through the microfluidic device, 2D simulations of the gel / molecular weight combinations discussed above were run while varying only the initial concentration from 0.1 -10 µM. The hypothesis was that with a lower concentration, the time needed to reach steady state would be increased. The COMSOL simulations, however, showed that the time for the gradient to reach steady-state conditions was nearly identical for all the three concentrations studied. Rather, it was observed that the overall concentration at steady-state at any location was typically reduced by a

factor of ten, from the 10 µM to the 1 µM and by a factor of ten again from the 1 µM to 0.1 µM. Table 3 and the data in Appendix C shows this held true for all diffusing molecule / gel combinations.

4.2.3 Calculation of steady-state conditions

Steady-state diffusion takes place at a constant rate, which means that over time, a given number of molecules crossing a particular point are constant. In these simulations, we attempt to find the time where the rate of diffusion becomes constant. To determine the steady state time, we calculated the slope of the diffusion curves at successive time points. Appendix A and Table 3 below shows the data used to calculate the steady state times.

For consistency between all calculations, concentration data was taken at the 0.8 mm and 1.0 mm locations (see Figure 15) and the resulting slopes calculated. When the slope between the 0.8 mm and 1.0 mm chamber locations became steady from one time point to the next, we declared that the gradient had reached steady state. In table 3, a sample of the calculations for 1 mg/mL collagen and a 10 kDa diffusing molecule is shown. It can be seen that after the 12 h time point, the slope of the gradient profile becomes constant. In this case the time needed to reach steady-state was set at 12 h. Similar calculations were done for all remaining gel and diffusing molecule combinations.

A wide range of times to reach steady-state was found, varying from as little as 0.75 h in the case of 1 kDa, 0 mg/mL collagen (water) up to 108 h for a 1,000 kDa molecule diffusing through 3 mg/mL collagen. Figures 18, 19, and 20

Determining Steady State Time from COMSOL Gradient Profiles

	Time Value (hrs)	Slope Between 0.8 & 1 mm				
		X_1	X_2	Y_1	Y_2	Slope
10 µM 100 kDa 1 mg/mL Collagen	6	0.8	1.0	0.0015	0.0008	-0.0035
	12	0.8	1.0	0.0028	0.0020	-0.0040
	18	0.8	1.0	0.0036	0.0028	-0.0040
	24	0.8	1.0	0.0041	0.0033	-0.0040
	30	0.8	1.0	0.0044	0.0036	-0.0040
1 µM 100 kDa 1 mg/mL Collagen	6	0.8	1.0	0.00015	0.00008	-0.00035
	12	0.8	1.0	0.00028	0.00020	-0.00040
	18	0.8	1.0	0.00036	0.00028	-0.00040
	24	0.8	1.0	0.00041	0.00033	-0.00040
	30	0.8	1.0	0.00044	0.00036	-0.00040
0.1 µM 100 kDa 1 mg/mL Collagen	6	0.8	1.0	0.000015	0.000008	-0.000035
	12	0.8	1.0	0.000028	0.000020	-0.000040
	18	0.8	1.0	0.000036	0.000028	-0.000040
	24	0.8	1.0	0.000041	0.000033	-0.000040
	30	0.8	1.0	0.000044	0.000036	-0.000040

Table II: Constant slope between successive time points seen after 12 hours in the 10, 1, and 0.1 µM simulations. Points prior to the 6 hour mark were removed to condense the chart. In this case, steady state time was determined to be approximately 12 hours. No difference was seen in steady state time between the three concentrations examined. As seen by the Y-values, steady state concentration dropped by a factor of 10 from one concentration to the next. X_1 and X_2 refers to the x location across the chamber while Y_1 and Y_2 are the concentrations seen at those locations.

show the resulting diffusion profile curves and snapshot images of the diffusion across the gel chamber for a 10 kDa molecule at 10 µM concentration diffusing through 1, 2 or 3 mg/ml collagen. Table 4 shows the steady-state times for each gel and diffusing molecule combination. Again, since the simulations showed virtually no difference in the steady-state times when the diffusing molecule concentration was changed, these steady state times also apply to the 1.0 µM and 0.1 µM concentrations.

Using this steady-state data, we were able to construct a 3D plot of the times required to reach steady-state, and perform a non-linear regression analysis that would enable predictability of the steady-state time, if the particular gel concentration and molecular weight of the diffusing molecule were known. Figure 17 shows the 3D graph and resulting equation for steady-state times. Statistical significance (*p*-values) was calculated for each of the coefficients as well as for the overall fit of the regression. In each case, the *p*-value obtained

showed that there was greater than a 99% chance that the relationship was real and did not emerge randomly. For instance, if the case of 1mg/mL collagen with a diffusing molecule molecular weight of 1,000 kDa was substituted into the formula, steady-state time would be calculated as 25.19 h which agrees well with the simulated steady state time of 24 h as shown in Table III.

	10 µM Dextran Concentration - Steady State Times			
	1 kDa	10 kDa	100 kDa	1,000 kDa
0 mg/mL	0.75	2	4	9
1 mg/mL	2	6	12	24
2 mg/mL	4	12	24	48
3 mg/mL	9	30	60	108
Matrigel	6	18	36	60

Table III: Time required to reach steady state diffusion for each gel & diffusing molecule molecular weight combination.

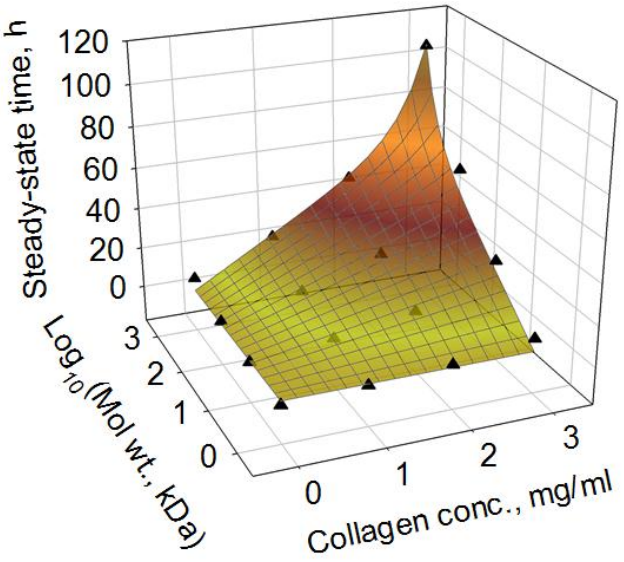

$z = a + b*x*y + c*\exp(x*y)$

a 2.6799 ($p < 0.0001$)
b 7.4726 ($p < 0.0001$)
c 0.0047 ($p = 0.0003$)

Overall regression fit: $p < 0.0001$

Fig 17: Regression analysis for determining steady state times when the collagen concentration and molecular weight of the diffusing molecule are known.

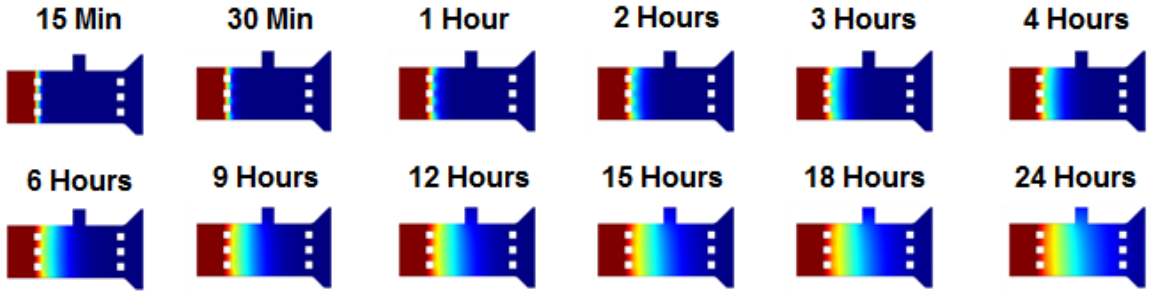

Fig 18: Left: Time lapse images of gradient progression across the microfluidic chamber. Below: Gradient profile curves at various time points across the device.

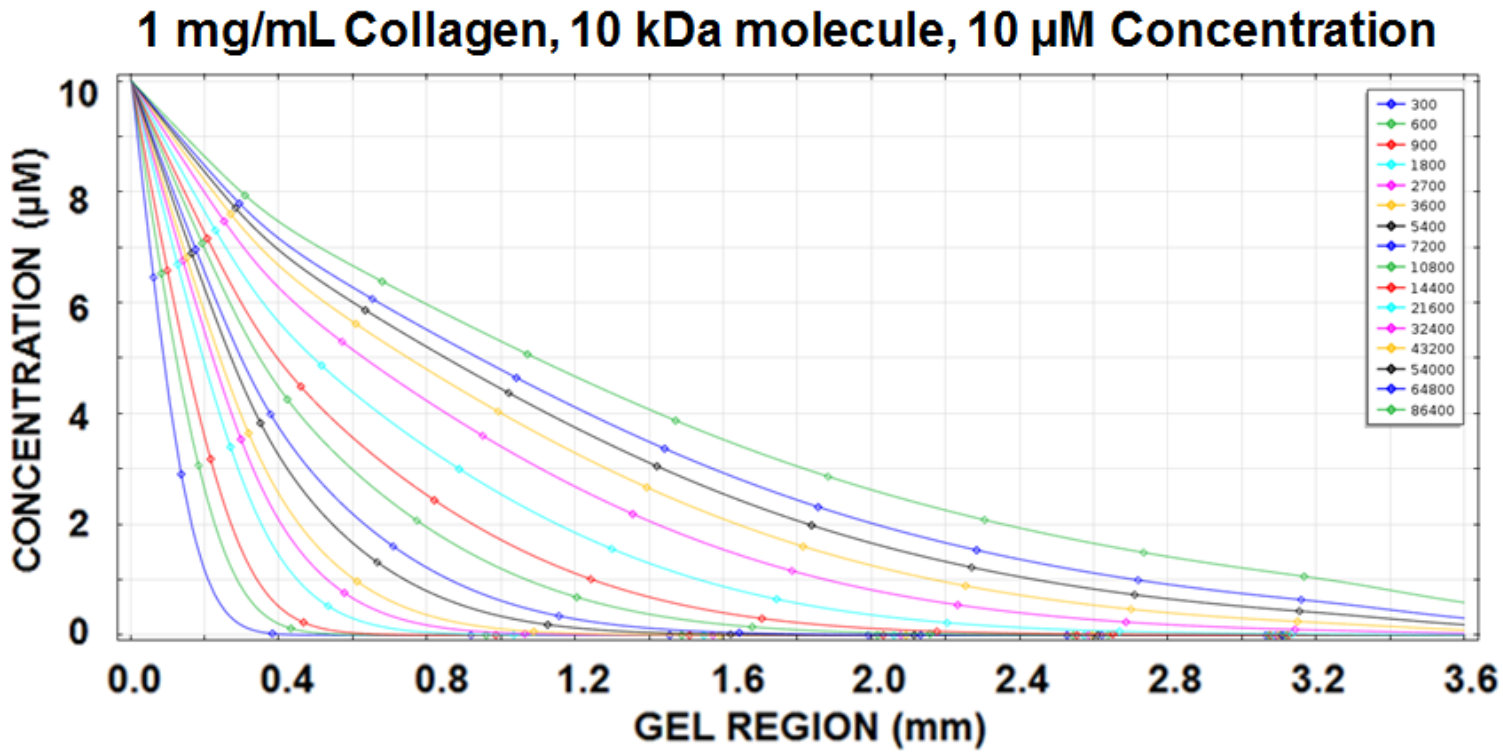

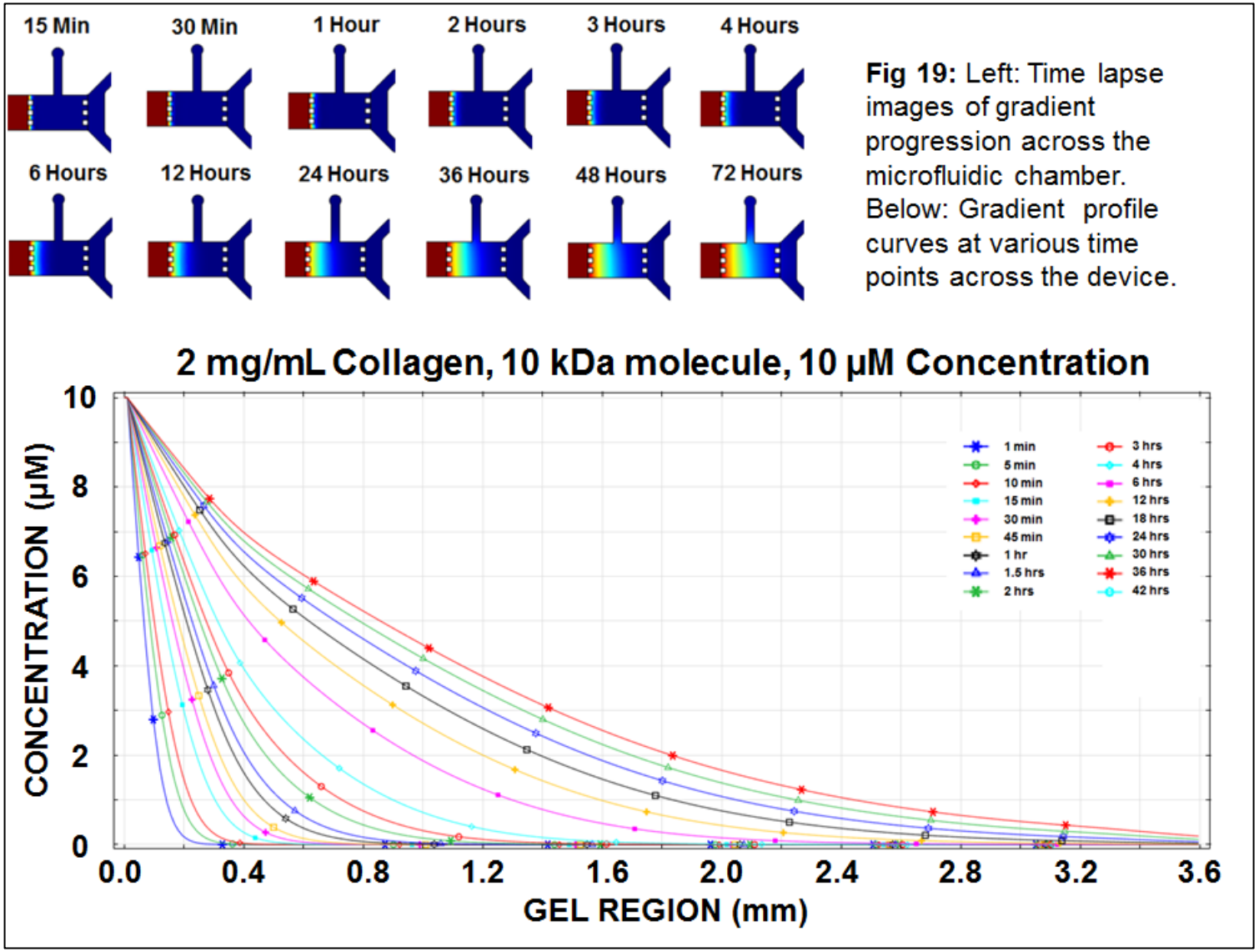

Fig 19: Left: Time lapse images of gradient progression across the microfluidic chamber. Below: Gradient profile curves at various time points across the device.

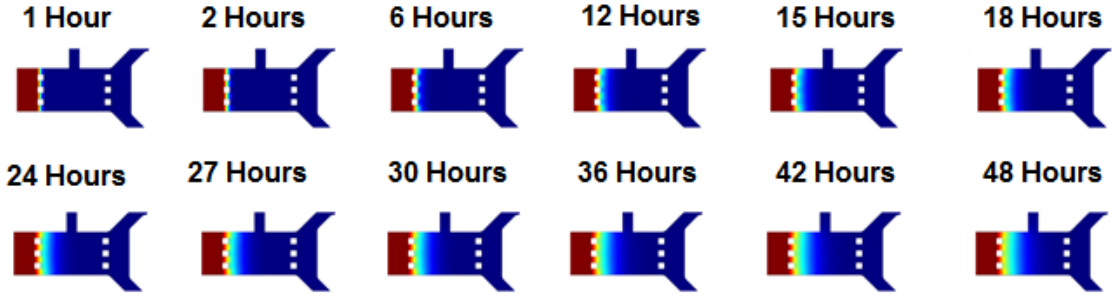

Fig 20: Left: Time lapse images of gradient progression across the microfluidic chamber. Below: Gradient profile curves at various time points across the device.

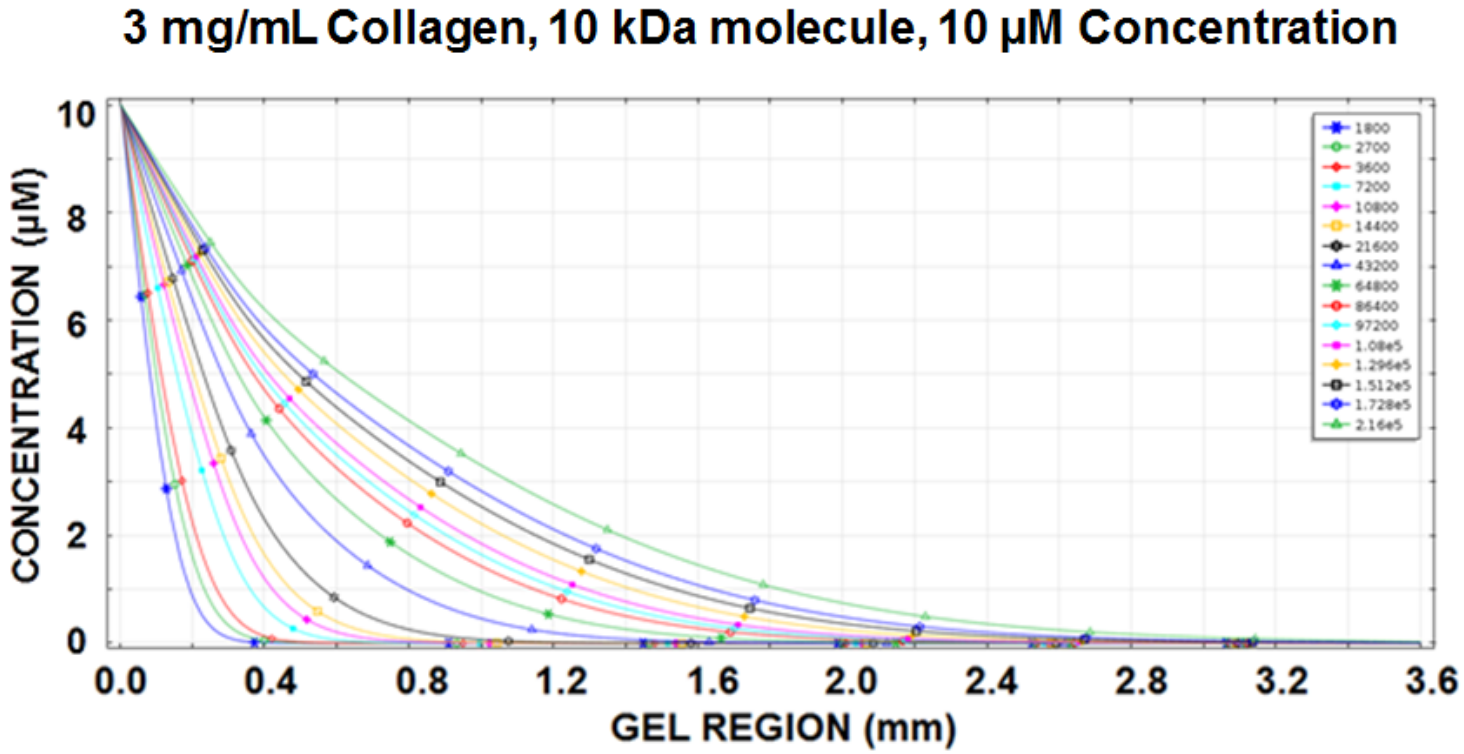

4.3 Calculation of theoretical diffusion time (τ) within microfluidic devices

The theoretical time (τ) for a molecule to diffuse across a known length L is approximated by $C(L^2/2D)$ for one dimensional diffusion or $C(L^2/4D)$, where D is the diffusion coefficient. In this section, we used the simulation data and graphs to calculate the constant C for diffusion through collagen and matrigel, and look at the accuracy of this formula for each of the steady-state conditions examined. This coefficient should be close to 1. Since this was to be compared to simulation data and diffusion was allowed to occur in the x and y directions, $L^2/4D$ was used for these calculations.

To calculate the constant for collagen gel, $C_{collagen}$, we used the simulation data from each of the four gel concentrations and all four diffusing molecule molecular weights. To determine this, the diffusion time at a specific location in the chamber was used while looking for a concentration increase of 10^{-6} M. For consistency, we found the time required for a molecule to diffuse across the entire 3.6 mm gel chamber. This time, in hours, was found for all 16 molecular weight / collagen gel concentrations. Next, we calculated $(L^2/4D)/3600$ to find the diffusion time for each gel/molecular weight combination, where L was 3.6 mm and D was the respective diffusion coefficient. Since the time calculated from the equation must be proportional to the time obtained from the simulations, the time calculated was divided by the diffusion time seen from the simulations. The resulting value is the $C_{collagen}$ coefficient. This coefficient was determined for all 16 collagen gel / molecular weight combinations and averaged to get one formula

for collagen. From this, we found this coefficient to be approximately 0.8768 for collagen for a final formula of $0.8768L^2/D$.

Matrigel was also examined using the same procedure in the "as-received" concentration. The coefficient for Matrigel was determined to be 0.7495. However, since only four points were used to calculate this coefficient, additional data points at other concentrations of Matrigel could be used to get a more accurate coefficient. The relationship of the simulated versus theoretical diffusion time can be seen in figure 21 below.

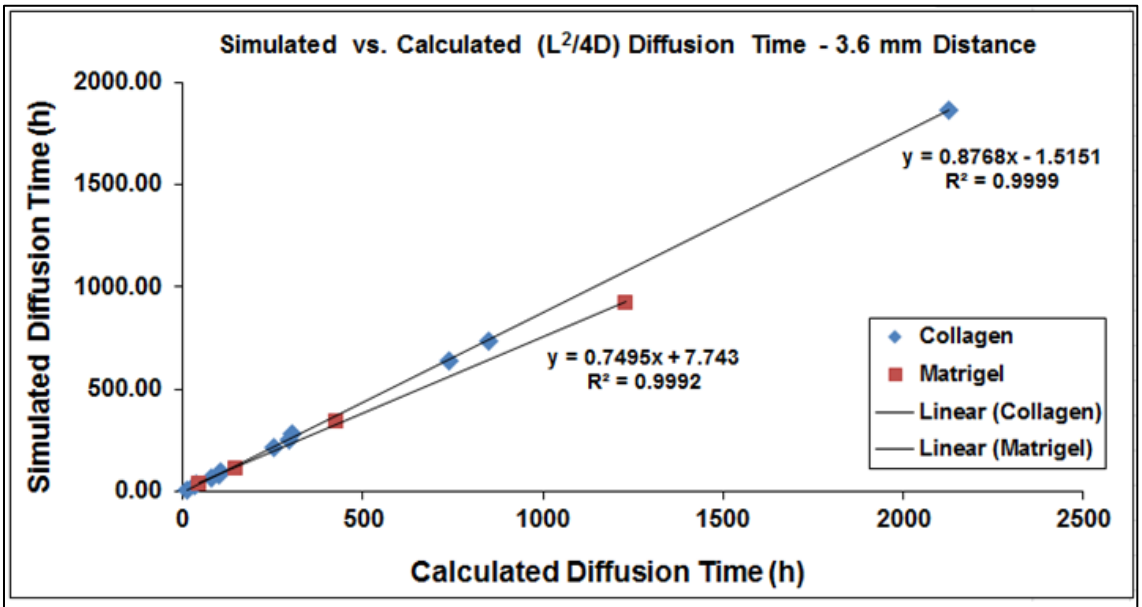

Fig. 21: Graph of observed vs. calculated diffusion times and the resulting equations for collagen and Matrigel. The observed times are the time points when an increase in concentration is first noticed at the 3.6 mm distance across the gel chamber. The high R^2 value indicates good correlation between the values seen in the COMSOL simulations and the theoretical, calculated times.

4.4 Calculation of average concentration and steepness

The steepness of a gradient is determined by the percentage difference in concentration of a particular diffusing molecule between two different locations. For example, physiologically this could be looked at as the difference in ion

concentrations inside versus outside the cell where the difference is measured over a distance equivalent to the thickness of a cell membrane. Since the microfluidic device used in these experiments was originally designed for neurite outgrowth and turning studies, the steepness across a distance equal to the size of an axonal growth cone was considered (~10 µm). The major hypothesis in developmental neuroscience is that axons are directed to specific targets in the body by sensing and responding to particular chemical gradients. The growth cones of neurons have been shown to respond to chemical gradients as low as 0.1%, with gradients of 1% or higher needed to induce substantial guidance [56]. It is hypothesized that since neurons are bombarded by many chemical signals in the body, they adapt their morphology and guidance depending on the chemical gradients seen at the growth cone [10].

From the simulation results we obtained, average concentration and steepness values were determined across the gel chambers. This was calculated at the steady-state time point for each simulation run. The gel chamber was divided into six regions, all 0.6 mm in width as shown in Figure 22. Average concentration and steepness were determined in each of the six regions and are shown for the case

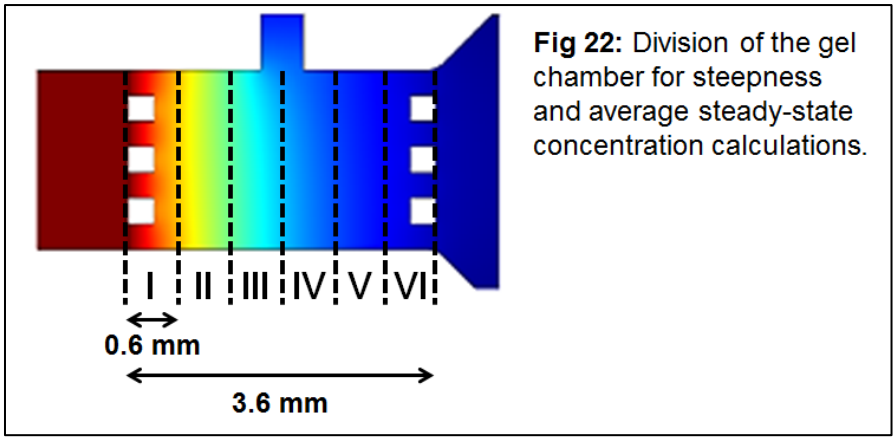

Fig 22: Division of the gel chamber for steepness and average steady-state concentration calculations.

of 2 mg/mL collagen in Figures 23 and 24, while the remaining cases are shown in the Appendix.

From the resulting data, steepness across a 10 µm distance (approximate width of a growth cone) was calculated. Literature shows that changes in concentration as small as 0.1% can be detected by the growth cone to induce changes in neurite outgrowth and directionality [56]. Simulation data for the 2 mg/mL collagen shows steepness values in the range of 0.67% (zone-I) in the case of a 10 kDa molecule in 2 mg/mL collagen and this steepness drops off as the growth cone progresses across the chamber. With steepness values in this range, some degree of neurite guidance should be observed and recorded.

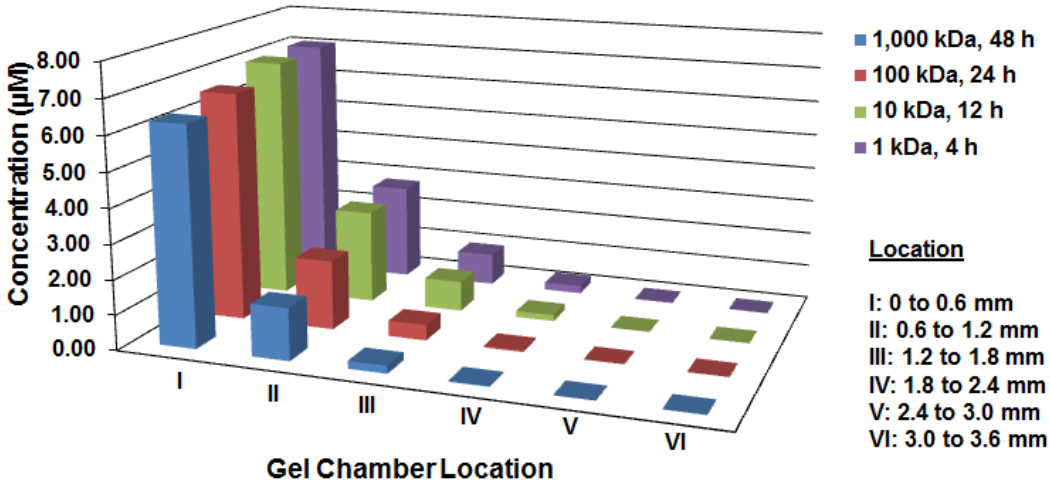

Fig. 23: Average steady state concentration in 2 mg/mL collagen at 0.6 mm increments across the gel chamber.

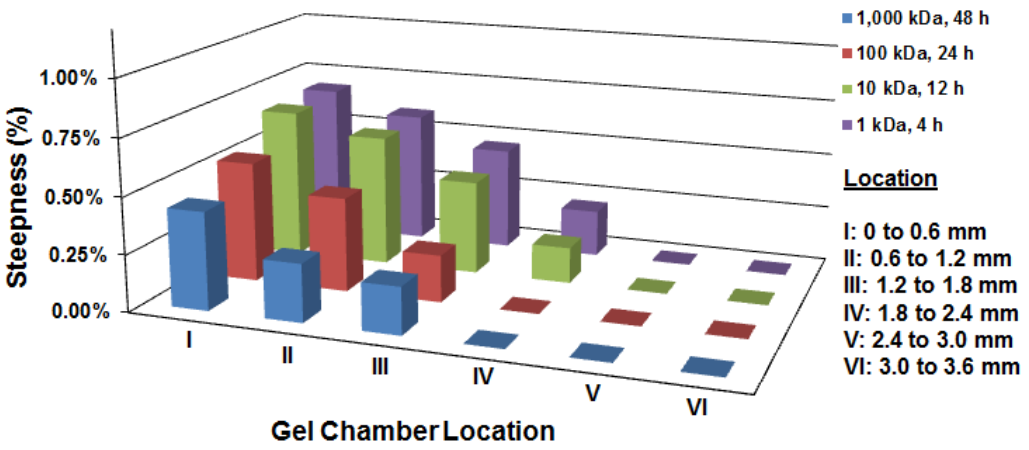

Fig. 24: Steepness at steady state across a 10μm distance in 2 mg/mL collagen at 0.6 mm increments across the gel chamber.

4.5 Characterization of neurite outgrowth & turning

IGF-I (insulin like growth factor) is a protein similar in function and structure to insulin and belongs to a family of proteins involved in mediating growth and development. IGF-1 has been shown to play an important role in promoting axonal growth from the dorsal root ganglion while also significantly enhancing neurite initiation and branching [57]. Outgrowth and guidance of neurons provides a potential therapy option to combat neurodegenerative diseases such as Alzheimer's and Parkinson's disease. Many new studies and therapies are focused on molecules that affect the differentiation, outgrowth, and guidance of neurites. In this experiment we attempt to characterize the effect of an IGF-1 gradient on neurite outgrowth and turning when compared to control samples.

4.5.1 Neurite outgrowth

To examine the effects of an IGF-I gradient on neurite outgrowth, an initial concentration of 10 µg/mL was added to the center chamber of the device (green region, Figure 11) and allowed to diffuse into the left and right chambers. Media containing no growth factors was added in the media channels on both the ends of the device (Figure 11, blue regions). Cortical neuronal cells mixed within 2 mg/ml collagen-1 gel were seeded in the left and right gel chambers (pink regions, Figure 11). Control devices received no IGF-1. In this setup, IGF-1 diffuses from the central chamber to the side channels, across the 3D scaffolds, forming a gradient, to which the cells are expected to sense and respond. Three devices, for a total of 6 cell chambers, were seeded for each experimental condition. All the devices were cultured for 48 h, fixed, stained, imaged and characterized. Figures 25, 26, and 27 shows representative fluorescence images as well as average neurite growth in zones I, III, and VI respectively, while fluorescence images of the control samples are shown for reference in the appendix. We chose these three zones within the gel region, based on their distinct average concentrations and gradient steepness (Figures 23 and 24). As shown in the graphs, higher average concentrations and steepness gradient of IGF-I promoted significantly more neurite outgrowth than seen in the cells exposed to lower concentrations IGF-I and the controls. Zone I, the highest concentration of IGF-1, showed the greatest increase in neurite outgrowth when compared to the controls in that zone. Here we saw an average of 90 µm of outgrowth compared to only approximately 20 µm in the control, a 4.5 fold

increase. Similar results were seen in zones III and VI although the increase in outgrowth was smaller due to the lower IGF-I concentration, as we all as the gradient steepness. In zone III, we observed a 2.5 fold increase in neurite outgrowth with averages of 37 μm for neurites exposed to the chemical gradient and 15 μm for those in the control devices. This effect continued to level off as the concentration decreased further towards zone VI. In this zone, only a 1.6 fold increase was seen with averages of 20 and 12 μm for the IGF-I and control samples.

Neurite length distribution analysis revealed that in the presence of IGF-1 gradient, a majority of the neurites (~ 80%) in zone-1 exhibited outgrowth within 50-130 μm range. However, in zone-III, ~ 78% of the cortical neurons showed outgrowth between the 11-50 μm range. Interestingly, 85% of neurites were between 0-30 μm range in zone-VI, suggesting the strong influence of gradient concentration as well as the steepness in regulating neurite outgrowth and turning within these zones. However, from this experimental setup and quantification, it cannot be determined whether the concentration of the IGF-I or the steepness of the chemical gradient has a greater effect on the neurite outgrowth.

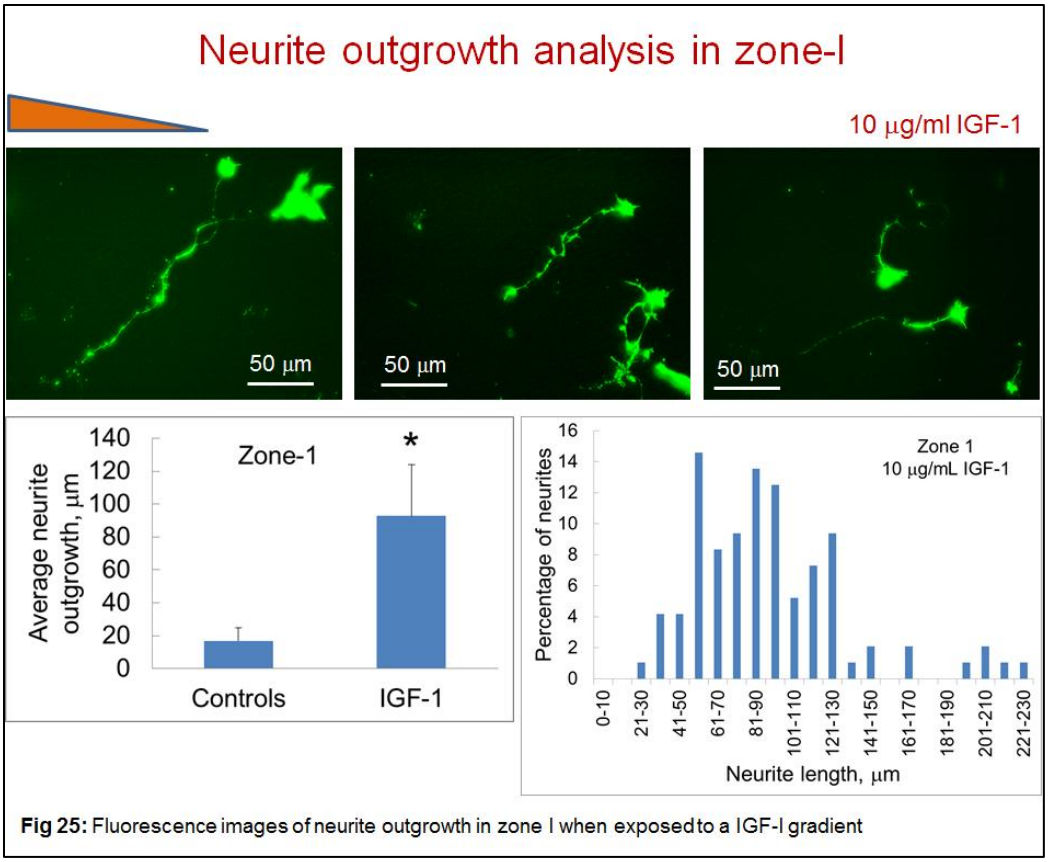

Fig 25: Fluorescence images of neurite outgrowth in zone I when exposed to a IGF-I gradient

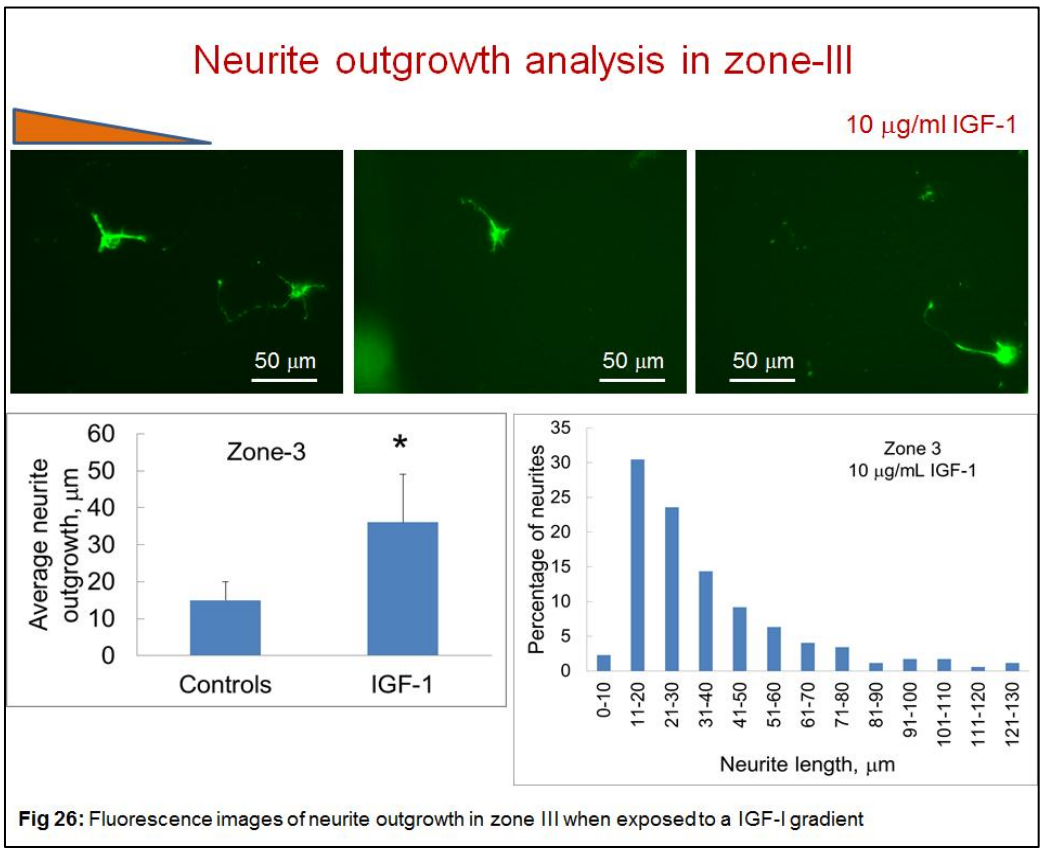

Fig 26: Fluorescence images of neurite outgrowth in zone III when exposed to a IGF-I gradient

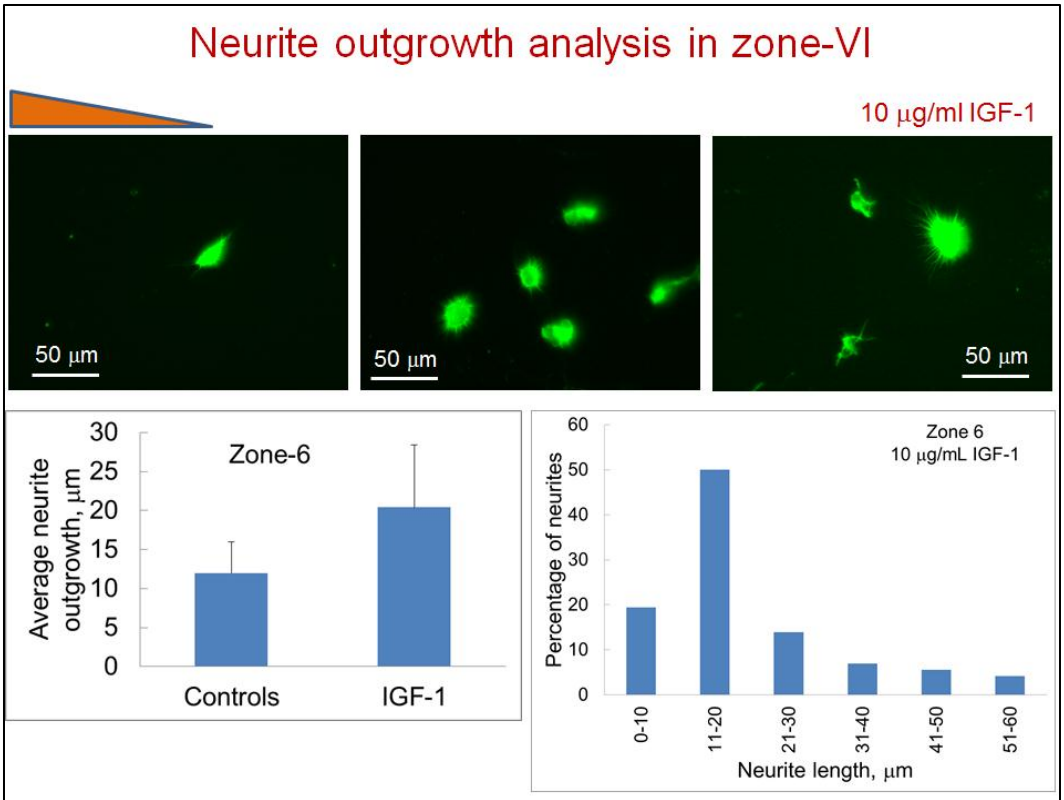

Fig 27: Fluorescence images of neurite outgrowth in zone VI when exposed to a IGF-I gradient

4.5.2 Neurite turning

In addition to characterizing the outgrowth of neurites in the presence of an IGF-I gradient, we also evaluated the role of IGF-I on neurite turning and guidance in microfluidic devices *in vitro*. When neurons were cultured in control devices with no influence of any guidance cues, outgrowth and turning appeared to be random as shown in Figure 28. Thus, in control cultures, outgrowth in Q1 and Q3 were nearly equal in zone I, with roughly 24% turning towards Q1 and 25% of neurites turning towards Q3. Similar outcome was seen in each of the three zones for the control samples, where no significant difference in neurite turning was observed between Q1 and Q3.This data in was in agreement with

our earlier devices as well, where neurite outgrowth was more random in control cultures, as expected.

When the neurons were exposed to a gradient of IGF-I, the outgrowth direction was more specific. In the presence of IGF-I, the majority of neurons from each of the three zones were attracted towards the gradient. Zone I, which had the highest concentration and steepness of the growth factor, showed ~53% of neurites turning towards the gradient, while less than 5% were turned away (Q1 vs. Q3, n = 96; $p < 0.0001$). Similar results were observed in zones III and VI, although the percentage turning towards and away from the gradient began to equalize with decreasing concentration. Zone III, where the average steady state concentration was only 12% of that seen in zone I, showed a fairly equal percentage of neurites turning towards and away from the gradient (27.6% in Q1, 22% in Q3; n = 174). In zone VI, 27.8% of the neurites showed movement towards the gradient and 17% away (n = 72). At steady state, the average concentration in zone VI approaches 0 µM. At this concentration, the turning would be more random as seen in the control samples. A larger sample size would be needed to see if the percentage of neurites turning towards and away from the gradient would equalize as expected from the controls. Table 6 summarizes the results seen from the IGF-I induced growth and turning compared to the controls. With decreasing average steady-state concentration and gradient steepness across the chamber, a dramatic decrease in the neurite outgrowth and turning towards the IGF-1 gradient was observed. Such stark

decreases were not noted in control cultures, where no IGF-1 gradient was introduced.

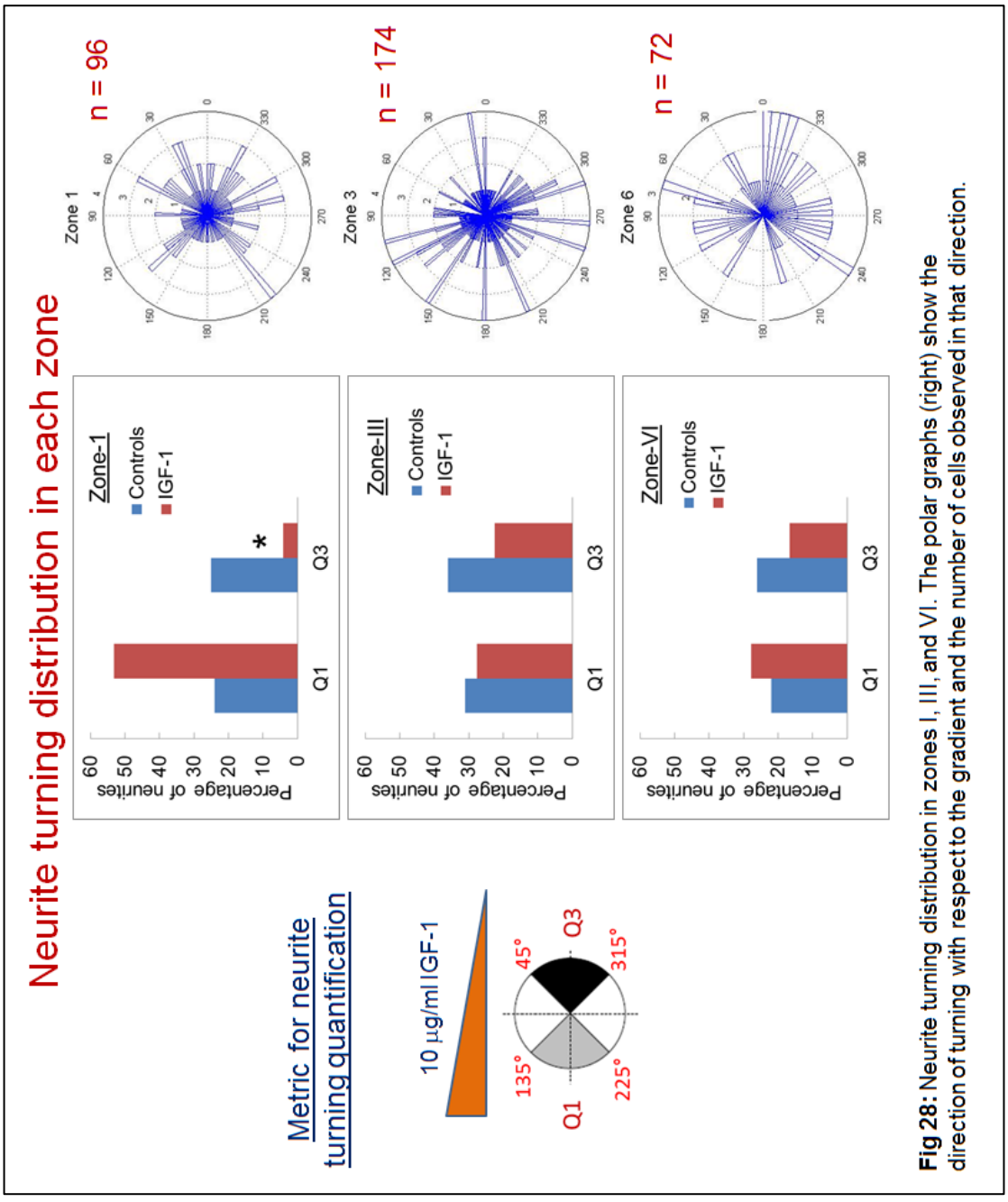

Fig 28: Neurite turning distribution in zones I, III, and VI. The polar graphs (right) show the direction of turning with respect to the gradient and the number of cells observed in that direction.

2 mg/ml collagen-1	10 μm IGF-1	~10 kDa molecule

Source	Parameter	Zone-1	Zone-3	Zone-6
Data from simulations	Average steady-state concentration across 10 μm distance	7 μM	0.88 μM	0 μM
	Average steepness at steady-state across 10 μm distance	0.67 %	0.42 %	0 %
Experimental observations (IGF-1 gradient)	Average neurite outgrowth	92 ± 31 μm	36 ± 13 μm	20 ± 7 μm
	% of neurites attracted towards chemogradient	53 %	27.6 %	27.8 %
Experimental observations (Controls)	Average neurite outgrowth	17 ± 8 μm	15 ± 5 μm	12 ± 4 μm
	% of neurites attracted towards chemogradient	24 %	31 %	22 %

Table V: Correlation between neurite outgrowth and chemogradient in each zone

CHAPTER V

CONCLUSIONS & RECOMMENDATIONS

5.1 Conclusions

In this study, a microfluidic device was designed and fabricated to quantify the spatio-temporal diffusion of solutes in 3D scaffolds. This device allows for simple fabrication and implementation to not only study molecular diffusion but also to be expanded to study biological applications such as neurite outgrowth and turning, cell migration and chemotaxis, among others. A combination of simulation data and actual fluorescent imaging was used to quantify and understand the diffusion across the device. Using this data, steady-state conditions such as time, average concentration and steepness could be determined and diffusion coefficients for various molecular weights in collagen and matrigel calculated and verified to give an idea of how cells would respond when placed in the device. The calculated diffusion coefficients seemed to agree well with what is currently published in literature while the concentrations and steepness observed across the gel chambers seems to provide an acceptable environment in which to further study neurite outgrowth and turning. Although no

imaging data was obtained to verify the steady-state conditions determined from simulation data (see recommendations for future work below), results from the neurite outgrowth and turning experiments provided promising results. While we were able to characterize the effects of an IGF-I gradient, a known guidance cue for neurite growth and turning, the flexibility of this device allows for the easy screening of other molecules that could potentially enhance neurite outgrowth or guidance. Such detailed analysis of gradient-induced concentration and steepness across a 3D scaffold within a microfluidic device has never been reported in literature. While other researchers have reported the effects of growth factors and their gradients on neurite outgrowth, the correlation between the gradient steepness and neurite response has never been elucidated earlier. We hypothesize that this device could also have potential applications in cancer cell biology, tissue engineering, regenerative medicine, stem cell differentiation and angiogenesis.

5.2 Recommendations for future work

Based on our understanding of this novel device, there are a few factors which merit further investigation to expand the scope of this research. The following are recommendations for future work that can add to or enhance the results obtained here.

1. While fluorescent imaging studies were attempted, no imaging was able to be completed. A few issues arose when attempting to load either the gels or the FITC-dextran into the microfluidic devices. In the first round of experiments, collagen gel was loaded into both the right

and left chambers while the center chamber remained empty. As the imaging was being conducted, the collagen started to pull away from the posts in the device and retract toward the center chamber, suggesting a potential pressure gradient between the media channels and chamber, although this hypothesis could not be verified or measured. In the second round of imaging attempts, the gel was only loaded into the left chamber only. While the gel did not appear to pull away from the posts over time as in the first round, there appeared to be some amount of gap between the collagen and either the surface of the glass cover slip or the PDMS device. This caused the dextran to flow between the gel and cover slip or PDMS and immediate move from one chamber to the next instead of diffusing through the collagen. One potential solution to this could be to coat the PDMS and/or the glass cover slip with laminin or fibronectin which could help facilitate better bonding to the collagen.

2. During steady state analysis, after the 12 hour time point successive time points were taken at a minimum of 6 hour intervals. If a more accurate estimate of steady state time is required, simulations could be rerun adding in additional time points where needed.
3. In this study we focused on 1, 10, 100, and 1000 kDa molecules. Curves were fitted to the steady state results in an attempt to determine a mathematical formula to represent steady state in collagen when the molecular weight of the diffusing molecule is known. To

make this formula more accurate, additional molecular weights such as 400 and 700 kDa should be simulated and the formulas for the best fit curve recalculated.

References

[1] Whitesides, George M. "The Origins and the Future of Microfluidics." *Nature*. 442.27 (2006): 368-73. Print.

[2] Tabeling, Patrick. *Introduction to Microfluidics*. New York: Oxford University Press, 2010. 1-21. Print.

[3] Alere Inc., "Triage Cardiac Panel Product Insert: Rapid Quantitative Test for Creatine Kinase MB (CK-MB), Myoglobin and Troponin I." *Alere Triage Cardiac Panel*. Alere Inc., n.d. Web. 23 Nov 2012. <https://sdmctrlprod.biosite.com/MC/main/mastercontrol/vault/view_doc.cfm?ls_id=9DC3B53406B1D048F0>.

[4] Lily, A . "FluidicMEMS- Perspectives on lab-on-a-chip, microfluidic, and bioMEMS technology." *Microfluidics for studying cancer metastasis*. FluidicMEM, 17 Jan 2010. Web. 7 Mar 2013. <http://fluidicmems.com/2010/01/17/microfluidics-for-studying-cancer-metastasis/>.

[5] Saadi, Wajeeh, Shur-Jen Wang, et al. "A parallel-gradient microfluidic chamber for quantitative analysis of breast cancer cell chemotaxis." *Biomedical Microdevices*. 8.2 (2006): 109-18. Print.

[6] Abhyankar, Vinay V., Michael W. Toepke, et al. "A platform for assessing chemotactic migration within a spatiotemporally defined 3D microenvironment." *Lab on a Chip*. 8.9 (2008): 1507-15. Print.

[7] Stanford Microfluidics Foundry, "Microfluidic Valve Technology." Stanford University, n.d. Web. 5 Nov 2012. <http://www.stanford.edu/group/foundry/Microfluidic valve technology.html>.

[8] Csete, Marie. "What can microfluidics do for stem cell research?." *Journal of Biology*. 9.1 (2010): n. page. Print.

[9] Dickson, BJ. "Molecular Mechanisms of Axon Guidance." *Science*. 298.5600 (2002): 1959-64. Print

[10] Kothapalli, Chandrasekhar R., Ed van Veen, Sarra de Valence, Seok Chung, Ioannis K. Zervantonakis, Frank B. Gertler, and Roger D. Kamm. "A high throughput microfluidic assay to study neurite response to growth factor gradients" *Lab on a Chip*. 11 (2011): 497-507. Print

[11] Genc, Baris, P. Hande Ozdinler, et al. "A Chemoattractant Role for NT-3 in Proprioceptive Axon Guidance." *PLoS Biology*. 2.12 (2004): 2112-21. Print.

[12] Gupta, Gaorav P., and Joan Massagu. "Cancer Metastasis: Building a Framework." *Cell*. 127. (2006): 679-95. Print.

[13] Lo, Chun-Min, Hong-Bei Wang, et al. "Cell Movement Is Guided by the Rigidity of the Substrate." *Biophysical Journal*. 79. (2000): 144-52. Print.

[14] Discher, Dennis E., Paul Janmey, and Yu-li Wang. "Tissue Cells Feel and Respond to the Stiffness of Their Substrate." *Science*. 310. (2005): 1139-43. Print.

[15] Keenan, Thomas M., and Albert Folch. "Biomolecular gradients in cell culture systems." *Lab on a Chip*. 8. (2008): 34-57. Print.

[16] Ratner, Buddy D., Allan S. Hoffman, Frederick J. Schoen, and Jack E. Lemons. *Biomaterials Science: An Introduction to Materials in Medicine*. 2nd ed. San Diego: Elsevier Academic Press, 2004. Print.

[17] Mosadegh, Bobak, Carlos Huang, et al. "Generation of Stable Complex Gradients Across Two-Dimensional Surfaces and Three-Dimensional Gels." *Langmuir: American Chemical Society*. 23. (2007): 10910-12. Print.

[18] Lye, Bethany. "Diffusion." . Kenyon College, n.d. Web. 16 Mar 2013. <http://biology.kenyon.edu/HHMI/Biol113/diffusion.htm>.

[19] Chen, Hong-Chen. "Boyden Chamber Assay." Trans. Array *Cell Migration: Developmental Methods & Protocols*. Jun-Lin Guan. Totowa, New Jersey: Humana Press, 2005. Print.

[20] Goodwin, Anne M. "In vitro assays of angiogenesis for assessment of angiogenic and anti-angiogenic agents." *Microvascular Research*. 74. (2007): 172-83. Print.

[21] Muinonen-Martin, Andrew J., Douwe M. Veltman, Gabriela Kalna, and Robert H. Insall. "An Improved Chamber for Direct Visualisation of Chemotaxis." *PLoS ONE*. 5.12 (2010): n. page. Print.

[22] Pujic, Zac, Duncan Mortimer, et al. "Assays for Eukaryotic Cell Chemotaxis." *Combinatorial Chemistry & High Throughput Screening*. 12. (2009): 580-88. Print.

[23] Crank, J. *The Mathematics of Diffusion*. 2nd ed. viii. New York: Oxford University Press, 1975. 414. Print.

[24] W. J. Rosoff, et al., “A new chemotaxis assay shows the extreme sensitivity of axons to molecular gradients”, *Nat. Neurosci*., 2004, 7(6), 678–682.

[25] T. Boland, et al., “Application of inkjet printing to tissue engineering”, *Biotechnology Journal*, 2006, 1(9), 910–917.

[26] Nolte, John. *The Human Brain: An Introduction to its Functional Anatomy*. 6th ed. Philadelphia: Mosby Elsevier, 2009. Print.

[27] E. Stein, M. Tessier-Lavigne, “Hierarchical organization of guidance receptors: Silencing of netrin attraction by slit through a Robo/DCC receptor complex”, *Science*, 2001, 291(5510), 1928–1938. Print

[28] H. J. Song, G. L. Ming, M. M. Poo, “cAMP-induced switching in turning direction of nerve growth cones”, *Nature*, 1997,388(6639), 275–279. Print

[29] V. H. Hopker, et al., “Growth-cone attraction to netrin-1 is converted to repulsion by laminin-1”, *Nature*, 1999, 401(6748), 69–73.Print

[30] Wang, Joanne, Xiong Li, Benjamin Lin, Sangwoo Shim, Guo-li Ming, and Andre Levchenko. "A microfluidics-based turning assay reveals complex growth cone responses to integrated gradients of substrate-bound ECM molecules and diffusible guidance cues." *Lab on a Chip*. 8. (2008): 227-37. Print.

[31] Sundararaghavan, Harini G., Gary A. Monteiro, et al. "Neurite Growth in 3D Collagen Gels with Gradients of Mechanical Properties." *Biotechnology & Bioengineering*. 102.2 (2009): 632-43. Print.

[32] Discher, Dennis E., Paul Janmey, and Yu-li Wang. "Tissue Cells Feel and Respond to the Stiffness of Their Substrate." *Science*. 310. (2005): 1139-43. Print.

[33] Lo, Chun-Min, Hong-Bei Wang, Micah Dembo, and Yu-Li Wang. "Cell Movement Is Guided by the Rigidity of the Substrate." *Biophysical Journal*. 79. (2000): 144-52. Print.

[34] Centers for Disease Control and Prevention, . "Spinal Cord Injury, SCI: Fact Sheet." *Injury Prevention and Control*. CDC, 04 2010. Web. 2 Dec 2012. <http://www.cdc.gov/traumaticbraininjury/scifacts.html>.

[35] Cajal, Ramon. *Cajal's Degeneration and Regeneration of the Nervous System*. New York: Oxford University Press, 1991. Print.

[36] Kim, Hyung Joon, Jeong Won Park, et al. "Integrated Microfluidics Platforms for Investigating Injury and Regeneration of CNS Axons." *Annals of Biomedical Engineering*. 40.6 (2012): 1268-76. Print.

[37] Fayaz, Imran, and Charles H. Tator. "Modeling Axonal Injury In Vitro: Injury and Regeneration Following Acute Neuritic Trauma." *Journal of Neuroscience Methods*. 102. (2000): 69-79. Print.

[38] Mandolesi, Georgia, Federico Madeddu, Yuri Bozzi, Lamberto Maffei, and Gian Michele Ratto. "Acute Physiological Response of Mammalian Central Neurons to Axotomy: Ionic Regulation and Electrical Activity." *FASEB Journal*. 18.December (2004): 1934-36. Print.

[39] Fawcett, James W., and Richard A. Asher. "The Glial Scar and Central Nervous System Repair." *Brain Research Bulletin*. 49.6 (1999): 377-91. Print.

[40] Abu-Rub, Mohammad, Siobhan McMahon, Dimitrios I. Zeugolis, Anthony Windebank, and Abhay Pandit. "Spinal Cord Injury In Vitro: Modelling Axon Growth Inhibition." *Drug Discovery Today*. 15.11 (2010): 436-43. Print.

[41] Panesar, Kiran. "Management of Nerve Injuries." *US Pharmacist*. 37.10 (2012): n. page. Print.

[42] Sharon, Idan. "Acute Nerve Injury." *Medscape Reference*. (2011): n. page. Web. 23 Mar. 2013. <http://emedicine.medscape.com/article/249621-overview>.

[43] Lee, K., and Brenda Lerner. "Neural Damage and Repair." *World of Anatomy and Physiology*. 2. Detroit: 2002.

[44] Sharon, Idan. "Acute Nerve Injury Treatment & Management." *Medscape Reference*. (2011): n. page. Web. 23 Mar. 2013. <http://emedicine.medscape.com/article/249621-overview>.

[45] University of Utah. "New Hope For Restoring Injured Nerves." *ScienceDaily*, 26 Jan. 2009. Web. 23 Mar. 2013.

[46] Gladman, Stacey J., Wenlong Huang, et al. "Improved Outcome after Peripheral Nerve Injury in Mice with Increased Levels of Endogenous Omega-3 Polyunsaturated Fatty Acids." *Journal of Neuroscience*. 32.2 (2012): 563-71. Print.

[47] Kronenberg, Golo, and Matthias Endres. "Neuronal Injury: Folate to the Rescue?." *Journal of Clinical Investigation*. 120.5 (2010): 1383-86. Print.

[48] Ali, Hamad, and Hussain Bahbahani. "Umbilical cord blood stem cells - potential therapeutic tool for neural injuries and disorders." *Acta Neurobiol Exp*. 70 (2010): 316-24. Print.

[49] Kelly Fitzgerald. "Revolutionary Stem Cell Treatment Repairs Spinal Cord Injuries In Paralyzed Dogs." *Medical News Today*. MediLexicon, Intl., 20 Nov.

2012. Web. 23 Mar. 2013.
http://www.medicalnewstoday.com/articles/252982.php
[50] Georgia Tech School of Electrical and Computer Engineering, "Photolithography." *Georgia Tech School of Electrical and Computer Engineering*. N.p., 16 Sept 2010. Web. 30 Sep 2012. <http://www.ece.gatech.edu/research/labs/vc/theory/photolith.html>.
[51] MacMillan, John H.. "Using Silanes as Adheshion Promoters." *UCT United Chemical Technologies*. UCT. Web. 16 Apr 2013. <http://www.ccl.net/cca/documents/MacMillan_Papers/adhesion.pdf>.
[52] BD Biosciences, . "Rat Tail Collagen High Concentration (HC), TYPE 1." *BD Biosciences*. N.p.. Web. 26 Jan 2013
[53] Sadoway, Donald R. "Diffusion." Introduction to Solid State Chemistry. MIT. 2005. Lecture.
[54] Weast, R.C. *CRC Handbook of Chemistry and Physics*. 50th ed. The Chemical Rubber Company 1969. F-36. Print.
[55] Guarnieri, D., S. Battista, A. Borzacchiello, et al. "Effects of fibronectin and laminin on structural, mechanical and transport properties of 3D collageneous network." *Journal of Materials Science: Materials in Medicine*. 18. (2007): 245-53. Print.
[56] Rosoff, William J., Jeffrey S. Urbach, Mark A. Esrick, et al. "A new chemotaxis assay shows the extreme sensitivity of axons to molecular gradients." *Nature Neuroscience*. 7.6 (2004): 678-82. Print.

[57] Jones, DM, BA Tucker, M Rahimtula , and KM Mearow. "The synergistic effects of NGF and IGF-1 on neurite growth in adult sensory neurons: convergence on the PI 3-kinase signaling pathway." *Journal of Neurochemistry*. 86.5 (2005): 1116-28. Print.

Image References

[P1] ALine Inc., . *Polymer Laminate Technology Enables Rapid Prototyping of Bio Microfluidic Devices*. 2011. MDT: Medical Design TechnologyWeb. 5 Nov 2012. <http://www.mdtmag.com/product-releases/2011/02/polymer-laminate-technology-enables-rapid-prototyping-bio-microfluidic-devices>.

[P2] Ostrovsky, Gene. "NanoVelcro Microfluidic Device for Detection, Isolation, and Molecular Analysis of Circulating Tumor Cells." *medGadget*. medGadget, 25 Feb 2013. Web. 5 Mar 2013. <http://www.medgadget.com/2013/02/nanovelcro-microfluidic-device-for-detection-isolation-and-molecular-analysis-of-circulating-tumor-cells.html>.

[P3] Wang, Yanju, Wei-Yu Lin, et al. "An integrated microfluidic device for large-scale in situ click chemistry screening." *Lab on a Chip*. 9. (2009): 2281-85. Print.

[P4] Genc, Baris, P. Hande Ozdinler, et al. "A Chemoattractant Role for NT-3 in Proprioceptive Axon Guidance." *PLoS Biology*. 2.12 (2004): 2112-21. Print.

[P5] Keenan, Thomas M., and Albert Folch. "Biomolecular gradients in cell culture systems." *Lab on a Chip*. 8. (2008): 34-57. Print.

[P6] Keenan, Thomas M., and Albert Folch. "Biomolecular gradients in cell culture systems." *Lab on a Chip*. 8. (2008): 34-57. Print.

[P7] Wang, Joanne, Xiong Li, Benjamin Lin, Sangwoo Shim, Guo-li Ming, and Andre Levchenko. "A microfluidics-based turning assay reveals complex growth cone responses to integrated gradients of substrate-bound ECM molecules and diffusible guidance cues." *Lab on a Chip*. 8. (2008): 227-37. Print.

[P8] Sundararaghavan, Harini G., Gary A. Monteiro, et al. "Neurite Growth in 3D Collagen Gels with Gradients of Mechanical Properties." *Biotechnology & Bioengineering*. 102.2 (2009): 632-43. Print.

[P9] Fayaz, Imran, and Charles H. Tator. "Modeling Axonal Injury In Vitro: Injury and Regeneration Following Acute Neuritic Trauma." *Journal of Neuroscience Methods*. 102. (2000): 69-79. Print

[P10] Kim, Hyung Joon, Jeong Won Park, et al. "Integrated Microfluidics Platforms for Investigating Injury and Regeneration of CNS Axons." *Annals of Biomedical Engineering*. 40.6 (2012): 1268-76. Print.

Appendix

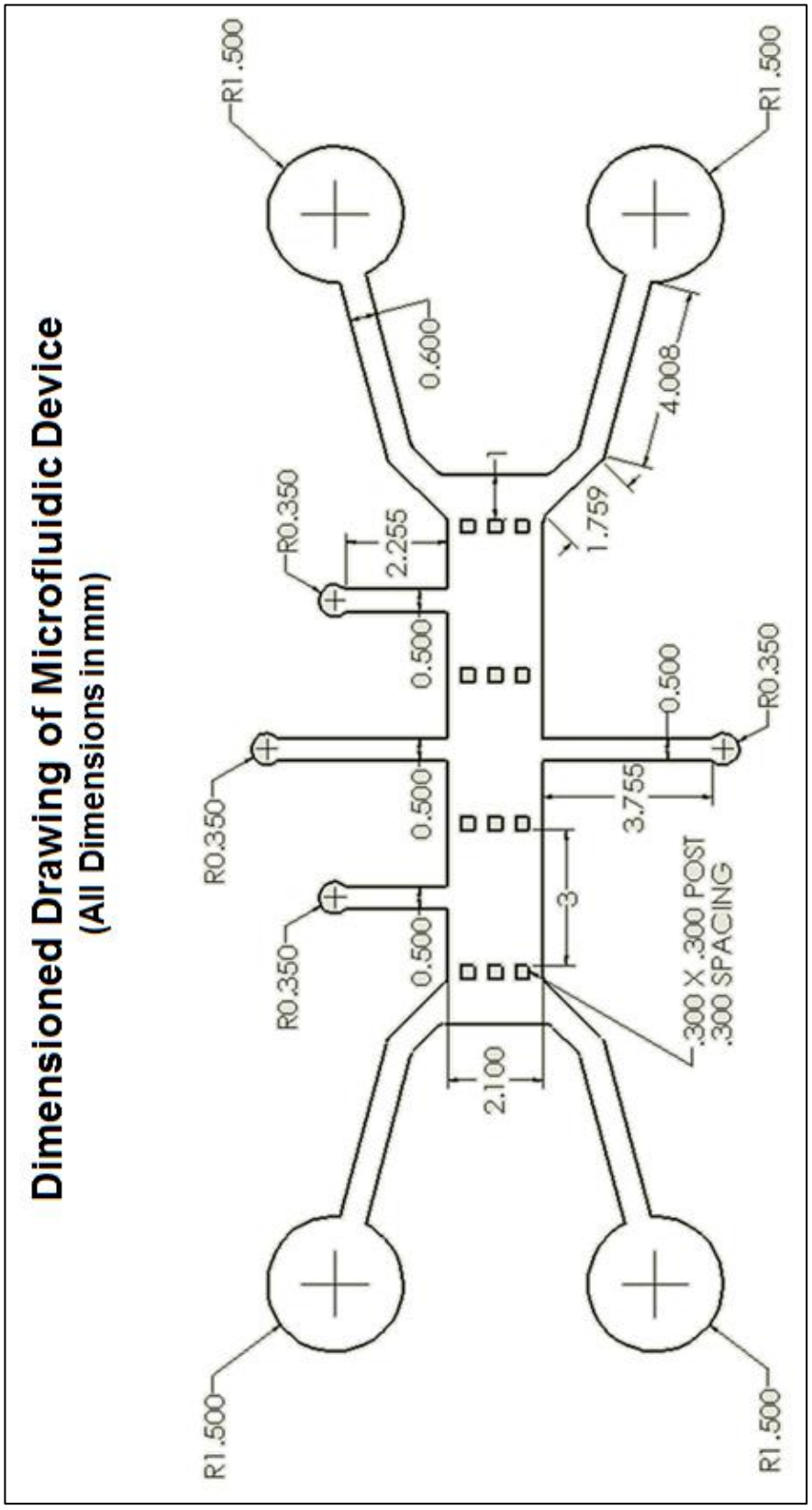
Dimensioned Drawing of Microfluidic Device
(All Dimensions in mm)
R1.500
R1.500
R1.500
R1.500
0.600
4.008
1.759
1
R0.350
2.255
0.500
R0.350
0.500
R0.350
0.500
R0.350
0.500
3.755
3
2.100
.300 X .300 POST
.300 SPACING

COMSOL Boundary Conditions & Equations

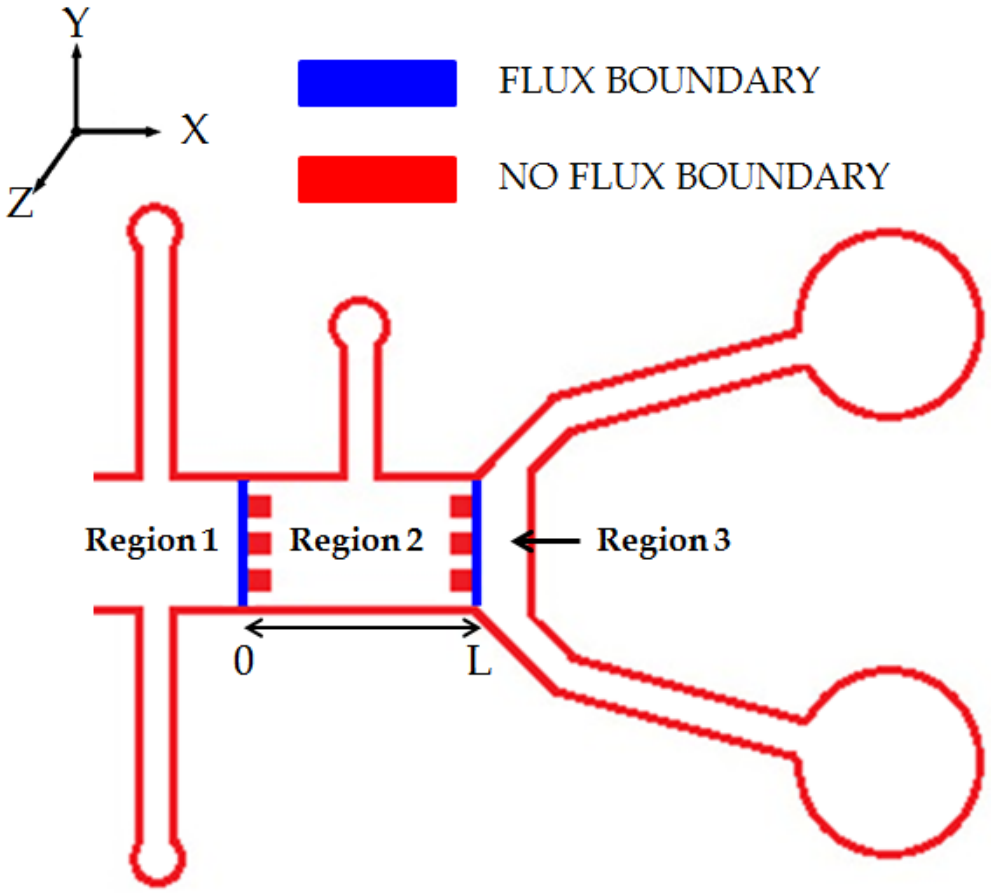

Governing Equation

$$\frac{\partial C}{\partial t} = D\frac{\partial^2 C}{\partial x^2}$$

Initial Conditions

Region 1: $C(0,t) = C_0$

Region 2: $C(0,t) = 0$

$$C(x,t) = D\frac{\partial C}{\partial t}$$

Region 3: $C(L,t) = 0$

Using separation of variables: $$C(x,t) = \sum_{n=1}^{\infty} C_n e^{-Dn^2\pi^2 t/l^2} \sin\left(\frac{n\pi x}{l}\right)$$

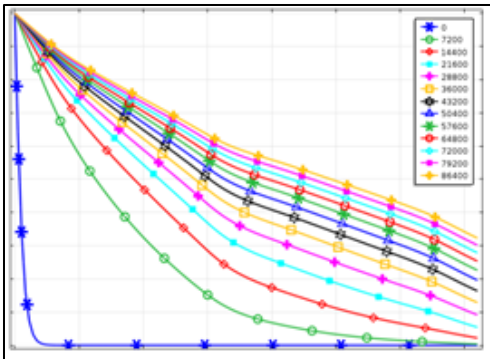

Line AB

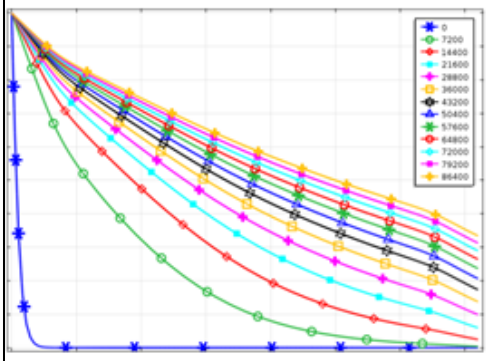

Line CD

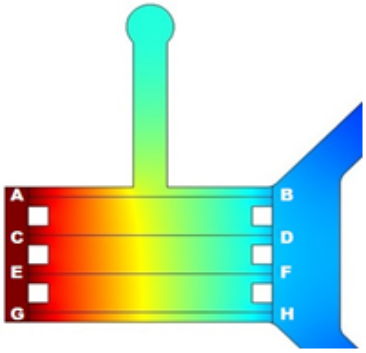

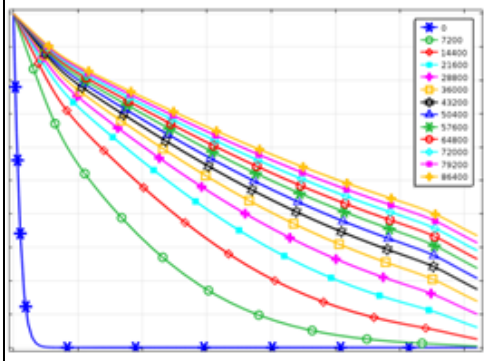

Line EF

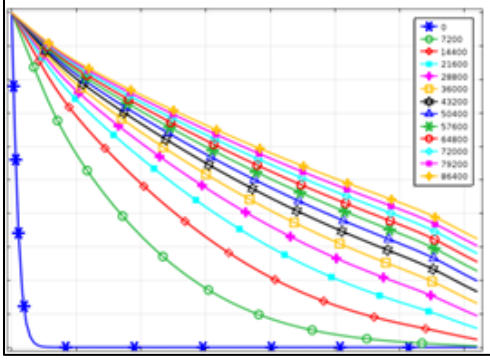

Line GH

Gradient profiles taken at four locations across the gel chamber. This was initially done to show that the diffusion across the gel chamber progressed as a straight line and did not exhibit any random flow patterns across the gel chambers

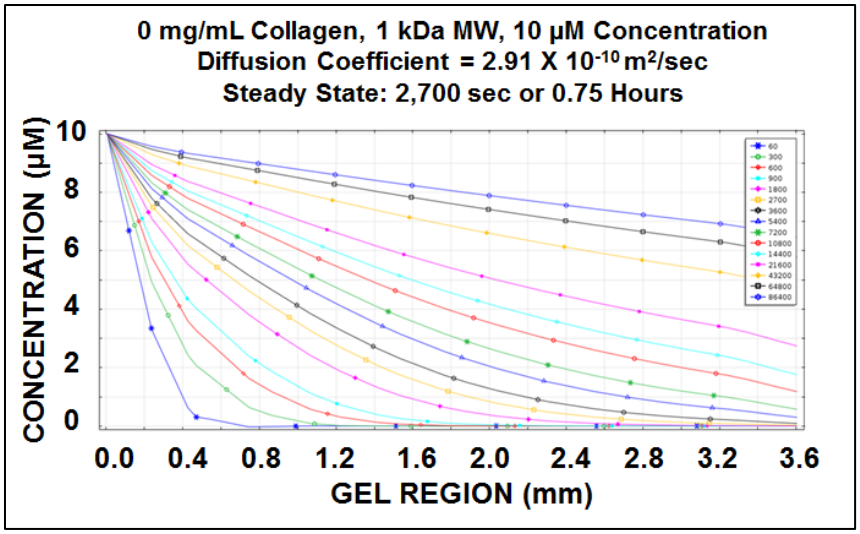
0 mg/mL Collagen, 1 kDa MW, 10 µM Concentration
Diffusion Coefficient = 2.91 X 10-10 m2/sec
Steady State: 2,700 sec or 0.75 Hours
CONCENTRATION (µM)
0 2 4 6 8 10
0.0 0.4 0.8 1.2 1.6 2.0 2.4 2.8 3.2 3.6
GEL REGION (mm)
60
300
600
900
1800
2700
3600
5400
7200
10800
14400
21600
43200
64800
86400

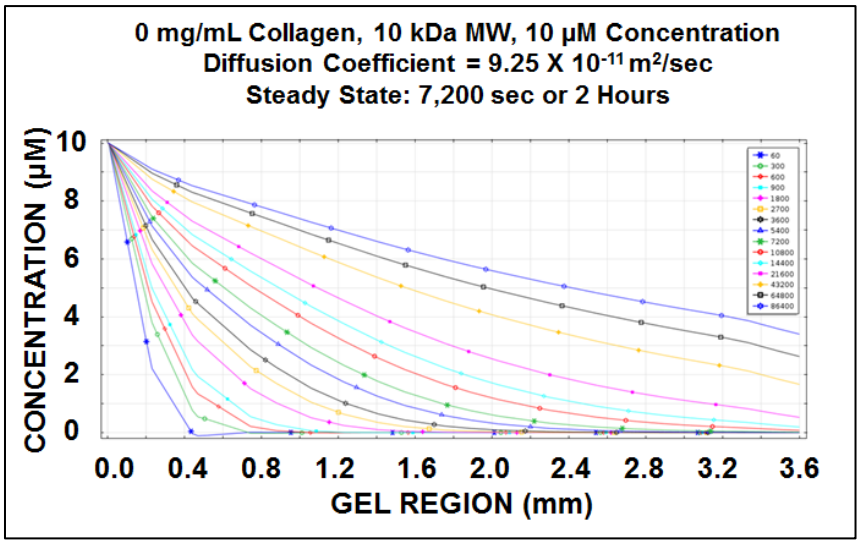
0 mg/mL Collagen, 10 kDa MW, 10 µM Concentration
Diffusion Coefficient = 9.25 X 10-11 m2/sec
Steady State: 7,200 sec or 2 Hours
CONCENTRATION (µM)
0 2 4 6 8 10
0.0 0.4 0.8 1.2 1.6 2.0 2.4 2.8 3.2 3.6
GEL REGION (mm)
60
300
600
900
1800
2700
3600
5400
7200
10800
14400
21600
43200
64800
86400

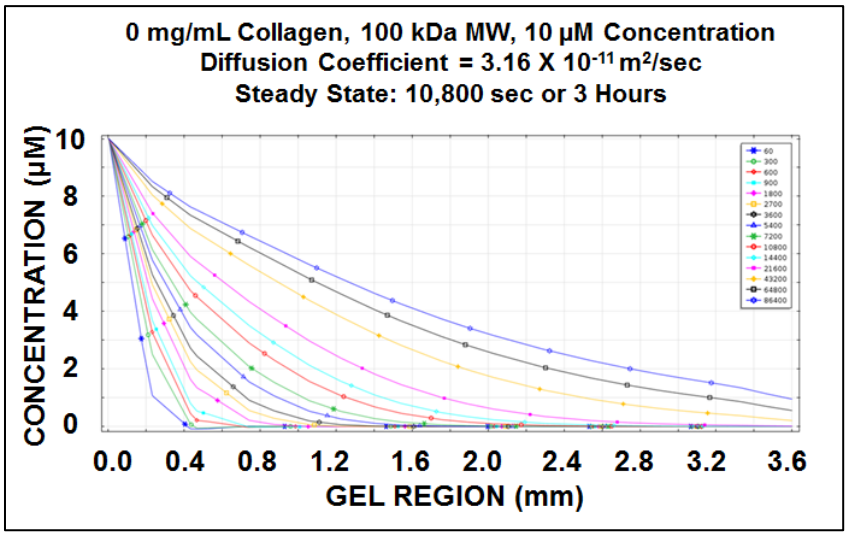
0 mg/mL Collagen, 100 kDa MW, 10 µM Concentration
Diffusion Coefficient = 3.16 X 10-11 m2/sec
Steady State: 10,800 sec or 3 Hours
CONCENTRATION (µM)
0 2 4 6 8 10
0.0 0.4 0.8 1.2 1.6 2.0 2.4 2.8 3.2 3.6
GEL REGION (mm)
60
300
600
900
1800
2700
3600
5400
7200
10800
14400
21600
43200
64800
86400

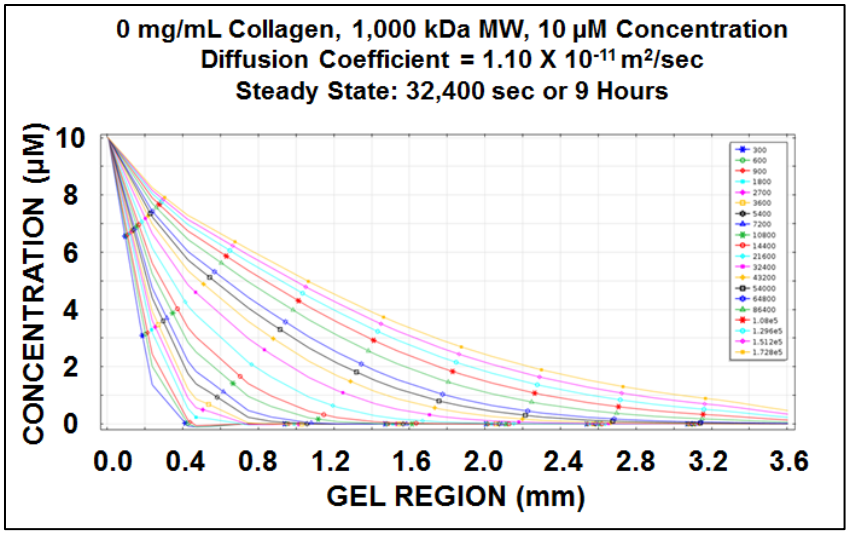
0 mg/mL Collagen, 1,000 kDa MW, 10 µM Concentration
Diffusion Coefficient = 1.10 X 10-11 m2/sec
Steady State: 32,400 sec or 9 Hours
CONCENTRATION (µM)
0 2 4 6 8 10
0.0 0.4 0.8 1.2 1.6 2.0 2.4 2.8 3.2 3.6
GEL REGION (mm)

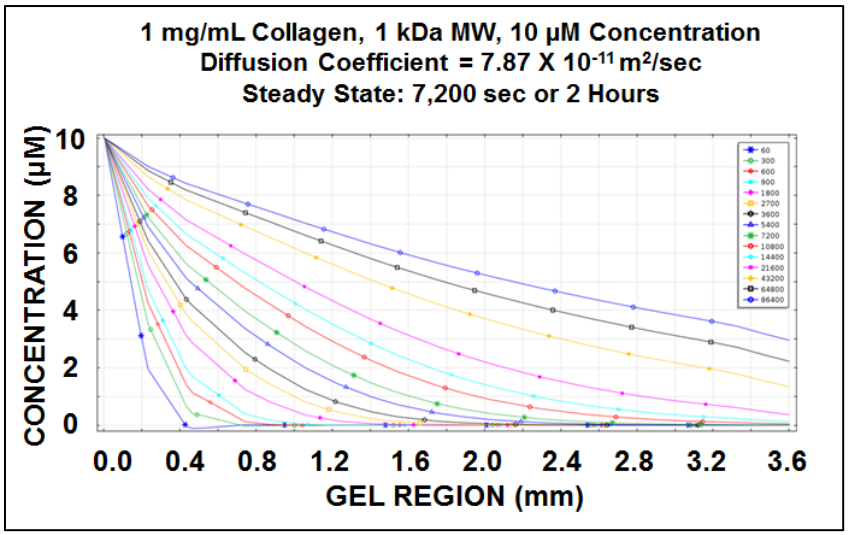
1 mg/mL Collagen, 1 kDa MW, 10 µM Concentration
Diffusion Coefficient = 7.87 X 10-11 m2/sec
Steady State: 7,200 sec or 2 Hours
CONCENTRATION (µM)
0 2 4 6 8 10
0.0 0.4 0.8 1.2 1.6 2.0 2.4 2.8 3.2 3.6
GEL REGION (mm)

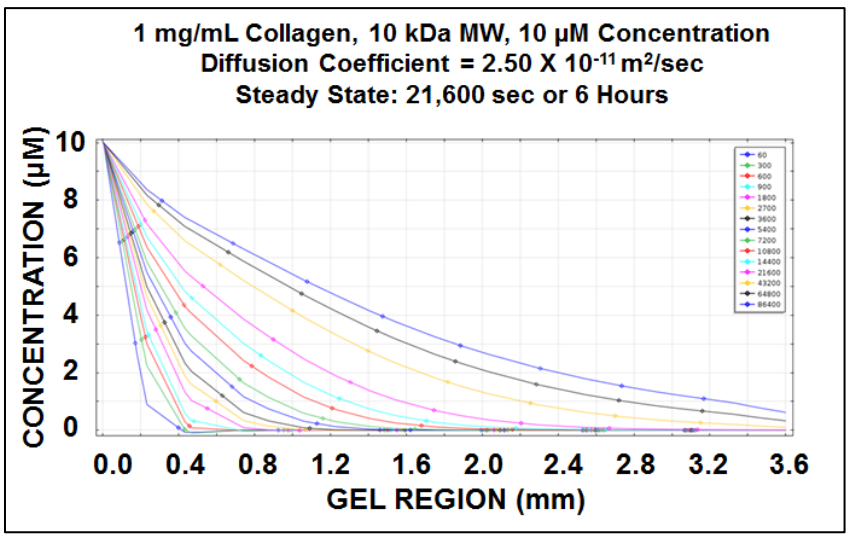
1 mg/mL Collagen, 10 kDa MW, 10 µM Concentration
Diffusion Coefficient = 2.50 X 10-11 m2/sec
Steady State: 21,600 sec or 6 Hours
CONCENTRATION (µM)
0 2 4 6 8 10
0.0 0.4 0.8 1.2 1.6 2.0 2.4 2.8 3.2 3.6
GEL REGION (mm)

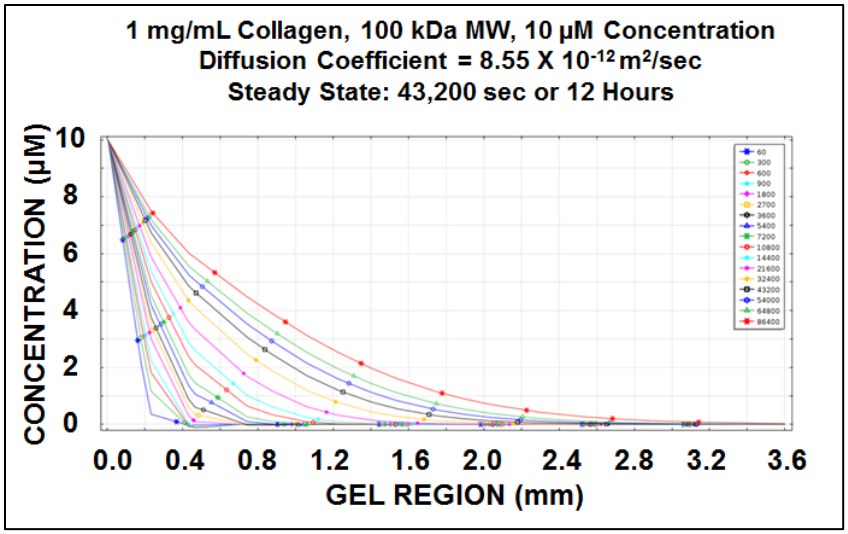
1 mg/mL Collagen, 100 kDa MW, 10 µM Concentration
Diffusion Coefficient = 8.55 X 10-12 m2/sec
Steady State: 43,200 sec or 12 Hours
CONCENTRATION (µM)
0
2
4
6
8
10
0.0
0.4
0.8
1.2
1.6
2.0
2.4
2.8
3.2
3.6
GEL REGION (mm)

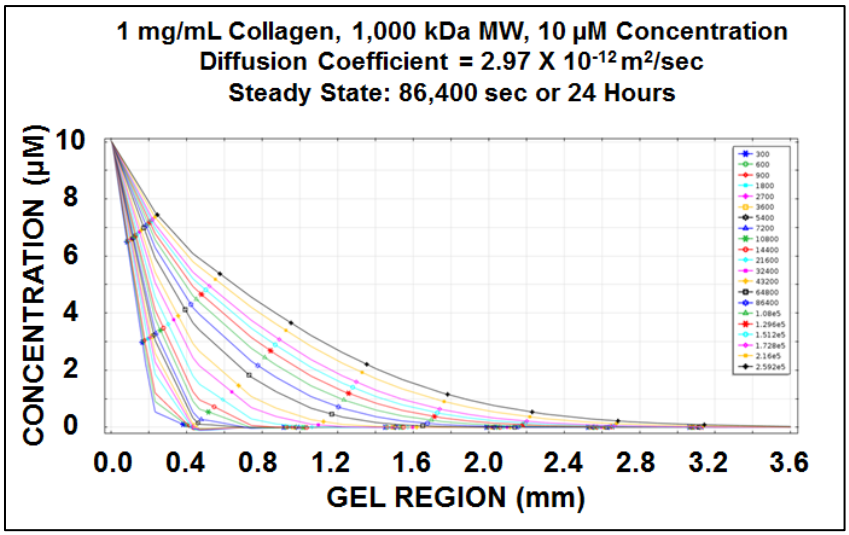
1 mg/mL Collagen, 1,000 kDa MW, 10 µM Concentration
Diffusion Coefficient = 2.97 X 10-12 m2/sec
Steady State: 86,400 sec or 24 Hours
CONCENTRATION (µM)
0
2
4
6
8
10
0.0
0.4
0.8
1.2
1.6
2.0
2.4
2.8
3.2
3.6
GEL REGION (mm)

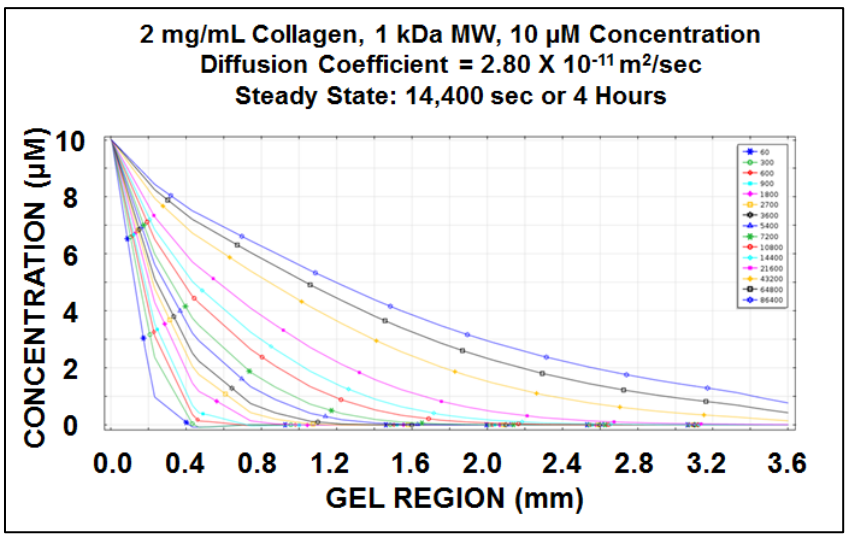
2 mg/mL Collagen, 1 kDa MW, 10 µM Concentration
Diffusion Coefficient = 2.80 X 10-11 m2/sec
Steady State: 14,400 sec or 4 Hours
CONCENTRATION (µM)
0
2
4
6
8
10
0.0
0.4
0.8
1.2
1.6
2.0
2.4
2.8
3.2
3.6
GEL REGION (mm)

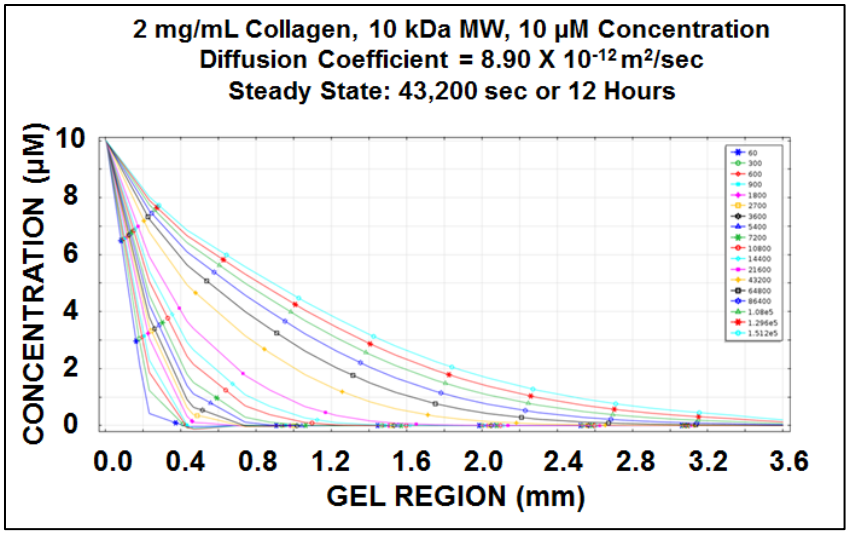
2 mg/mL Collagen, 10 kDa MW, 10 µM Concentration
Diffusion Coefficient = 8.90 X 10-12 m2/sec
Steady State: 43,200 sec or 12 Hours
CONCENTRATION (µM)
0
2
4
6
8
10
0.0
0.4
0.8
1.2
1.6
2.0
2.4
2.8
3.2
3.6
GEL REGION (mm)

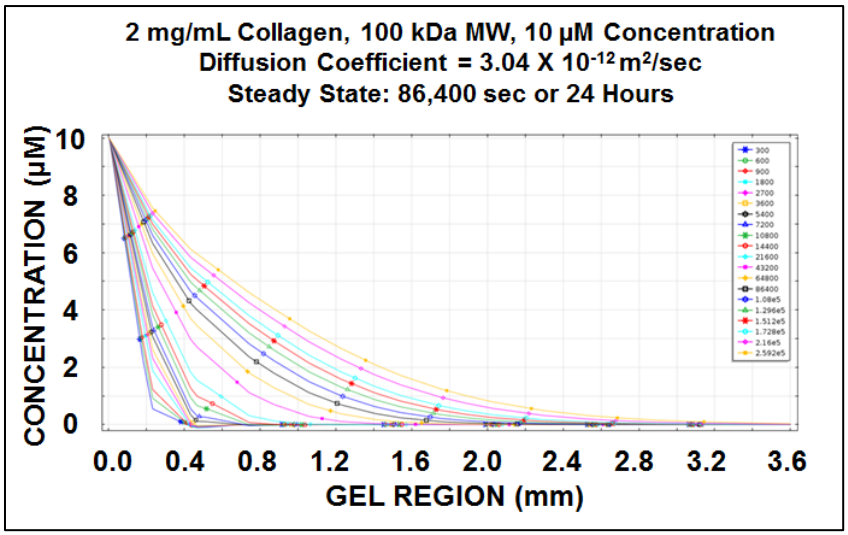
2 mg/mL Collagen, 100 kDa MW, 10 µM Concentration
Diffusion Coefficient = 3.04 X 10-12 m2/sec
Steady State: 86,400 sec or 24 Hours
CONCENTRATION (µM)
0
2
4
6
8
10
0.0
0.4
0.8
1.2
1.6
2.0
2.4
2.8
3.2
3.6
GEL REGION (mm)

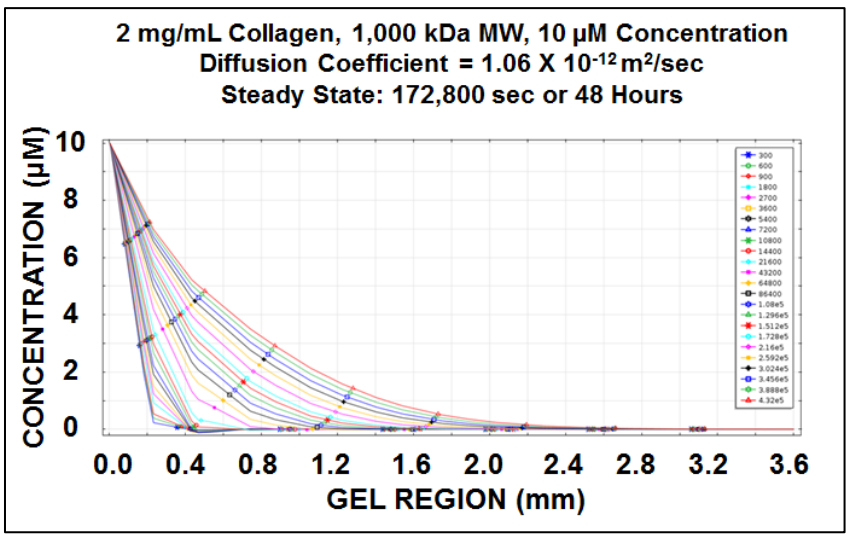
2 mg/mL Collagen, 1,000 kDa MW, 10 µM Concentration
Diffusion Coefficient = 1.06 X 10-12 m2/sec
Steady State: 172,800 sec or 48 Hours
CONCENTRATION (µM)
0
2
4
6
8
10
0.0
0.4
0.8
1.2
1.6
2.0
2.4
2.8
3.2
3.6
GEL REGION (mm)

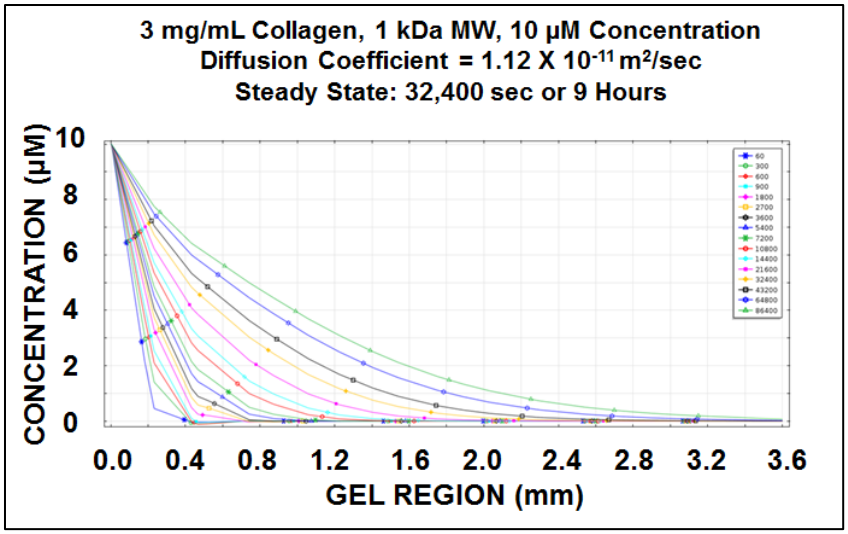
3 mg/mL Collagen, 1 kDa MW, 10 µM Concentration
Diffusion Coefficient = 1.12 X 10-11 m2/sec
Steady State: 32,400 sec or 9 Hours
CONCENTRATION (µM)
0
2
4
6
8
10
0.0
0.4
0.8
1.2
1.6
2.0
2.4
2.8
3.2
3.6
GEL REGION (mm)

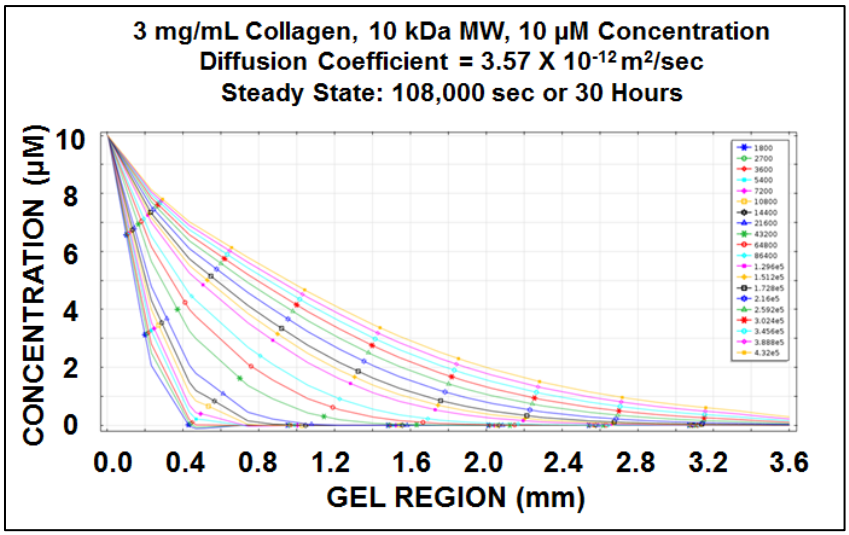
3 mg/mL Collagen, 10 kDa MW, 10 µM Concentration
Diffusion Coefficient = 3.57 X 10-12 m2/sec
Steady State: 108,000 sec or 30 Hours
CONCENTRATION (µM)
0
2
4
6
8
10
0.0
0.4
0.8
1.2
1.6
2.0
2.4
2.8
3.2
3.6
GEL REGION (mm)

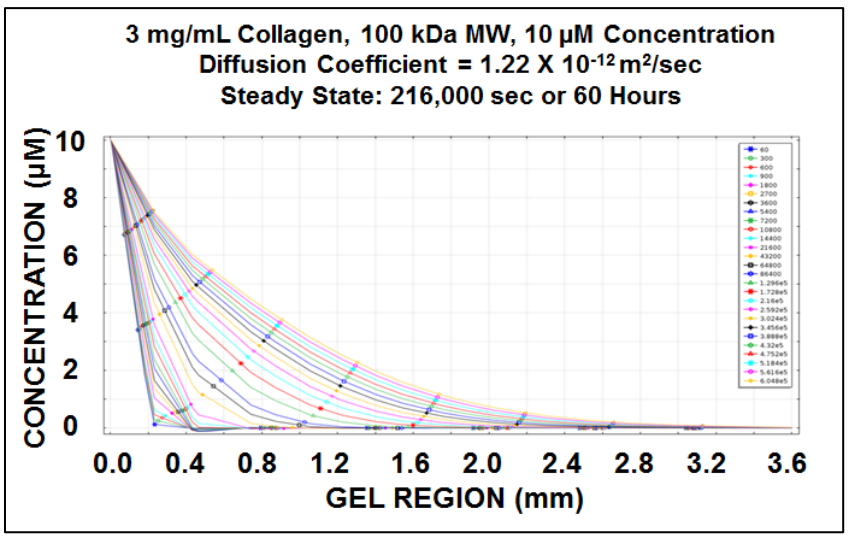
3 mg/mL Collagen, 100 kDa MW, 10 µM Concentration
Diffusion Coefficient = 1.22 X 10-12 m2/sec
Steady State: 216,000 sec or 60 Hours
CONCENTRATION (µM)
0
2
4
6
8
10
0.0
0.4
0.8
1.2
1.6
2.0
2.4
2.8
3.2
3.6
GEL REGION (mm)

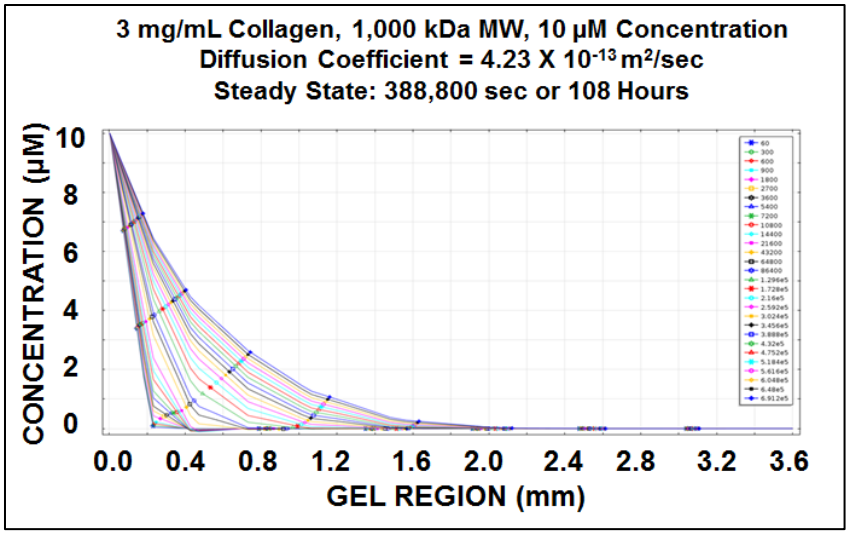
3 mg/mL Collagen, 1,000 kDa MW, 10 µM Concentration
Diffusion Coefficient = 4.23 X 10-13 m2/sec
Steady State: 388,800 sec or 108 Hours
CONCENTRATION (µM)
0
2
4
6
8
10
0.0
0.4
0.8
1.2
1.6
2.0
2.4
2.8
3.2
3.6
GEL REGION (mm)

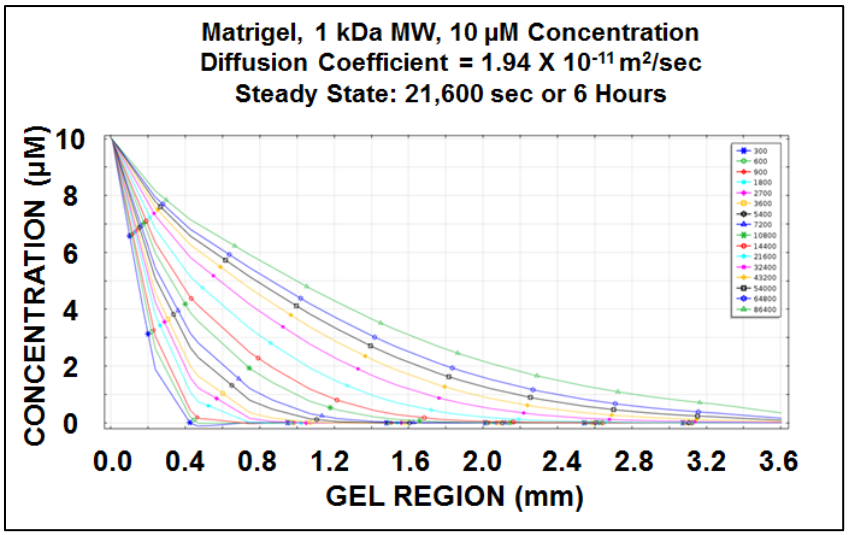
Matrigel, 1 kDa MW, 10 µM Concentration
Diffusion Coefficient = 1.94 X 10-11 m2/sec
Steady State: 21,600 sec or 6 Hours
CONCENTRATION (µM)
0
2
4
6
8
10
0.0
0.4
0.8
1.2
1.6
2.0
2.4
2.8
3.2
3.6
GEL REGION (mm)

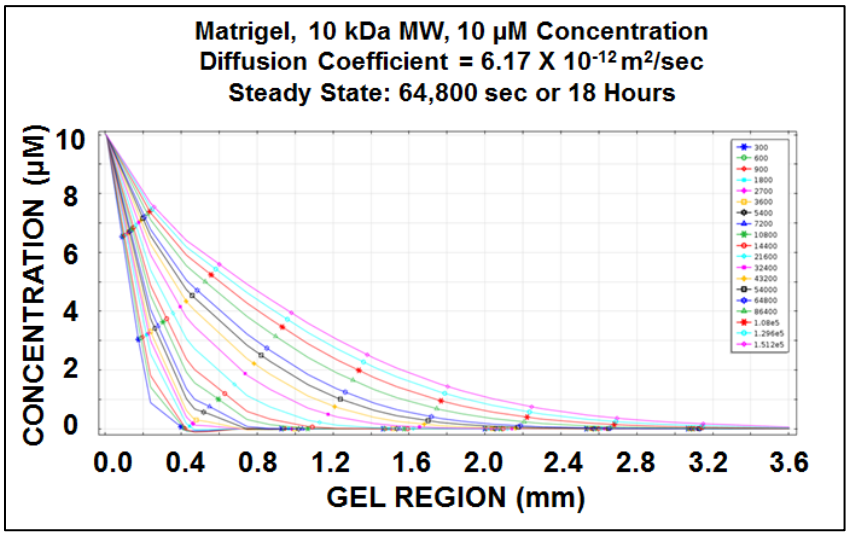
Matrigel, 10 kDa MW, 10 µM Concentration
Diffusion Coefficient = 6.17 X 10-12 m2/sec
Steady State: 64,800 sec or 18 Hours
CONCENTRATION (µM)
0
2
4
6
8
10
0.0
0.4
0.8
1.2
1.6
2.0
2.4
2.8
3.2
3.6
GEL REGION (mm)

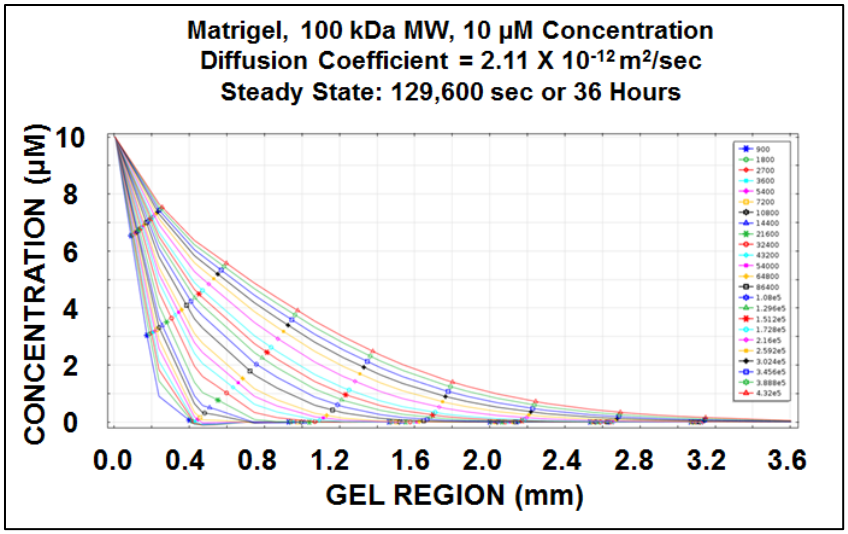
Matrigel, 100 kDa MW, 10 µM Concentration
Diffusion Coefficient = 2.11 X 10-12 m2/sec
Steady State: 129,600 sec or 36 Hours
CONCENTRATION (µM)
10
8
6
4
2
0
0.0 0.4 0.8 1.2 1.6 2.0 2.4 2.8 3.2 3.6
GEL REGION (mm)

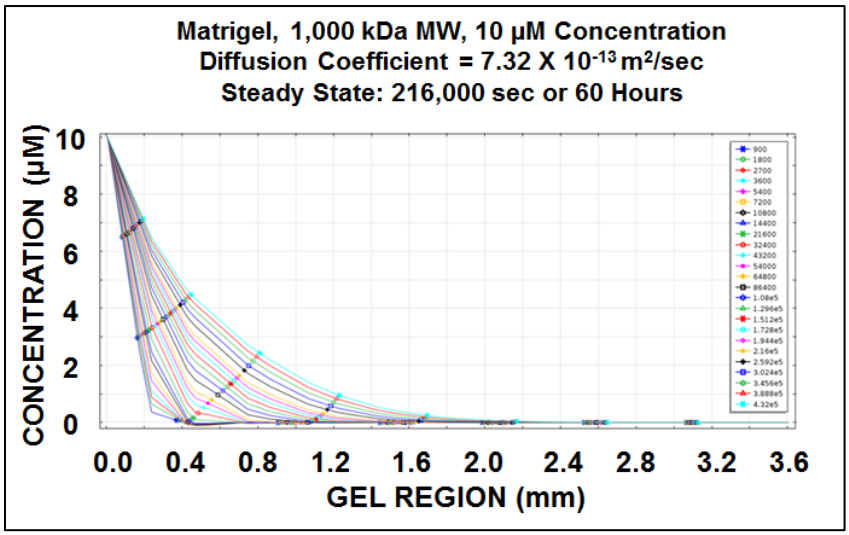
Matrigel, 1,000 kDa MW, 10 µM Concentration
Diffusion Coefficient = 7.32 X 10-13 m2/sec
Steady State: 216,000 sec or 60 Hours
CONCENTRATION (µM)
10
8
6
4
2
0
0.0 0.4 0.8 1.2 1.6 2.0 2.4 2.8 3.2 3.6
GEL REGION (mm)

10 µM Concentration - Steady State Calculation

	Molecular Weight	Time Value (s)	Time Value (hrs)	Slope Between 0.8 & 1 mm					Slope Between 1.2 & 1.4 mm					% Difference Between Slopes
				X_1	X_2	Y_1	Y_2	Slope	X_1	X_2	Y_1	Y_2	Slope	
0 mg/mL Collagen	1 kDa	1800	0.5	0.8	1.0	0.0035	0.0027	-0.0040	1.2	1.4	0.0019	0.0014	-0.0025	37.50%
		2700	0.75	0.8	1.0	0.0044	0.0035	-0.0045	1.2	1.4	0.0027	0.0021	-0.0030	33.33%
		3600	1	0.8	1.0	0.0049	0.0041	-0.0040	1.2	1.4	0.0033	0.0027	-0.0030	25.00%
		5400	1.5	0.8	1.0	0.0056	0.0049	-0.0035	1.2	1.4	0.0042	0.0036	-0.0030	14.29%
		7200	2	0.8	1.0	0.0061	0.0054	-0.0035	1.2	1.4	0.0047	0.0041	-0.0030	14.29%
		10800	3	0.8	1.0	0.0066	0.0060	-0.0030	1.2	1.4	0.0055	0.0049	-0.0030	0.00%
		14400	4	0.8	1.0	0.0070	0.0065	-0.0025	1.2	1.4	0.0060	0.0055	-0.0025	0.00%
		21600	6	0.8	1.0	0.0075	0.0070	-0.0025	1.2	1.4	0.0067	0.0062	-0.0025	0.00%
		43200	12	0.8	1.0	0.0083	0.0080	-0.0015	1.2	1.4	0.0078	0.0075	-0.0015	0.00%
		64800	18	0.8	1.0	0.0088	0.0085	-0.0015	1.2	1.4	0.0083	0.0080	-0.0015	0.00%
		86400	24	0.8	1.0	0.0090	0.0088	-0.0010	1.2	1.4	0.0086	0.0084	-0.0010	0.00%
	10 kDa	1800	0.5	0.8	1.0	0.0013	0.0007	-0.0030	1.2	1.4	0.0004	0.0002	-0.0010	66.67%
		2700	0.75	0.8	1.0	0.0020	0.0012	-0.0040	1.2	1.4	0.0007	0.0004	-0.0015	62.50%
		3600	1	0.8	1.0	0.0026	0.0017	-0.0045	1.2	1.4	0.0011	0.0007	-0.0020	55.56%
		5400	1.5	0.8	1.0	0.0035	0.0026	-0.0045	1.2	1.4	0.0018	0.0013	-0.0025	44.44%
		7200	2	0.8	1.0	0.0041	0.0032	-0.0045	1.2	1.4	0.0024	0.0018	-0.0030	33.33%
		10800	3	0.8	1.0	0.0049	0.0040	-0.0045	1.2	1.4	0.0033	0.0026	-0.0035	22.22%
		14400	4	0.8	1.0	0.0054	0.0047	-0.0035	1.2	1.4	0.0038	0.0032	-0.0030	14.29%
		21600	6	0.8	1.0	0.0060	0.0054	-0.0030	1.2	1.4	0.0046	0.0040	-0.0030	0.00%
		43200	12	0.8	1.0	0.0070	0.0064	-0.0030	1.2	1.4	0.0059	0.0053	-0.0030	0.00%
		64800	18	0.8	1.0	0.0075	0.0070	-0.0025	1.2	1.4	0.0065	0.0060	-0.0025	0.00%
		86400	24	0.8	1.0	0.0078	0.0074	-0.0020	1.2	1.4	0.0070	0.0066	-0.0020	0.00%
	100 kDa	5400	1.5	0.8	1.0	0.0014	0.0007	-0.0035	1.2	1.4	0.0004	0.0001	-0.0015	57.14%
		7200	2	0.8	1.0	0.0018	0.0011	-0.0035	1.2	1.4	0.0006	0.0003	-0.0015	57.14%
		10800	3	0.8	1.0	0.0026	0.0018	-0.0040	1.2	1.4	0.0012	0.0007	-0.0025	37.50%
		14400	4	0.8	1.0	0.0032	0.0024	-0.0040	1.2	1.4	0.0017	0.0011	-0.0030	25.00%
		21600	6	0.8	1.0	0.0041	0.0033	-0.0040	1.2	1.4	0.0025	0.0018	-0.0035	12.50%
		43200	12	0.8	1.0	0.0053	0.0047	-0.0030	1.2	1.4	0.0039	0.0033	-0.0030	0.00%
		64800	18	0.8	1.0	0.0060	0.0053	-0.0035	1.2	1.4	0.0047	0.0040	-0.0035	0.00%
		86400	24	0.8	1.0	0.0064	0.0058	-0.0030	1.2	1.4	0.0052	0.0046	-0.0030	0.00%
	1,000 kDa	14400	4	0.8	1.0	0.0012	0.0007	-0.0025	1.2	1.4	0.0003	0.0001	-0.0010	60.00%
		21600	6	0.8	1.0	0.0019	0.0012	-0.0035	1.2	1.4	0.0007	0.0003	-0.0020	42.86%
		43200	12	0.8	1.0	0.0033	0.0025	-0.0040	1.2	1.4	0.0018	0.0012	-0.0030	25.00%
		64800	18	0.8	1.0	0.0041	0.0033	-0.0040	1.2	1.4	0.0026	0.0019	-0.0035	12.50%
		86400	24	0.8	1.0	0.0047	0.0039	-0.0040	1.2	1.4	0.0031	0.0024	-0.0035	12.50%
		108000	30	0.8	1.0	0.0050	0.0044	-0.0030	1.2	1.4	0.0036	0.0030	-0.0030	0.00%
		129600	36	0.8	1.0	0.0054	0.0048	-0.0030	1.2	1.4	0.0039	0.0033	-0.0030	0.00%

10 µM Concentration - Steady State Calculation

	Molecular Weight	Time Value (s)	Time Value (hrs)	Slope Between 0.8 & 1 mm					Slope Between 1.2 & 1.4 mm					% Difference Between Slopes
				X_1	X_2	Y_1	Y_2	Slope	X_1	X_2	Y_1	Y_2	Slope	
1 mg/mL Collagen	1 kDa	1800	0.5	0.8	1.0	0.0011	0.0005	-0.0030	1.2	1.4	0.0002	0.0001	-0.0005	83.33%
		2700	0.75	0.8	1.0	0.0017	0.0010	-0.0035	1.2	1.4	0.0006	0.0003	-0.0015	57.14%
		3600	1	0.8	1.0	0.0023	0.0015	-0.0040	1.2	1.4	0.0009	0.0005	-0.0020	50.00%
		5400	1.5	0.8	1.0	0.0031	0.0022	-0.0045	1.2	1.4	0.0015	0.0010	-0.0025	44.44%
		7200	2	0.8	1.0	0.0037	0.0028	-0.0045	1.2	1.4	0.0021	0.0015	-0.0030	33.33%
		10800	3	0.8	1.0	0.0045	0.0037	-0.0040	1.2	1.4	0.0029	0.0023	-0.0030	25.00%
		14400	4	0.8	1.0	0.0050	0.0042	-0.0040	1.2	1.4	0.0035	0.0028	-0.0035	12.50%
		21600	6	0.8	1.0	0.0057	0.0050	-0.0035	1.2	1.4	0.0043	0.0037	-0.0030	14.29%
		43200	12	0.8	1.0	0.0067	0.0062	-0.0025	1.2	1.4	0.0056	0.0051	-0.0025	0.00%
		64800	18	0.8	1.0	0.0073	0.0068	-0.0025	1.2	1.4	0.0063	0.0058	-0.0025	0.00%
		86400	24	0.8	1.0	0.0076	0.0072	-0.0020	1.2	1.4	0.0067	0.0063	-0.0020	0.00%
	10 kDa	3600	1	0.8	1.0	0.0005	0.0001	-0.0020	1.2	1.4	0.0001	0.0000	-0.0005	75.00%
		5400	1.5	0.8	1.0	0.0010	0.0005	-0.0025	1.2	1.4	0.0002	0.0001	-0.0008	70.00%
		7200	2	0.8	1.0	0.0014	0.0007	-0.0035	1.2	1.4	0.0004	0.0002	-0.0013	64.29%
		10800	3	0.8	1.0	0.0022	0.0014	-0.0040	1.2	1.4	0.0008	0.0004	-0.0020	50.00%
		14400	4	0.8	1.0	0.0028	0.0019	-0.0045	1.2	1.4	0.0012	0.0007	-0.0025	44.44%
		21600	6	0.8	1.0	0.0036	0.0027	-0.0045	1.2	1.4	0.0020	0.0014	-0.0030	33.33%
		43200	12	0.8	1.0	0.0050	0.0042	-0.0040	1.2	1.4	0.0034	0.0028	-0.0030	25.00%
		64800	18	0.8	1.0	0.0056	0.0049	-0.0035	1.2	1.4	0.0042	0.0036	-0.0030	14.29%
		86400	24	0.8	1.0	0.0061	0.0055	-0.0030	1.2	1.4	0.0048	0.0042	-0.0030	0.00%
	100 kDa	21600	6	0.8	1.0	0.0015	0.0008	-0.0035	1.2	1.4	0.0004	0.0001	-0.0015	57.14%
		43200	12	0.8	1.0	0.0028	0.0020	-0.0040	1.2	1.4	0.0012	0.0008	-0.0020	50.00%
		64800	18	0.8	1.0	0.0036	0.0028	-0.0040	1.2	1.4	0.0020	0.0015	-0.0025	37.50%
		86400	24	0.8	1.0	0.0041	0.0033	-0.0040	1.2	1.4	0.0027	0.0020	-0.0035	12.50%
		108000	30	0.8	1.0	0.0044	0.0038	-0.0030	1.2	1.4	0.0029	0.0023	-0.0030	0.00%
		129600	36	0.8	1.0	0.0049	0.0042	-0.0035	1.2	1.4	0.0035	0.0028	-0.0035	0.00%
		151200	42	0.8	1.0	0.0051	0.0045	-0.0030	1.2	1.4	0.0038	0.0032	-0.0030	0.00%
	1,000 kDa	43200	12	0.8	1.0	0.0009	0.0004	-0.0025	1.2	1.4	0.0001	0.0000	-0.0005	80.00%
		64800	18	0.8	1.0	0.0016	0.0009	-0.0035	1.2	1.4	0.0004	0.0002	-0.0010	71.43%
		86400	24	0.8	1.0	0.0021	0.0013	-0.0040	1.2	1.4	0.0008	0.0005	-0.0015	62.50%
		108000	30	0.8	1.0	0.0025	0.0017	-0.0040	1.2	1.4	0.0010	0.0006	-0.0020	50.00%
		129600	36	0.8	1.0	0.0028	0.0020	-0.0040	1.2	1.4	0.0013	0.0007	-0.0030	25.00%
		151200	42	0.8	1.0	0.0030	0.0023	-0.0035	1.2	1.4	0.0016	0.0010	-0.0030	14.29%
		172800	48	0.8	1.0	0.0033	0.0026	-0.0035	1.2	1.4	0.0020	0.0013	-0.0035	0.00%
		194400	54	0.8	1.0	0.0035	0.0028	-0.0035	1.2	1.4	0.0023	0.0016	-0.0035	0.00%

10 µM Concentration - Steady State Calculation

	Molecular Weight	Time Value (s)	Time Value (hrs)	Slope Between 0.8 & 1 mm					Slope Between 1.2 & 1.4 mm					% Difference Between Slopes
				X_1	X_2	Y_1	Y_2	Slope	X_1	X_2	Y_1	Y_2	Slope	
2 mg/mL Collagen	1 kDa	7200	2	0.8	1.0	0.0016	0.0009	-0.0035	1.2	1.4	0.0005	0.0002	-0.0015	57.14%
		10800	3	0.8	1.0	0.0024	0.0016	-0.0040	1.2	1.4	0.0010	0.0005	-0.0025	37.50%
		14400	4	0.8	1.0	0.0030	0.0021	-0.0045	1.2	1.4	0.0015	0.0009	-0.0030	33.33%
		21600	6	0.8	1.0	0.0038	0.0030	-0.0040	1.2	1.4	0.0022	0.0016	-0.0030	25.00%
		43200	12	0.8	1.0	0.0052	0.0044	-0.0040	1.2	1.4	0.0037	0.0030	-0.0035	12.50%
		64800	18	0.8	1.0	0.0058	0.0051	-0.0035	1.2	1.4	0.0045	0.0038	-0.0035	0.00%
		86400	24	0.8	1.0	0.0062	0.0056	-0.0030	1.2	1.4	0.0050	0.0044	-0.0030	0.00%
	10 kDa	14400	4	0.8	1.0	0.0009	0.0004	-0.0025	1.2	1.4	0.0002	0.0000	-0.0010	60.00%
		21600	6	0.8	1.0	0.0016	0.0009	-0.0035	1.2	1.4	0.0005	0.0002	-0.0015	57.14%
		43200	12	0.8	1.0	0.0029	0.0020	-0.0045	1.2	1.4	0.0013	0.0008	-0.0025	44.44%
		64800	18	0.8	1.0	0.0037	0.0029	-0.0040	1.2	1.4	0.0021	0.0016	-0.0025	37.50%
		86400	24	0.8	1.0	0.0043	0.0035	-0.0040	1.2	1.4	0.0027	0.0020	-0.0035	12.50%
		108000	30	0.8	1.0	0.0047	0.0039	-0.0040	1.2	1.4	0.0033	0.0025	-0.0040	0.00%
		129600	36	0.8	1.0	0.0051	0.0043	-0.0040	1.2	1.4	0.0035	0.0027	-0.0040	0.00%
	100 kDa	43200	12	0.8	1.0	0.0009	0.0004	-0.0025	1.2	1.4	0.0002	0.0000	-0.0010	60.00%
		64800	18	0.8	1.0	0.0016	0.0009	-0.0035	1.2	1.4	0.0005	0.0002	-0.0015	57.14%
		86400	24	0.8	1.0	0.0021	0.0013	-0.0040	1.2	1.4	0.0008	0.0005	-0.0015	62.50%
		108000	30	0.8	1.0	0.0024	0.0017	-0.0035	1.2	1.4	0.0011	0.0007	-0.0020	42.86%
		129600	36	0.8	1.0	0.0027	0.0021	-0.0030	1.2	1.4	0.0014	0.0009	-0.0025	16.67%
		151200	42	0.8	1.0	0.0030	0.0024	-0.0030	1.2	1.4	0.0017	0.0011	-0.0030	0.00%
		172800	48	0.8	1.0	0.0033	0.0027	-0.0030	1.2	1.4	0.0019	0.0013	-0.0030	0.00%
	1,000 kDa	129600	36	0.8	1.0	0.0008	0.0005	-0.0015	1.2	1.4	0.0002	0.0000	-0.0010	33.33%
		172800	48	0.8	1.0	0.0011	0.0007	-0.0020	1.2	1.4	0.0004	0.0001	-0.0015	25.00%
		216000	60	0.8	1.0	0.0015	0.0012	-0.0015	1.2	1.4	0.0007	0.0004	-0.0015	0.00%
		259200	72	0.8	1.0	0.0017	0.0014	-0.0015	1.2	1.4	0.0008	0.0005	-0.0015	0.00%

10 µM Concentration - Steady State Calculation

	Molecular Weight	Time Value (s)	Time Value (hrs)	Slope Between 0.8 & 1 mm					Slope Between 1.2 & 1.4 mm					% Difference Between Slopes
				X_1	X_2	Y_1	Y_2	Slope	X_1	X_2	Y_1	Y_2	Slope	
3 mg/mL Collagen	1 kDa	14400	4	0.8	1.0	0.0012	0.0006	-0.0030	1.2	1.4	0.0003	0.0001	-0.0010	66.67%
		21600	6	0.8	1.0	0.0019	0.0012	-0.0035	1.2	1.4	0.0007	0.0004	-0.0015	57.14%
		43200	12	0.8	1.0	0.0033	0.0025	-0.0040	1.2	1.4	0.0018	0.0012	-0.0030	25.00%
		64800	18	0.8	1.0	0.0042	0.0034	-0.0040	1.2	1.4	0.0026	0.0019	-0.0035	12.50%
		86400	24	0.8	1.0	0.0047	0.0040	-0.0035	1.2	1.4	0.0032	0.0025	-0.0035	0.00%
	10 kDa	64800	18	0.8	1.0	0.0015	0.0011	-0.0020	1.2	1.4	0.0006	0.0003	-0.0015	25.00%
		86400	24	0.8	1.0	0.0020	0.0016	-0.0020	1.2	1.4	0.0008	0.0005	-0.0015	25.00%
		108000	30	0.8	1.0	0.0029	0.0021	-0.0040	1.2	1.4	0.0013	0.0007	-0.0030	25.00%
		129600	36	0.8	1.0	0.0032	0.0024	-0.0040	1.2	1.4	0.0018	0.0011	-0.0035	12.50%
		172800	48	0.8	1.0	0.0038	0.0030	-0.0040	1.2	1.4	0.0024	0.0016	-0.0040	0.00%
		216000	60	0.8	1.0	0.0043	0.0035	-0.0040	1.2	1.4	0.0028	0.0020	-0.0040	0.00%
	100 kDa	129600	36	0.8	1.0	0.0012	0.0006	-0.0030	1.2	1.4	0.0003	0.0001	-0.0010	66.67%
		172800	48	0.8	1.0	0.0017	0.0010	-0.0035	1.2	1.4	0.0005	0.0002	-0.0015	57.14%
		216000	60	0.8	1.0	0.0023	0.0014	-0.0045	1.2	1.4	0.0007	0.0004	-0.0015	66.67%
		259200	72	0.8	1.0	0.0025	0.0016	-0.0045	1.2	1.4	0.0010	0.0006	-0.0020	55.56%
		302400	84	0.8	1.0	0.0028	0.0019	-0.0045	1.2	1.4	0.0013	0.0008	-0.0025	44.44%
		345600	96	0.8	1.0	0.0031	0.0022	-0.0045	1.2	1.4	0.0015	0.0009	-0.0030	33.33%
		388800	108	0.8	1.0	0.0033	0.0025	-0.0040	1.2	1.4	0.0018	0.0012	-0.0030	25.00%
		432000	120	0.8	1.0	0.0034	0.0026	-0.0040	1.2	1.4	0.0019	0.0013	-0.0030	25.00%
		475200	132	0.8	1.0	0.0037	0.0029	-0.0040	1.2	1.4	0.0022	0.0015	-0.0035	12.50%
		518400	144	0.8	1.0	0.0038	0.0031	-0.0035	1.2	1.4	0.0023	0.0016	-0.0035	0.00%
		561600	156	0.8	1.0	0.0041	0.0033	-0.0040	1.2	1.4	0.0025	0.0017	-0.0040	0.00%
		604800	168	0.8	1.0	0.0042	0.0035	-0.0035	1.2	1.4	0.0027	0.0020	-0.0035	0.00%
	1,000 kDa	259200	72	0.8	1.0	0.0007	0.0003	-0.0020	1.2	1.4	0.00020	0.00000	-0.0010	50.00%
		302400	84	0.8	1.0	0.0009	0.0004	-0.0025	1.2	1.4	0.00025	0.00010	-0.0008	70.00%
		345600	96	0.8	1.0	0.0012	0.0005	-0.0035	1.2	1.4	0.00033	0.00020	-0.0007	81.43%
		388800	108	0.8	1.0	0.0014	0.0006	-0.0040	1.2	1.4	0.00040	0.00025	-0.0008	81.25%
		432000	120	0.8	1.0	0.0015	0.0007	-0.0040	1.2	1.4	0.00045	0.00030	-0.0008	81.25%
		475200	132	0.8	1.0	0.0016	0.0008	-0.0040	1.2	1.4	0.00050	0.00035	-0.0008	81.25%
		518400	144	0.8	1.0	0.0018	0.0010	-0.0040	1.2	1.4	0.00060	0.00040	-0.0010	75.00%
		561600	156	0.8	1.0	0.0019	0.0012	-0.0035	1.2	1.4	0.00070	0.00043	-0.0014	61.43%
		604800	168	0.8	1.0	0.0021	0.0013	-0.0040	1.2	1.4	0.00080	0.00045	-0.0018	56.25%
		648000	180	0.8	1.0	0.0023	0.0014	-0.0045	1.2	1.4	0.00090	0.00048	-0.0021	53.33%
		691200	192	0.8	1.0	0.0024	0.0015	-0.0045	1.2	1.4	0.00100	0.00050	-0.0025	44.44%

10 µM Concentration - Steady State Calculation

	Molecular Weight	Time Value (s)	Time Value (hrs)	Slope Between 0.8 & 1 mm					Slope Between 1.2 & 1.4 mm					% Difference Between Slopes
				X_1	X_2	Y_1	Y_2	Slope	X_1	X_2	Y_1	Y_2	Slope	
Matrigel	1 kDa	5400	1.5	0.8	1.0	0.0006	0.0003	-0.0015	1.2	1.4	0.0001	0.0000	-0.0005	66.67%
		7200	2	0.8	1.0	0.0010	0.0005	-0.0025	1.2	1.4	0.0002	0.0001	-0.0005	80.00%
		10800	3	0.8	1.0	0.0017	0.0010	-0.0035	1.2	1.4	0.0005	0.0002	-0.0015	57.14%
		14400	4	0.8	1.0	0.0023	0.0015	-0.0040	1.2	1.4	0.0008	0.0005	-0.0015	62.50%
		21600	6	0.8	1.0	0.0031	0.0022	-0.0045	1.2	1.4	0.0015	0.0010	-0.0025	44.44%
		32400	9	0.8	1.0	0.0039	0.0031	-0.0040	1.2	1.4	0.0023	0.0017	-0.0030	25.00%
		43200	12	0.8	1.0	0.0045	0.0037	-0.0040	1.2	1.4	0.0029	0.0022	-0.0035	12.50%
		54000	15	0.8	1.0	0.0049	0.0041	-0.0040	1.2	1.4	0.0034	0.0026	-0.0040	0.00%
		64800	18	0.8	1.0	0.0052	0.0045	-0.0035	1.2	1.4	0.0038	0.0031	-0.0035	0.00%
		86400	24	0.8	1.0	0.0057	0.0050	-0.0035	1.2	1.4	0.0043	0.0036	-0.0035	0.00%
	10 kDa	43200	12	0.8	1.0	0.0022	0.0014	-0.0040	1.2	1.4	0.00070	0.00040	-0.0015	62.50%
		54000	15	0.8	1.0	0.0026	0.0017	-0.0043	1.2	1.4	0.00110	0.00070	-0.0020	52.94%
		64800	18	0.8	1.0	0.0030	0.0021	-0.0045	1.2	1.4	0.00140	0.00090	-0.0025	44.44%
		86400	24	0.8	1.0	0.0036	0.0027	-0.0045	1.2	1.4	0.00200	0.00140	-0.0030	33.33%
		108000	30	0.8	1.0	0.0040	0.0031	-0.0045	1.2	1.4	0.00240	0.00170	-0.0035	22.22%
		129600	36	0.8	1.0	0.0044	0.0035	-0.0045	1.2	1.4	0.00280	0.00210	-0.0035	22.22%
		151200	42	0.8	1.0	0.0047	0.0038	-0.0045	1.2	1.4	0.00310	0.00240	-0.0035	22.22%
	100 kDa	64800	18	0.8	1.0	0.0010	0.0005	-0.0025	1.2	1.4	0.00015	0.00005	-0.0005	80.00%
		86400	24	0.8	1.0	0.0015	0.0008	-0.0035	1.2	1.4	0.00040	0.00020	-0.0010	71.43%
		108000	30	0.8	1.0	0.0018	0.0011	-0.0035	1.2	1.4	0.00060	0.00030	-0.0015	57.14%
		129600	36	0.8	1.0	0.0022	0.0014	-0.0040	1.2	1.4	0.00085	0.00050	-0.0018	56.25%
		151200	42	0.8	1.0	0.0025	0.0017	-0.0040	1.2	1.4	0.00100	0.00060	-0.0020	50.00%
		172800	48	0.8	1.0	0.0027	0.0019	-0.0040	1.2	1.4	0.00130	0.00080	-0.0025	37.50%
		194400	54	0.8	1.0	0.0030	0.0022	-0.0040	1.2	1.4	0.00150	0.00090	-0.0030	25.00%
		216000	60	0.8	1.0	0.0032	0.0024	-0.0040	1.2	1.4	0.00170	0.00110	-0.0030	25.00%
		259200	72	0.8	1.0	0.0036	0.0028	-0.0040	1.2	1.4	0.00200	0.00140	-0.0030	25.00%
		302400	84	0.8	1.0	0.0039	0.0031	-0.0040	1.2	1.4	0.00230	0.00170	-0.0030	25.00%
	1,000 kDa	172800	48	0.8	1.0	0.0008	0.0004	-0.0020	1.2	1.4	0.00015	0.00005	-0.0005	75.00%
		194400	54	0.8	1.0	0.0011	0.0005	-0.0030	1.2	1.4	0.00020	0.00008	-0.0006	80.00%
		216000	60	0.8	1.0	0.0013	0.0006	-0.0035	1.2	1.4	0.00025	0.00010	-0.0008	78.57%
		259200	72	0.8	1.0	0.0015	0.0008	-0.0035	1.2	1.4	0.00040	0.00020	-0.0010	71.43%
		302400	84	0.8	1.0	0.0018	0.0011	-0.0035	1.2	1.4	0.00060	0.00030	-0.0015	57.14%
		345600	96	0.8	1.0	0.0020	0.0013	-0.0035	1.2	1.4	0.00070	0.00040	-0.0015	57.14%
		388800	108	0.8	1.0	0.0023	0.0016	-0.0036	1.2	1.4	0.00080	0.00050	-0.0015	58.33%
		432000	120	0.8	1.0	0.0024	0.0017	-0.0035	1.2	1.4	0.00105	0.00065	-0.0020	42.86%

Average Steady State Concentration - 10 µM initial concentration

	Dextran MW (kDa)	Steady State Time (Hrs)	Average Steady State Concentration (in µM) Chamber Location in mm					
			0 to 0.6 mm	0.6 to 1.2 mm	1.2 to 1.8 mm	1.8 to 2.4 mm	2.4 to 3.0 mm	3.0 to 3.6 mm
0 mg/mL Collagen (Water)	1 kDa	0.75	7.70	4.08	1.98	0.85	0.33	0.08
	10 kDa	2.00	7.55	3.78	1.68	0.63	0.23	0.05
	100 kDa	4.00	7.15	3.00	1.10	0.30	0.05	0.00
	1,000 kDa	9.00	6.90	2.50	0.75	0.18	0.03	0.00
1 mg/mL Collagen	1 kDa	2.00	7.35	3.40	1.40	0.45	0.13	0.03
	10 kDa	6.00	7.30	3.30	1.30	0.38	0.08	0.01
	100 kDa	12.00	6.95	2.60	0.80	0.18	0.03	0.00
	1,000 kDa	24.00	6.60	1.95	0.40	0.05	0.00	0.00
2 mg/mL Collagen	1 kDa	4.00	7.05	2.78	0.93	0.23	0.03	0.00
	10 kDa	12.00	7.00	2.70	0.88	0.18	0.01	0.00
	100 kDa	24.00	6.60	2.00	0.45	0.05	0.00	0.00
	1,000 kDa	48.00	6.30	1.50	0.23	0.03	0.00	0.00
3 mg/mL Collagen	1 kDa	9.00	6.90	2.55	0.83	0.18	0.01	0.00
	10 kDa	30.00	6.95	2.60	0.80	0.15	0.00	0.00
	100 kDa	60.00	6.60	1.95	0.40	0.05	0.00	0.00
	1,000 kDa	108.00	6.20	1.40	0.21	0.01	0.00	0.00
Matrigel	1 kDa	6.00	7.10	2.88	1.00	0.28	0.05	0.00
	10 kDa	18.00	7.05	2.75	0.90	0.23	0.03	0.00
	100 kDa	36.00	6.65	2.05	0.45	0.05	0.00	0.00
	1,000 kDa	60.00	6.15	1.30	0.17	0.02	0.00	0.00

Average Steady State Concentration at 0.6 mm Increments Across Gel Chamber

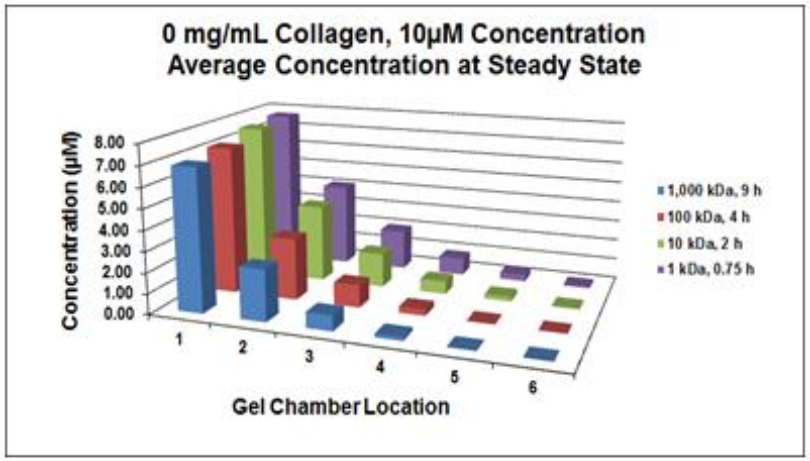

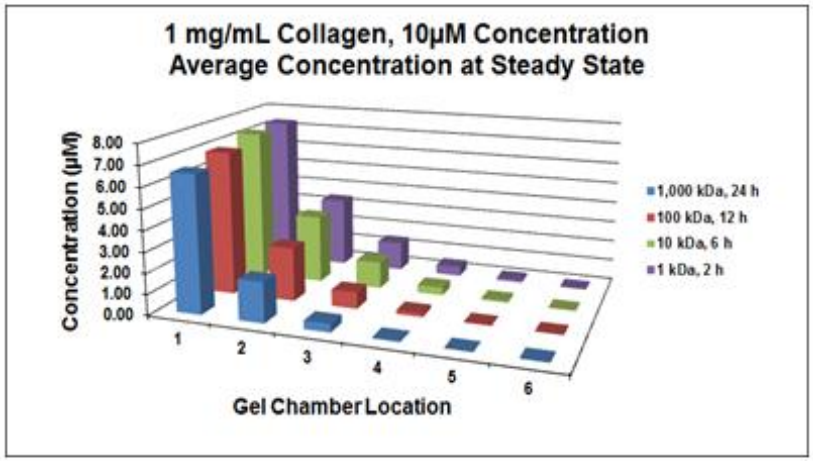

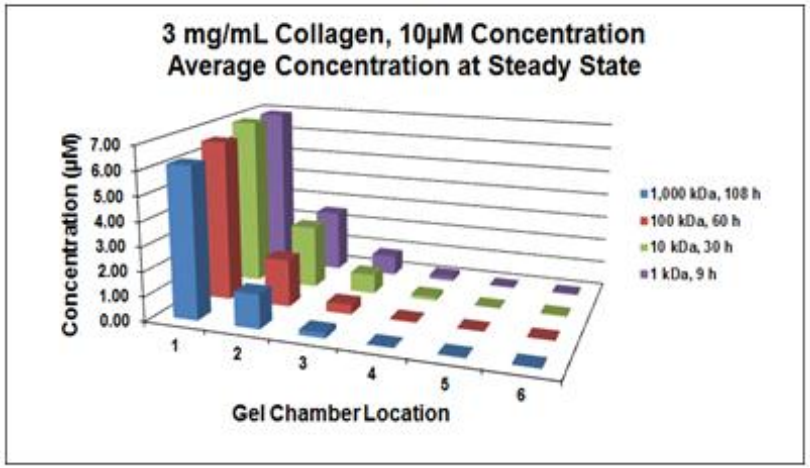

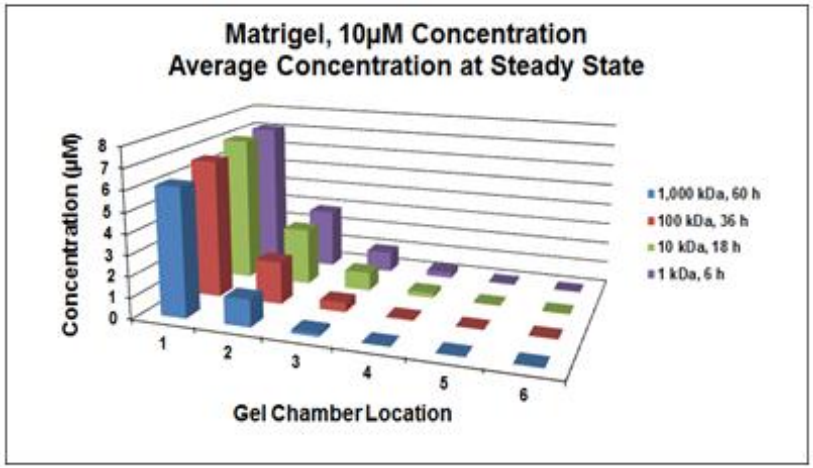

Steepness at Steady State Conditions

	Dextran MW (kDa)	Steady State Time (Hrs)	Steepness % at 10 microns at Steady State Chamber Location in mm					
			0 to 0.6 mm	0.6 to 1.2 mm	1.2 to 1.8 mm	1.8 to 2.4 mm	2.4 to 3.0 mm	3.0 to 3.6 mm
0 mg/mL Collagen (Water)	1 kDa	0.75	0.90%	0.85%	0.73%	0.69%	0.50%	0.02%
	10 kDa	2.00	0.85%	0.80%	0.61%	0.65%	0.48%	0.01%
	100 kDa	4.00	0.72%	0.66%	0.49%	0.33%	0.00%	0.00%
	1,000 kDa	9.00	0.63%	0.53%	0.42%	0.28%	0.00%	0.00%
1 mg/mL Collagen	1 kDa	2.00	0.78%	0.74%	0.56%	0.48%	0.42%	0.05%
	10 kDa	6.00	0.77%	0.72%	0.50%	0.42%	0.11%	0.00%
	100 kDa	12.00	0.65%	0.56%	0.38%	0.28%	0.00%	0.00%
	1,000 kDa	24.00	0.53%	0.36%	0.24%	0.00%	0.00%	0.00%
2 mg/mL Collagen	1 kDa	4.00	0.68%	0.59%	0.46%	0.21%	0.00%	0.00%
	10 kDa	12.00	0.67%	0.58%	0.42%	0.16%	0.00%	0.00%
	100 kDa	24.00	0.53%	0.42%	0.21%	0.00%	0.00%	0.00%
	1,000 kDa	48.00	0.43%	0.26%	0.21%	0.00%	0.00%	0.00%
3 mg/mL Collagen	1 kDa	9.00	0.63%	0.57%	0.45%	0.05%	0.00%	0.00%
	10 kDa	30.00	0.65%	0.56%	0.38%	0.00%	0.00%	0.00%
	100 kDa	60.00	0.53%	0.36%	0.24%	0.00%	0.00%	0.00%
	1,000 kDa	108.00	0.40%	0.28%	0.04%	0.00%	0.00%	0.00%
Matrigel	1 kDa	6.00	0.70%	0.62%	0.48%	0.37%	0.00%	0.00%
	10 kDa	18.00	0.68%	0.57%	0.48%	0.21%	0.00%	0.00%
	100 kDa	36.00	0.55%	0.40%	0.21%	0.00%	0.00%	0.00%
	1,000 kDa	60.00	0.38%	0.22%	0.17%	0.00%	0.00%	0.00%

Average Steepness at Steady State across 10µm at 0.6 mm Increments across Gel Chamber

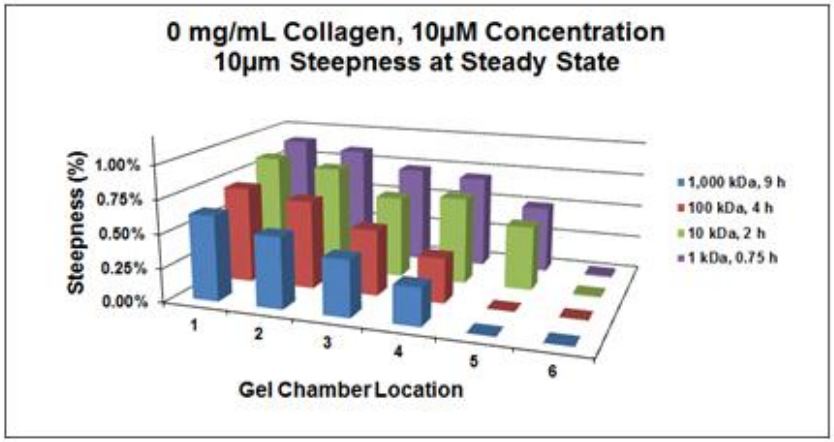

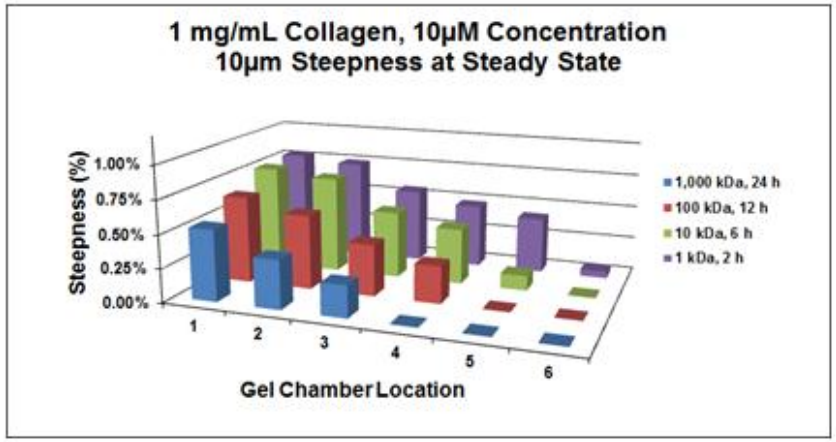

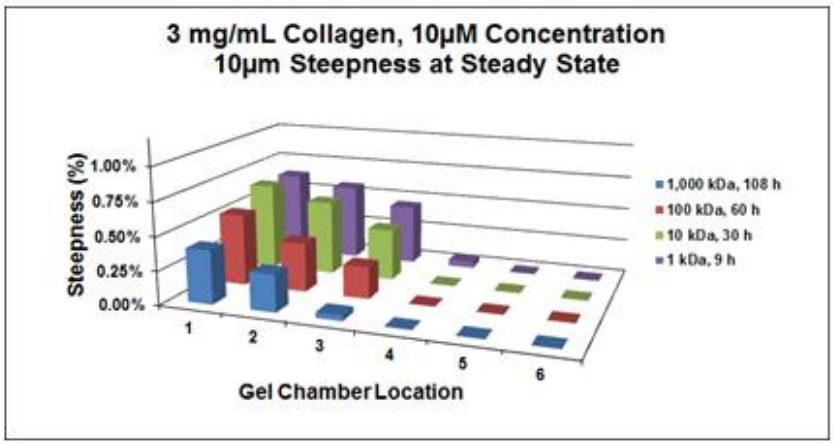

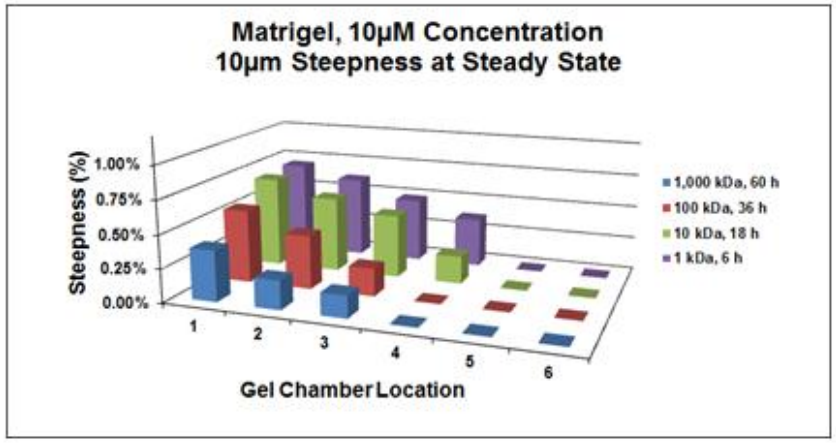

Neurite outgrowth in control cultures

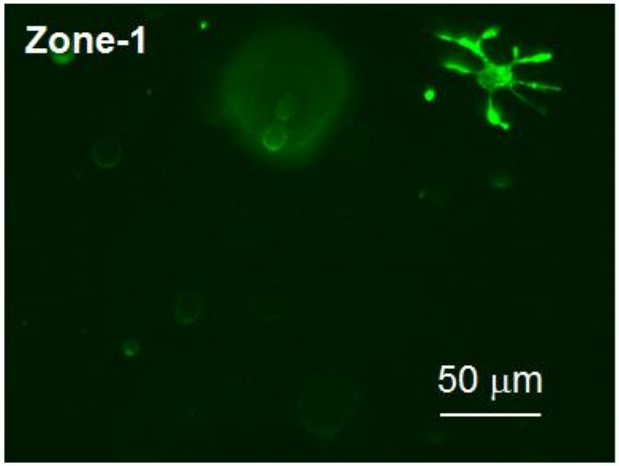

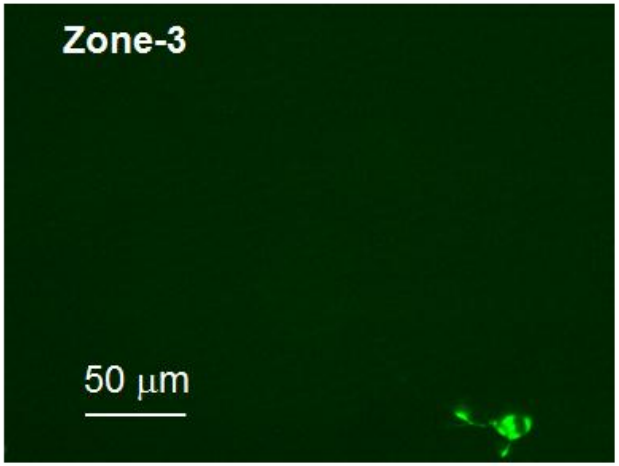

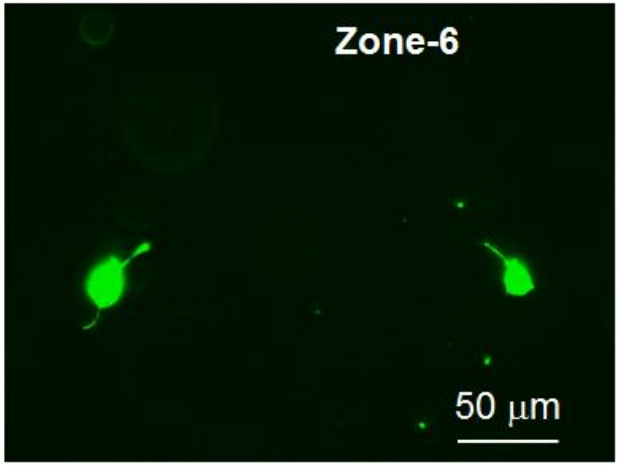

Fluorescence images of control samples used as comparison to those exposed to the gradient of IGF-I. Significantly lower neurite outgrowth was seen in the controls compared to the IGF-I samples